NOVEL THEORETICAL TOOLS AND APPLICATIONS FOR THE STUDY OF ELECTRONIC STRUCTURE AND OPTIMIZING REACTION ENERGETICS

A Thesis

Submitted to the Graduate Faculty

in Partial Fulfillment of the Requirements

for the Degree of Master of Science

Department of Chemistry

Faculty of Science

University of Prince Edward Island

Adam J. Proud

Charlottetown, Prince Edward Island

December 2011

Your file Votre référence
ISBN: 978-0-494-82241-8
Our file Notre référence
ISBN: 978-0-494-82241-8

CONDITIONS FOR THE USE OF THE THESIS

SIGNATURE

PAGE(S)

(iii) & (iv)

REMOVED

Abstract

This thesis is comprised of two distinct areas: the first area representing the bulk of the work to be presented here, focusses on the development of novel analytical tools for the study of electronic structure. The second area highlights the refinement of potential energy surfaces algorithmically.

There is a great deal of interest in understanding electronic interactions within atoms and molecules. As we are confined to only 3-dimensions when visualizing a set of data, it is impossible to completely visualize the effects of particle interactions. Nonetheless, over the years, there have been numerous methods devised in order to analyze these interactions in different ways. In the first part of this thesis, the development of novel tools to examine electronic structure effects will be highlighted.

We introduce the intex density $X(R,u)$, which combines both the intracular and extracular coordinates to yield a simultaneous probability density for the position of the centre-of-mass radius (R) and relative separation (u) of electron pairs. The principle application of the intex density explored here is in the investigation of the recently observed secondary Coulomb hole. The Hartree-Fock (HF) intex densities for the helium atom and heliumlike ions are symmetric functions that may be used to prove the isomorphism $2P(2R) = E(R)$, where $P(u)$ is the intracule density and $E(R)$ is the extracule density. This is not true of the densities that have been constructed from explicitly correlated wave functions. The difference between these asymmetric functions and their symmetric HF counterparts produces a topologically rich intex correlation hole. We conclude that the probability of observing an electron pair with a very large interelectronic separation increases with the inclusion of correlation only when their centre-of-mass radius is close to half of their separation.

Despite providing more details regarding the correlation hole than the intracule alone, the intex density is still limited in nature by its lack of information regarding the spatial orientation of the $\boldsymbol{R}$ and $\boldsymbol{u}$ vectors. This led to the development of the probability density for the angle between these two vectors using both Hartree-Fock (HF) and explicitly correlated Kinoshita wave functions. This angular density, $A(\theta_{Ru})$, and the angular-dependent intex density, $X(R,u,\theta_{Ru})$, are explored for the helium isoelectronic series from He to Ne^{8+} to study the distribution of electron pairs in atomic systems (both HF and exact). We demonstrate that the most probable angle depends significantly on the scalar values of R and u for both the HF and exact treatments. As R and u simultaneously increase, the favoured angle for these densities approach 0 and π.

With a more complete description and understanding of the secondary Coulomb hole, the focus of our study was directed towards determining the origin of the hole. These analyses were carried out by examining the correlation hole in intracules, $\Delta P(u)$, for atoms with varying electron-nuclear potentials including systems with Coulombic potentials, harmonic potentials, and those with a zero potential (aside from an infinite confining potential). These studies have highlighted the role of a non-zero potential in the presence of the secondary hole and have suggested this counter-intuitive effect is the result of shielding. This theory is well supported by evidence in the literature including an analogous effect (i.e. contraction of electron pairs at large values of u) that has been observed for excited states and has been attributed to shielding.

In addition to these electronic structure analyses with respect to correlation, we also present findings regarding the effects of using polarization functions in basis sets to describe atoms and molecules. Previous research has indicated that the introduction of polarization functions into a basis set leads to an overall contraction of the intracule density. We examine this contraction of electron pairs through analysis of position intracules, various components of the energy, and differences in electron densities. This combined data has yielded conclusive evidence that the inclusion of polarization functions leads to an increase in density in the bonding regions in order to improve bond descriptions.

The second area explored in this thesis is regarding the development of novel software to be used for the optimization of chemical reactions. This optimization is based on a new method described herein, known as the linear combination of functional groups. In this process, a large set of substituents is superimposed at a functional site within a reactant complex. By allowing these substituents to interact with the fixed part of the molecule while prohibiting interactions between each of the functional groups, one can effectively determine the contribution of each moiety to the overall energy. Localized molecular orbitals are used in this study as they are highly transferable from molecule to the next. This allows for the construction of a library of coefficients specific for each functional group to determine the form of the molecular orbitals of said group that would be applicable in any chemical environment. Through the use of minimization/maximization algorithms one can optimize the energy difference between two states (e.g. products and reactants) with respect to each of these functional groups. The details of the method and the results of an optimization on the deprotonation of HO-X (X being the set of functional groups) is demonstrated herein. The results obtained in the proof-of-concept stage of this project demonstrate great merit for this concept.

Acknowledgements

Performing a graduate research project and preparing a thesis summarizing the details of said research is no simple task and I could not have succeeded without the help and support of a number of people. For all of your help over the past two years, I would like to thank you all.

More specifically, I would first like to thank my supervisor, Dr. Jason Pearson. I simply could not have done this without you. Coming into the Masters of Science program, I knew very little about theoretical chemistry. But in the past two years, you have taught me so much and pushed me to learn whatever I could about the field and about science in general. I know there is still much to learn, but I now feel confident in my abilities and knowledge of theoretical chemistry. You have always been there to discuss my research or to *try* and help me formulate a plan for my future. For all of these reasons and more, I am truly grateful.

I would next like to thank the members of my graduate supervisory committee: Dr. James Polson of the Physics Department and Dr. Michael Shaver of the Chemistry Department. You have both been very supportive in our discussions regarding my research and I appreciate all of your feedback and support over the past two years. I realize that my research is quite different from your respective fields of study, but this has allowed me to see my research from different perspectives. I would also like to thank Dr. Ajit Thakkar from the University of New Brunswick, who agreed to be the external examiner for my thesis defence. You are a very well respected member in our field of study and it was a pleasure meeting you through conferences during my graduate studies. I am grateful that you accepted the role of the external examiner in the thesis review and defence portion of this program.

I am also very grateful to all of the remaining faculty and staff in the Chemistry Department for all of their help over the years during my undergraduate and graduate studies. I would especially like to thank Dr. Rabin Bissessur who gave me my start in research and whose door was always open whenever I needed to chat about something. Janette Paquet, Dawna Lund and Jill MacDonald also deserve a great deal of gratitude for ensuring that our department runs smoothly.

Dr. Pedro Quijon deserves a great deal of thanks as well. You have done a wonderful job as the Graduate Studies Coordinator for the Faculty of Science. Whenever I have had questions regarding the program, you have always been very helpful and I greatly appreciate it.

Outside of the faculty and staff at the University of Prince Edward Island, I was fortunate enough to have received advice and participated in fruitful discussions with Dr. Peter Gill and Dr. Pierre-Francois Loos of the Australian National University. Furthermore, Dr. Toshikatsu Koga was very generous in providing atomic orbital coefficients for the development of the highly accurate Kinoshita wavefunctions. To each of these individuals, I am very grateful for your help.

With regards to financial support, I would like to extend my thanks to the National Sciences and Engineering Research Council, the University of Prince Edward Island, Dr. Regis Duffy, and my supervisor Dr. Jason Pearson.

Finally, I would like to thank my parents, Mike and Anne, and my girlfriend, Jillian McInnis. I realize that graduate studies not only take a toll on the students but also on those closest to them. I am very grateful for your unconditional support over the years. I would not be here without you. Thank you.

Contents

List of Figures

List of Tables

List of Abbreviations and Symbols

Abbreviations

AO	Atomic orbital
BSIE	Basis set incompleteness error
BO	Born-Oppenheimer
CC	Coupled cluster
CI	Configuration interaction
DFT	Density functional theory
GTO	Gaussian-type orbital
HF	Hartree-Fock
LCAO	Linear combination of atomic orbitals
LCFG	Linear combination of functional groups
MO	Molecular orbital
MPn	MPPT applied up to and including the n^{th} order corrections
MPPT	Møller Plesset perturbation theory
RHF	Restricted Hartree-Fock
SCF	Self-consistent field
STO	Slater-type orbital
STO-nG	Denotes a minimal basis set containing a contracted set of n GTOs
UHF	Unrestricted Hartree-Fock

Symbols

Ψ	Molecular wave function
ψ	Spatial molecular orbital
χ	Spin molecular orbital
ϕ	Basis function
$\hat{H}$	Hamiltonian operator
$\hat{T}$	Kinetic energy operator
$\hat{V}$	Potential energy operator
$\hat{H}^{elec}$	Electronic Hamiltonian operator

$\hat{P}_{ij}$	Permutation operator
$\hat{J}$	Coulomb operator
$\hat{K}$	Exchange operator
$\boldsymbol{r}$	Electron position vector
$\boldsymbol{r_i}$	Position vector for electron i
r_{ij}	Distance between electrons i and j
$\boldsymbol{R}$	Nuclear position vector
R_{AB}	Distance between nuclei A and B
Z_A	Atomic number of nucleus A
N	Number of electrons
M	Number of nuclei
K	Number of basis functions
$S_{\mu\nu}$	Element of overlap matrix, $\boldsymbol{S}$
$T_{\mu\nu}$	Element of kinetic energy matrix
$V^{en}_{\mu\nu}$	Element of electron nuclear attraction matrix
$V^{ee}_{\mu\nu\lambda\sigma}$	Element of electron repulsion matrix
$\Gamma^{ee}_{\mu\nu\lambda\sigma}$	Element of two-particle density matrix
$P_{\lambda\sigma}$	Element of charge density matrix
c	Orbital expansion coefficient
d	Basis function contraction coefficient
α	Spin-up function
β	Spin-down function
δ_{ij}	Kronecker delta ($\delta_{ij} = 1$ if $i = j$; $\delta_{ij} = 0$ if $i \neq j$)
$\boldsymbol{F}$	Fock matrix
$\boldsymbol{C}$	Molecular orbital coefficient matrix
$\boldsymbol{X}$	Overlap transformation matrix
E	Energy
ε_a	Energy of orbital a
$\boldsymbol{u}$	Intracule coordinate vector ($u = \lvert\boldsymbol{r_1} - \boldsymbol{r_2}\rvert$)
$\boldsymbol{R}$	Extracule coordinate vector ($R = \frac{1}{2}\lvert\boldsymbol{r_1} + \boldsymbol{r_2}\rvert$)
θ_{12}	Angular separation of electronic position vectors $\boldsymbol{r_1}$ and $\boldsymbol{r_2}$
θ_{Ru}	Angular separation of extracule, $\boldsymbol{R}$, and intracule, $\boldsymbol{u}$, coordinate vectors
s	Hylleraas coordinate ($s = \lvert\boldsymbol{r_1}\rvert + \lvert\boldsymbol{r_2}\rvert$)
t	Hyleraas coordinate ($t = \lvert\boldsymbol{r_1}\rvert - \lvert\boldsymbol{r_2}\rvert$)
$\rho(\boldsymbol{r})$	Electron density
$\rho(\boldsymbol{r_1}, \boldsymbol{r_2})$	Two-electron density
$P(u)$	Position intracule density
$E(R)$	Extracule density
$X(R, u)$	Intex density
$\mathrm{d}\Omega$	Indicates an integration over all angular coordinates
∇^2	Laplacian operator ($\nabla^2 \equiv \frac{\partial^2}{\partial x^2} + \frac{\partial^2}{\partial y^2} + \frac{\partial^2}{\partial z^2}$)

1 Introduction

Computational chemistry is a relatively new branch of science having only truly been developed within the past 100 years. In fact, the first theoretical calculations to be performed in the field of chemistry were not conducted until 1927 by the German physicists, Walter Heitler and Fritz London.[1,2] The difficulty in performing such calculations stems from the unorthodox behaviour (wave-particle duality) of microscopic particles and the many-body problem. Unlike the objects observed in everyday life, these subatomic particles must be treated with quantum mechanics rather than the more traditional classical mechanics.

1.1 Classical Mechanics

Sir Isaac Newton's contributions to the field of science simply cannot be overstated. In the latter part of the 17^{th} century, it was he who first formulated what is now referred to as classical mechanics, which describes the laws that govern the motion of macroscopic objects.[1] Newton's second law of motion, which is commonly expressed as

$$\vec{F} = m\,\vec{a}\,, \tag{1.1}$$

where $\vec{F}$ defines the force acting on an object while m and $\vec{a}$ represent the mass and acceleration of the object, respectively, can be used to determine the past, present, and future positions of any object under the specified boundary conditions. In a more general form, this law states that the net force which is acting on a particle is equal to the rate of change

in the particle's momentum with time. This can be denoted by

$$\vec{F} = \frac{d\vec{p}}{dt} = \frac{d(m\vec{v})}{dt} = \vec{v}\frac{dm}{dt} + m\frac{d\vec{v}}{dt} = m\frac{d^2\vec{r}}{dt^2}\,, \tag{1.2}$$

where the $\vec{v}\,\frac{dm}{dt}$ term vanishes as the mass is constant. Since the force is given by $m\,\frac{d^2\vec{r}}{dt^2}$, it is easily shown that, if said force is constant, the position, $\vec{r}$, is a function of time, t, expressed as

$$\vec{r}(t) = \int\int \frac{\vec{F}}{m}\mathrm{d}t\,\mathrm{d}t = \frac{\vec{F}}{m}t^2 + \vec{c}_1 t + \vec{c}_2 \tag{1.3}$$

Here, $\vec{c}_1$ is obtained from the first indefinite integral, which yields the velocity function and $\vec{c}_2$ is obtained from the second integration yielding the final position function, $\vec{r}(t)$. At time $t = 0$, $\vec{r}(t) = \vec{c}_2$, and thus $\vec{c}_2$ is simply the initial position, $\vec{r}_0$, of the object. Similarly, $\vec{c}_1$ is found to be equal to the initial velocity, $\vec{v}_0$, of the object and thus we can write (1.3) as

$$\vec{r}(t) = \frac{\vec{F}}{m}t^2 + \vec{v}_0 t + \vec{r}_0 \tag{1.4}$$

From this equation, it is noted that by knowing the initial position and velocity of a macroscopic particle as well as the mass of the object and the constant net force acting on it, one can readily determine the future motion of this particle. This expression demonstrates the incredible utility of Newton's second law of motion; however, systems are often more complicated than this as there are numerous variables to consider. Nonetheless, by considering all parameters, one can effectively determine the position of the object at any time, t. Unfortunately, these laws of motion do not apply to microscopic particles. Consequently, this idea led to the development of quantum mechanics in the early twentieth century. The reason these particles cannot be described using classical mechanics can be explained in part by the Heisenberg Uncertainty Principle. The Heisenberg Uncertainty Principle states, "The more precisely the position is determined, the less precisely the momentum is known in this instant, and vice versa" (translation by American Institute of Physics).[3] Mathemat-

ically, this principle is given by $\Delta x \Delta \rho \geq h/4\pi$ where Δx and $\Delta \rho$ are the uncertainties in the position and momentum respectively and h is Planck's constant.[1] When considering the size of the particles (i.e. macroscopic) that are treated with classical mechanics, this level of uncertainty is negligible even for high accuracy studies; however, in the study of microscopic particles, the uncertainty is relevant and thus, the exact position and momentum of these particles cannot be known simultaneously with reasonable accuracy. Instead, one must rely on quantum mechanics which describes the motion of such particles in a probabilistic or statistical manner.

1.2 Quantum Mechanics

Without the development of quantum mechanics, we would not be capable of understanding the behaviour of subatomic particles, and thus our fundamental understanding of how atoms and molecules function would be severely limited.

1.2.1 The Schrödinger Equation

The Schrödinger equation is the foundation for non-relativistic quantum mechanics. It is as essential to quantum mechanics as Newton's Laws of Motion are to classical mechanics.[4] It is the fundamental equation on which most quantum chemical models are based and it can be expressed as

$$-\frac{\hbar}{i}\frac{\partial \Psi(\boldsymbol{r},t)}{\partial t} = -\frac{\hbar^2}{2m}\sum_i \nabla_i^2 \Psi(\boldsymbol{r},t) - \sum_A \frac{\hbar}{2M_A}\nabla_A^2 \Psi(\boldsymbol{r},t) + V(\boldsymbol{r},t)\Psi(\boldsymbol{r},t)\,, \quad (1.5)$$

where $\Psi(\boldsymbol{r},t)$ is the state or wave function of the system, $V(\boldsymbol{r},t)$ is the potential energy operator, and ∇_j^2 is the Laplacian operator involving the second partial derivatives over the set of Cartesian coordinates ($\nabla^2 \equiv \frac{\partial^2}{\partial x^2} + \frac{\partial^2}{\partial y^2} + \frac{\partial^2}{\partial z^2}$) of particle j (e.g. electron i or nucleus A). The $\boldsymbol{r}$ ($\boldsymbol{r} = \{(x_i, y_i, z_i)\}$) and t variables denote the position and time coordinates, respectively.[1] The expression shown above is the time-dependent Schrödinger

Table 1.1: Definition of atomic units.

Measure	Unit	Value in Atomic Units	Value in SI Units
Length	a_0	1 bohr	5.2918×10^{-11} m
Mass	m_e	1	9.1095×10^{-31} kg
Charge	e	1	1.6022×10^{-19} C
Energy	E	1 hartree (E_h)	4.3598×10^{-18} J
Energy	E	1 hartree (E_h)	27.211 eV
Energy	E	1 hartree (E_h)	627.51 kcal/mol
Angular momentum	$\hbar$	1	1.0546×10^{-34} J s
Vacuum permittivity	$4\pi\varepsilon_0$	1	1.113×10^{-10} C^2/(J m)

equation for a general system in 3-dimensions. The solution to the time-dependent equation can be separated into time and space components and fortunately, many applications of quantum chemistry can be accurately described by the time-independent Schrödinger equation which observes stationary states of the wave function. Throughout this thesis, we will only be concerned with the time-independent expression and will simply refer to it as the Schrödinger equation. This expression for a system consisting of N electrons and M nuclei is given by[1,5]

$$\left[-\frac{\hbar}{2m}\sum_{i=1}^{N}\nabla_i^2 - \sum_{A=1}^{M}\frac{\hbar}{2M_A}\nabla_A^2 + V(\boldsymbol{r})\right]\Psi(\boldsymbol{r},\boldsymbol{R}) = E\,\Psi(\boldsymbol{r},\boldsymbol{R})\,, \tag{1.6}$$

where $V(\boldsymbol{r})$ is once again the potential energy operator, E is the total energy of the system, and $\Psi(\boldsymbol{r},\boldsymbol{R})$ is the time-independent wave function which depends on the set of all electronic ($\boldsymbol{r} \equiv \boldsymbol{r_1}, \boldsymbol{r_2}, \ldots, \boldsymbol{r_N}$) and nuclear ($\boldsymbol{R} \equiv \boldsymbol{R_1}, \boldsymbol{R_2}, \ldots, \boldsymbol{R_N}$) coordinate vectors.

There are a number of simplifications that can be applied to the Schrödinger equation. The first that is discussed here is the conversion from SI units to atomic units. These atomic units are defined in order to simplify the expressions and the conversions are given in Table 1.1.[5]

There has yet to be any mention of the form of the potential energy operator. This was done intentionally, in order to simplify the form of the expression. Using the atomic unit

simplification, the Schrödinger equation can be expressed fully as

$$\left[-\frac{1}{2}\sum_{i=1}^{N}\nabla_i^2 - \sum_{A=1}^{M}\frac{1}{2M_A}\nabla_A^2 + \left(\sum_{i=1}^{N-1}\sum_{j>i}^{N}\frac{1}{r_{ij}} - \sum_{i=1}^{N}\sum_{A=1}^{M}\frac{Z_A}{r_{iA}} + \sum_{A=1}^{M-1}\sum_{B>A}^{M}\frac{Z_A Z_B}{R_{AB}}\right)\right]\Psi(\boldsymbol{r},\boldsymbol{R}) = E\,\Psi(\boldsymbol{r},\boldsymbol{R}) \quad (1.7)$$

where the terms enclosed in round brackets represent the potential energy operator, V. In this expression, r_{ij} and R_{AB} are the interelectronic and internuclear distances, respectively, while r_{iA} is the distance between electron i and nucleus A. Finally, Z_A is the atomic number of nucleus A and the remaining terms are as previously described.

In this final expression, there are five separate terms in square brackets. Each term represents an operator for a particular component of the energy. The first two terms, with the Laplacian operators, represent the kinetic energy operators for the electrons and nuclei, respectively. The potential energy operator is comprised of the electronic repulsion (term 3), electron nuclear attraction (term 4) and nuclear repulsion (term 5) operators. The sum of these five terms can be expressed as a single Hermitian operator known as the Hamiltonian operator, $\hat{H}$. It is defined by the terms in square brackets and using this operator, the Schrödinger equation can be written in its most common form as

$$\hat{H}\,\Psi(\boldsymbol{r},\boldsymbol{R}) = E\,\Psi(\boldsymbol{r},\boldsymbol{R}) \quad (1.8)$$

This equation is an eigenvalue problem where the eigenfunctions of the Hamiltonian operator represent the ground and excited state wave functions and the eigenvalues are the corresponding energy values for these states.

1.2.2 The Born-Oppenheimer Approximation

As shown in equation (1.7), the operators consist of both electronic and nuclear terms. However, since nuclei are far more massive than electrons ($M_A/m_e \approx 1840$ for **H** atom),[1]

they move at a much slower pace. This is the basis of the Born-Oppenheimer (BO) approximation developed by said researchers in 1926.[6] This approximation assumes that as electronic motion is much faster than nuclear motion, one can treat the system as if the electrons move within a field of static nuclei. Using this approximation, the Hamiltonian operator is greatly simplified. First and foremost, since the nuclei are considered fixed, the nuclear kinetic energy operator can be omitted. The Hamiltonian operator is then given by

$$\hat{H} = -\frac{1}{2}\sum_{i=1}^{N}\nabla_i^2 + \sum_{i=1}^{N-1}\sum_{j>i}^{N}\frac{1}{r_{ij}} - \sum_{i=1}^{N}\sum_{A=1}^{M}\frac{Z_A}{r_{iA}} + \sum_{A=1}^{M-1}\sum_{B>A}^{M}\frac{Z_A Z_B}{R_{AB}} \tag{1.9}$$

Furthermore, as the nuclei are fixed in space, the final term representing the nuclear repulsion operator simply becomes a constant. Since constants do not affect the eigenfunctions in an eigenvalue problem, but simply add said constant to each of the eigenvalues, this term can be removed from the Hamiltonian operator to form the electronic Hamiltonian, $\hat{H}_{elec}$, given by

$$\hat{H}_{elec} = -\frac{1}{2}\sum_{i=1}^{N}\nabla_i^2 + \sum_{i=1}^{N-1}\sum_{j>i}^{N}\frac{1}{r_{ij}} - \sum_{i=1}^{N}\sum_{A=1}^{M}\frac{Z_A}{r_{iA}} \tag{1.10}$$

Using this newly defined operator, the electronic Schrödinger equation can be expressed as

$$\hat{H}_{elec}\Psi(\boldsymbol{r};\boldsymbol{R}) = E_{elec}\Psi(\boldsymbol{r};\boldsymbol{R}) \tag{1.11}$$

where E_{elec} is the electronic energy. Here, the wave function has been denoted by $\Psi(\boldsymbol{r};\boldsymbol{R})$ which indicates that it is no longer a function of the nuclear coordinates, $\boldsymbol{R}$, but instead has a parametric dependence. This indicates that if the coordinates of the nuclei were to change, the wave function would also change. The BO approximation will be used throughout this thesis, and thus the wave function will simply be given by $\Psi(\boldsymbol{r})$. Upon solving the electronic Schrödinger equation, the total energy, E, is given by the sum of the electronic and nuclear repulsion components as follows

$$E = E_{elec} + \sum_{A=1}^{M-1} \sum_{B>A}^{M} \frac{Z_A Z_B}{R_{AB}} \tag{1.12}$$

1.3 Solving the Schrödinger Equation

Despite the approximations described in the previous section, solving the Schrödinger equation remains a formidable task. The solution for the one-electron hydrogen atom is well established, as are the solutions for a variety of fictional systems (e.g. particle in a box, the linear rigid rotor, Hooke's law atom, etc.);[1] however, in real chemical systems (i.e. molecules and multi-electron atoms), the introduction of a second electron leads to the inseparability of the Schrödinger equation and the inability to obtain analytical solutions. This has led to the development of a wide range of techniques to approximate the solution for these more complicated systems. These techniques can be grouped into a number of classes, including perturbative methods, variational methods, quantum Monte Carlo simulations, and density functional theories. The majority of the work in this thesis will involve variational methods and it is these techniques that will be discussed in detail here.

1.3.1 The Variational Theorem

With any approximation, it is essential to have a measure of its accuracy. In quantum chemistry, the variational theorem is used for this purpose. The theorem states that for any normalized trial wavefunction, ϕ_G, that obeys the boundary conditions imposed upon the true wave function, the expectation value (predicted mean value) of the Hamiltonian operator, E_G, will always be greater than the exact ground state energy, E_0.[5] This is represented mathematically as

$$\langle \phi_G | \hat{H} | \phi_G \rangle = E_G \geq E_0 \tag{1.13}$$

Using this principle, one can effectively measure the quality of any approximation to the wave function as lower energies reflect more accurate guesses. If one obtains the true

ground state energy, then ϕ_G must be identical to the exact wave function. This principle is used in many quantum chemical methods for the determination of accuracy; however, not all techniques are variational. It is only true when the energy determined by the method is obtained from the expectation value of the Hamiltonian operator as shown in (1.13).

1.4 The Hartree Method

One of the earliest methods developed to obtain approximate solutions to the Schrödinger equation was developed by Douglas Hartree in the late 1920s.[7,8] This method is commonly referred to as the Hartree self-consistent field method or simply the Hartree method. It is also the basis for the more popular Hartree-Fock (HF) method that will be discussed in the next section.

The Hartree method involves the use of a Hartree product wave function,[5] Ψ^{HP}, which approximates the true wave function as a product of single particle functions (i.e. orbitals) as follows:

$$\Psi^{HP}(\boldsymbol{x_1}, \boldsymbol{x_2}, ..., \boldsymbol{x_n}) = \prod_{i=1}^{N} \chi_i(\boldsymbol{x_i}) \tag{1.14}$$

Here, $\boldsymbol{x_i}$ is the combined position-spin coordinate vector ($\boldsymbol{x_i} \equiv (\boldsymbol{r_i}, \omega_i)$, where ω_i is the spin coordinate) of electron i, N is the number of electrons and χ_i is the i^{th} spin orbital. A spin orbital is simply an orbital function that contains a single spin-up (α) or spin-down (β) electron.[1,5] In freshman chemistry classes, one is often told that an orbital can hold up to two electrons. This statement describes spatial orbitals, $\psi(\boldsymbol{r})$, which can hold one electron of each spin type. The relationship between spin and spatial orbitals is as follows:

$$\begin{aligned} \chi_i(\boldsymbol{x}) &= \psi_i(\boldsymbol{r})\,\alpha(\omega) = \psi_i^{\alpha}(\boldsymbol{r}) \\ \chi_{i+1}(\boldsymbol{x}) &= \psi_i(\boldsymbol{r})\,\beta(\omega) = \psi_i^{\beta}(\boldsymbol{r}) \end{aligned} \tag{1.15}$$

where i is restricted to be odd so that the first electron in a spatial orbital has spin α and

the second has spin β. The functional form of the spin functions is undefined; however, it is important to know that the spin functions are chosen to be orthonormal. Thus

$$\langle\alpha(\omega_i)|\alpha(\omega_i)\rangle = \langle\beta(\omega_i)|\beta(\omega_i)\rangle = 1 \qquad \langle\alpha(\omega_i)|\beta(\omega_i)\rangle = \langle\beta(\omega_i)|\alpha(\omega_i)\rangle = 0 \tag{1.16}$$

There are a number of deficiencies in the Hartree method that led to the development of Hartree-Fock theory. The first problem is that electrons are assigned to specific orbitals. This disobeys the laws of quantum mechanics that state that electrons should be indistinguishable. A second, related problem is that the wave function is not antisymmetric. The antisymmetry principle states that the wave function for any fermion (particle with a half-integer spin) must be antisymmetric with respect to the interchange of two electrons; in other words, the sign of the wave function must change upon the permutation of an electron pair.[1,5] Therefore the following must be true:

$$\Psi(\boldsymbol{x_1}, \boldsymbol{x_2}, ..., \boldsymbol{x_i}, ... \boldsymbol{x_j}, ..., \boldsymbol{x_N}) = -\Psi(\boldsymbol{x_1}, \boldsymbol{x_2}, ..., \boldsymbol{x_j}, ..., \boldsymbol{x_i}, ..., \boldsymbol{x_N}) \tag{1.17}$$

This is clearly not true for a Hartree product wave function. Consider the two-electron case as an example. The antisymmetry principle would require that

$$\chi_1(\boldsymbol{x_1})\chi_2(\boldsymbol{x_2}) = -\chi_1(\boldsymbol{x_2})\chi_2(\boldsymbol{x_1}) \tag{1.18}$$

but this is not true for all choices of χ_1 and χ_2. The final problem results from the idea that the positions of the electrons are not correlated in any manner. The position of one electron is completely independent of the positions of any of the other electrons.

1.5 The Hartree-Fock (HF) Method

Building on the foundation laid out by Hartree, in 1930 Vladimir Fock modified the theory to address the previously described problems.[9] All of these problems are resolved, at least

to some extent, by expressing the wave function as a combination of all signed permutations of the Hartree products as shown below for a two-electron system.

$$\Psi^{HF} = \frac{1}{\sqrt{2!}}[\chi_1(\boldsymbol{x_1})\chi_2(\boldsymbol{x_2}) - \chi_1(\boldsymbol{x_2})\chi_2(\boldsymbol{x_1})] \tag{1.19}$$

where $1/\sqrt{2!}$ is a normalization constant. At first glance, it may appear that the electrons are once again designated to specific orbitals; however, with the inclusion of each of the permutations (in this case, just the second term), one can note that each electron is associated with every orbital. For systems containing a large number of electrons, writing out all of the signed permutations is an undesirable task. However, there is a simple method for obtaining each of these terms. This approach involves the construction of a Slater determinant.[10,11]

A Slater determinant consists of columns corresponding to molecular orbitals and rows corresponding to electrons. For the two-electron system, it is given by

$$\Psi^{HF} = \frac{1}{\sqrt{2!}}\begin{vmatrix} \chi_1(\boldsymbol{x_1}) & \chi_2(\boldsymbol{x_1}) \\ \chi_1(\boldsymbol{x_2}) & \chi_2(\boldsymbol{x_2}) \end{vmatrix} = \frac{1}{\sqrt{2!}}[\chi_1(\boldsymbol{x_1})\chi_2(\boldsymbol{x_2}) - \chi_1(\boldsymbol{x_2})\chi_2(\boldsymbol{x_1})] \tag{1.20}$$

Using a Slater determinant to write the Hartree-Fock (HF) wave function is very useful due to some of the properties of determinants.[1] First, if two columns (or rows) in a matrix are identical, the determinant is equal to zero. For a chemical system, this is analagous to having two electrons of the same spin in the same orbital which is prohibited by the Pauli exclusion principle.[1] Secondly, upon the interchange of two columns (or rows) in a matrix, the determinant is multiplied by a factor of -1, which ensures the antisymmetric behaviour of the HF wave function.

Thus far, a Slater determinant has only been shown for a two-electron system, but systems containing any number of electrons, N, can be represented in the same fashion.

For the general N-electron case, the HF wave function is given by

$$\Psi^{HF} = \frac{1}{\sqrt{N!}} \begin{vmatrix} \chi_1(\boldsymbol{x_1}) & \chi_2(\boldsymbol{x_1}) & \cdots & \chi_N(\boldsymbol{x_1}) \\ \chi_1(\boldsymbol{x_2}) & \chi_2(\boldsymbol{x_2}) & \cdots & \chi_N(\boldsymbol{x_2}) \\ \vdots & \vdots & \ddots & \vdots \\ \chi_1(\boldsymbol{x_N}) & \chi_2(\boldsymbol{x_N}) & \cdots & \chi_N(\boldsymbol{x_N}) \end{vmatrix} \tag{1.21}$$

For large systems, it is inefficient to write out the entire Slater determinant, and thus it is often expressed in a more concise form given by

$$|\Psi^{HF}\rangle = |\chi_1\chi_2\cdots\chi_i\chi_j\cdots\chi_N\rangle \tag{1.22}$$

The HF energy, E^{HF}, is given by the expectation value of the Hamiltonian operator with the HF wave function. From the definition of the electronic Hamiltonian in (1.10), it can be noted that the first and third terms are one-electron operators, while the second term representing the electronic repulsions is a two-electron operator. Therefore, $\hat{H}$ can be simplified by grouping the one-electron operators into a single operator, $\hat{h}_i$, and the electron repulsion operator can be simply expressed as $\hat{v}_{ij}$.[1,5] These new operators are thus defined as

$$\hat{h}_i = -\frac{1}{2}\nabla_i^2 + \sum_{A=1}^{M} \frac{Z_A}{r_{iA}} \qquad \hat{v}_{ij} = \frac{1}{r_{ij}} \tag{1.23}$$

which simplifies the Hamiltonian operator to

$$\hat{H} = \sum_{i=1}^{N} \hat{h}_i + \sum_{i=1}^{N-1} \sum_{j>i}^{N} \hat{v}_{ij} \tag{1.24}$$

For the purposes of this thesis, it is essential for the reader to have a good understanding of the theory involved in the HF method in order to truly understand its deficiencies. For this reason, we will show here how to derive the Hartree-Fock equations for a two-electron system. The equations will then be generalized for a system with N-electrons. We will not,

however, show the full derivation for the general N-electron case as it is beyond the scope of this document.

We first focus on the one-electron operator. The expectation value resulting from this operator is given by

$$\langle \Psi^{HF} | \sum_{i=1}^{N} \hat{h}_i | \Psi^{HF} \rangle = \int \Psi^{*HF}\, \hat{h}_1\, \Psi^{HF}\, \mathrm{d}\boldsymbol{x_1}\mathrm{d}\boldsymbol{x_2} + \int \Psi^{*HF}\, \hat{h}_2\, \Psi^{HF}\, \mathrm{d}\boldsymbol{x_1}\mathrm{d}\boldsymbol{x_2} \tag{1.25}$$

where Ψ^{HF} is the HF wave function given by the Slater determinant consisting of two spin orbitals shown by

$$\Psi^{HF} = |\chi_1\chi_2\rangle = \frac{1}{\sqrt{2!}}[\chi_1(\boldsymbol{x_1})\chi_2(\boldsymbol{x_2}) - \chi_1(\boldsymbol{x_2})\chi_2(\boldsymbol{x_1})] \tag{1.26}$$

We will begin with the derivation with respect to the first integral in (1.25). Substituting the definition of the wave function from (1.26) into the expectation value of the one-electron operator for electron one in (1.25), we obtain

$$\frac{1}{2}\int [\chi_1^*(\boldsymbol{x_1})\chi_2^*(\boldsymbol{x_2}) - \chi_1^*(\boldsymbol{x_2})\chi_2^*(\boldsymbol{x_1})]\hat{h}_1[\chi_1(\boldsymbol{x_1})\chi_2(\boldsymbol{x_2}) - \chi_1(\boldsymbol{x_2})\chi_2(\boldsymbol{x_1})]\, \mathrm{d}\boldsymbol{x_1}\mathrm{d}\boldsymbol{x_2} \tag{1.27}$$

Expanding this expression yields the following four terms

$$\begin{aligned}\frac{1}{2}\int [&\chi_1^*(\boldsymbol{x_1})\chi_2^*(\boldsymbol{x_2})\hat{h}_1\chi_1(\boldsymbol{x_1})\chi_2(\boldsymbol{x_2}) - \chi_1^*(\boldsymbol{x_2})\chi_2^*(\boldsymbol{x_1})\hat{h}_1\chi_1(\boldsymbol{x_1})\chi_2(\boldsymbol{x_2}) \\ &- \chi_1^*(\boldsymbol{x_1})\chi_2^*(\boldsymbol{x_2})\hat{h}_1\chi_1(\boldsymbol{x_2})\chi_2(\boldsymbol{x_1}) + \chi_1^*(\boldsymbol{x_2})\chi_2^*(\boldsymbol{x_1})\hat{h}_1\chi_1(\boldsymbol{x_2})\chi_2(\boldsymbol{x_1})]\, \mathrm{d}\boldsymbol{x_1}\mathrm{d}\boldsymbol{x_2}\end{aligned} \tag{1.28}$$

Since $\hat{h}_1$ only operates on electron 1, all functions of electron 2 can be integrated out. Due to the orthonormality of the spin functions (α and β), the two negative terms integrate to zero while the two positive terms integrate to unity yielding

$$\frac{1}{2}\int [\chi_1^*(\boldsymbol{x_1})\hat{h}_1\chi_1(\boldsymbol{x_1}) + \chi_2^*(\boldsymbol{x_1})\hat{h}_1\chi_2(\boldsymbol{x_1})]\, \mathrm{d}\boldsymbol{x_1} \tag{1.29}$$

One can perform an analogous derivation for the expectation value of $\hat{h}_2$ (second integral in (1.25)) and find that, due to the indistinguishable nature of electrons, it is equivalent to that shown for $\hat{h}_1$ (i.e. $\langle \Psi^{HF} | \hat{h}_2 | \Psi^{HF} \rangle = \langle \Psi^{HF} | \hat{h}_1 | \Psi^{HF} \rangle$). Thus for the sum of all of the one-electron operators for this two-electron system, the expectation value is

$$\langle \Psi^{HF} | \sum_{i=1}^{2} \hat{h}_i | \Psi^{HF} \rangle = \langle \Psi^{HF} | \hat{h}_1 + \hat{h}_2 | \Psi^{HF} \rangle = \int [\chi_1(\boldsymbol{x_1}) \hat{h} \chi_1(\boldsymbol{x_1}) + \chi_2(\boldsymbol{x_1}) \hat{h} \chi_2(\boldsymbol{x_1})] \, \mathrm{d}\boldsymbol{x_1} \tag{1.30}$$

Instead of writing out the integrals in every equation, there is a common shorthand notation to describe these one-electron integrals.[5] This notation, given by

$$\langle \chi_i | \hat{h} | \chi_j \rangle = \langle i | \hat{h} | j \rangle = \int \chi_i^*(\boldsymbol{x_1}) \, \hat{h} \, \chi_j(\boldsymbol{x_1}) \mathrm{d}\boldsymbol{x_1} \tag{1.31}$$

simplifies (1.30) to

$$\langle \Psi^{HF} | \hat{h}_1 + \hat{h}_2 | \Psi^{HF} \rangle = \langle 1 | \hat{h} | 1 \rangle + \langle 2 | \hat{h} | 2 \rangle \tag{1.32}$$

For the general N-electron case, one can show that[5]

$$\langle \Psi^{HF} | \sum_{i=1}^{N} \hat{h}_i | \Psi^{HF} \rangle = \sum_{i=1}^{N} \langle i | \hat{h} | i \rangle \tag{1.33}$$

Thus far, the derivation has only involved spin orbitals. To modify these equations for the use of spatial orbitals, we must integrate over the spin components of the orbitals. Since a spin orbital is simply the product of a spatial orbital, $\psi(\boldsymbol{r})$, and a spin function ($\alpha(\omega_i)$ or $\beta(\omega_i)$), as given by (1.15), we can use this definition to adapt (1.30) for spatial orbitals as follows:

$$\langle i | \hat{h} | i \rangle = \int \psi_1^*(\boldsymbol{r_1}) \alpha^*(\omega_1) \hat{h} \psi_1(\boldsymbol{r_1}) \alpha(\omega_1) \, \mathrm{d}\boldsymbol{r_1} \mathrm{d}\omega_1 = \int \psi_1^*(\boldsymbol{r_1}) \hat{h} \psi_1(\boldsymbol{r_1}) \, \mathrm{d}\boldsymbol{r_1} = (i | \hat{h} | i) \tag{1.34}$$

Here we have used the orthonormality condition of the spin orbitals in the integration over the spin components. One could have just as easily used an orbital with a β spin component

in the previous expression and obtained the same result. The reader may have noticed the use of round brackets in the final expression on the right-hand side. These round brackets have an equivalent definition as $\langle i|\hat{h}|i\rangle$ except the round brackets indicate that spatial orbitals are involved instead of spin orbitals and thus the expectation value now involves the sum over the $N/2$ spatial orbitals (i.e. $\sum_{i=1}^{N}\langle i|\hat{h}|i\rangle = \sum_{i=1}^{N/2}(i|\hat{h}|i)$).[5]

We now turn our attention to the two-electron operator, $\hat{v}_{ij}$, given by r_{ij}^{-1}. For the two-electron system, the expectation value of said operator is

$$\langle \Psi^{HF}|\hat{v}_{ij}|\Psi^{HF}\rangle = \frac{1}{2}\int [\chi_1^*(\boldsymbol{x_1})\chi_2^*(\boldsymbol{x_2}) - \chi_1^*(\boldsymbol{x_2})\chi_2^*(\boldsymbol{x_1})] \times \frac{1}{r_{12}}[\chi_1(\boldsymbol{x_1})\chi_2(\boldsymbol{x_2}) - \chi_1(\boldsymbol{x_2})\chi_2(\boldsymbol{x_1})]\mathrm{d}\boldsymbol{x_1}\mathrm{d}\boldsymbol{x_2} \quad (1.35)$$

As in the case of the one-electron operator, we multiply to expand the integrand yielding four terms given by

$$\frac{1}{2}\int \left[\chi_1^*(\boldsymbol{x_1})\chi_2^*(\boldsymbol{x_2})\frac{1}{r_{12}}\chi_1(\boldsymbol{x_1})\chi_2(\boldsymbol{x_2}) - \chi_1^*(\boldsymbol{x_2})\chi_2^*(\boldsymbol{x_1})\frac{1}{r_{12}}\chi_1(\boldsymbol{x_1})\chi_2(\boldsymbol{x_2}) - \chi_1^*(\boldsymbol{x_1})\chi_2^*(\boldsymbol{x_2})\frac{1}{r_{12}}\chi_1(\boldsymbol{x_2})\chi_2(\boldsymbol{x_1}) + \chi_1^*(\boldsymbol{x_2})\chi_2^*(\boldsymbol{x_1})\frac{1}{r_{12}}\chi_1(\boldsymbol{x_2})\chi_2(\boldsymbol{x_1})\right] \mathrm{d}\boldsymbol{x_1}\mathrm{d}\boldsymbol{x_2} \quad (1.36)$$

Since $r_{12} = r_{21}$, we can interchange $\boldsymbol{x_1}$ and $\boldsymbol{x_2}$ in terms 3 and 4 of the integrand giving

$$\frac{1}{2}\int \left[\chi_1^*(\boldsymbol{x_1})\chi_2^*(\boldsymbol{x_2})\frac{1}{r_{12}}\chi_1(\boldsymbol{x_1})\chi_2(\boldsymbol{x_2}) - \chi_1^*(\boldsymbol{x_2})\chi_2^*(\boldsymbol{x_1})\frac{1}{r_{12}}\chi_1(\boldsymbol{x_1})\chi_2(\boldsymbol{x_2}) - \chi_1^*(\boldsymbol{x_2})\chi_2^*(\boldsymbol{x_1})\frac{1}{r_{12}}\chi_1(\boldsymbol{x_1})\chi_2(\boldsymbol{x_2}) + \chi_1^*(\boldsymbol{x_1})\chi_2^*(\boldsymbol{x_2})\frac{1}{r_{12}}\chi_1(\boldsymbol{x_1})\chi_2(\boldsymbol{x_2})\right] \mathrm{d}\boldsymbol{x_1}\mathrm{d}\boldsymbol{x_2} \quad (1.37)$$

Using this alternative form, it is easy to note that term 1 is equal to term 4 while terms 2 and 3 are also equivalent. This simplifies the expression to

$$\int \left[\chi_1^*(\boldsymbol{x_1})\chi_2^*(\boldsymbol{x_2})\frac{1}{r_{12}}\chi_1(\boldsymbol{x_1})\chi_2(\boldsymbol{x_2}) - \chi_1^*(\boldsymbol{x_2})\chi_2^*(\boldsymbol{x_1})\frac{1}{r_{12}}\chi_1(\boldsymbol{x_1})\chi_2(\boldsymbol{x_2})\right] \mathrm{d}\boldsymbol{x_1}\mathrm{d}\boldsymbol{x_2} \quad (1.38)$$

The form in which (1.38) is expressed is known as the physicists' notation.[5] Chemists tend to rearrange this equation to simplify the integration over the spin components. This is achieved by placing orbitals containing electron 1 on the left side of the operator, and those pertaining to electron 2 on the right side. Thus, the equivalent chemists' notation is

$$\int \left[\chi_1^*(\boldsymbol{x_1})\chi_1(\boldsymbol{x_1})\frac{1}{r_{12}}\chi_2^*(\boldsymbol{x_2})\chi_2(\boldsymbol{x_2}) - \chi_1(\boldsymbol{x_1})\chi_2^*(\boldsymbol{x_1})\frac{1}{r_{12}}\chi_1^*(\boldsymbol{x_2})\chi_2(\boldsymbol{x_2})\right] \mathrm{d}\boldsymbol{x_1}\mathrm{d}\boldsymbol{x_2} \quad (1.39)$$

Much like the expectation value of the one-electron operator, there is also a short hand notation for that of the two-electron operator. For the physicists' notation, angled brackets are used as follows:

$$\langle \Psi^{HF}|\hat{v}_{12}|\Psi^{HF}\rangle = \langle 12|12\rangle - \langle 12|21\rangle \quad (1.40)$$

while the chemists' notation employs square brackets as shown below.

$$\langle \Psi^{HF}|\hat{v}_{12}|\Psi^{HF}\rangle = [11|22] - [12|21] \quad (1.41)$$

For a general N-electron system, it can be shown that the expectation value with respect to spin orbitals is given by

$$\langle \Psi^{HF}|\sum_{i=1}^{N-1}\sum_{j>i}^{N}\hat{v}_{ij}|\Psi^{HF}\rangle = \sum_{i=1}^{N-1}\sum_{j>i}^{N}\Big(\langle ij|ij\rangle - \langle ij|ji\rangle\Big) = \sum_{i=1}^{N-1}\sum_{j>i}^{N}\Big([ii|jj] - [ij|ji]\Big) \quad (1.42)$$

For spin orbitals, we can now derive a full expression for the expectation value of the full electronic Hamiltonian by combining (1.33) and (1.42) to give

$$\begin{aligned} E^{HF} = \langle \Psi^{HF}|\hat{H}^{elec}|\Psi^{HF}\rangle &= \sum_{i=1}^{N}\langle i|\hat{h}|i\rangle + \sum_{i=1}^{N-1}\sum_{j>i}^{N}\Big(\langle ij|ij\rangle - \langle ij|ji\rangle\Big) \\ &= \sum_{i=1}^{N}\langle i|\hat{h}|i\rangle + \sum_{i=1}^{N-1}\sum_{j>i}^{N}\Big([ii|jj] - [ij|ji]\Big) \end{aligned} \quad (1.43)$$

To determine the final form of the expectation value of the electronic Hamiltonian with

respect to spatial orbitals, the two-electron integral terms in (1.42) must be defined more carefully. Due to the orthogonality of the spin functions, this expression can be given by

$$\langle \Psi^{HF} | \hat{v}_{12} | \Psi^{HF} \rangle = \sum_{i=1}^{N-1} \sum_{j>i}^{N} \Big([ii|jj] - \delta_{m_{si},m_{sj}} [ij|ji] \Big) \tag{1.44}$$

where m_s is the spin quantum number (m_s=$\pm\frac{1}{2}$) and $\delta_{i,j}$ is the Kronecker delta, which equals 1 if $i = j$ and 0 when $i \neq j$. When converting to spatial orbitals, $\chi_i = \psi_i^\alpha$ or ψ_i^β, and thus there are four unique possibilities for the combination of spins when $i \neq j$:

$$(ii|jj): \qquad [\psi_i^\alpha \psi_i^\alpha | \psi_j^\alpha \psi_j^\alpha] \quad [\psi_i^\alpha \psi_i^\alpha | \psi_j^\beta \psi_j^\beta] \quad [\psi_i^\beta \psi_i^\beta | \psi_j^\alpha \psi_j^\alpha] \quad [\psi_i^\beta \psi_i^\beta | \psi_j^\beta \psi_j^\beta] \tag{1.45}$$

$$(ij|ji): \qquad [\psi_i^\alpha \psi_j^\alpha | \psi_j^\alpha \psi_i^\alpha] \quad [\psi_i^\alpha \psi_j^\beta | \psi_j^\beta \psi_i^\alpha] \quad [\psi_i^\beta \psi_j^\alpha | \psi_j^\alpha \psi_i^\beta] \quad [\psi_i^\beta \psi_j^\beta | \psi_j^\beta \psi_i^\beta] \tag{1.46}$$

In (1.45), all of these integrals would give non-zero values as the spin functions would integrate to unity. However, in (1.46) only the first and fourth expressions would yield non-zero values. One can see that when $i \neq j$ there are four possible $(ii|jj)$ integrals but only two possible $(ij|ji)$ integrals for each set of i and j. However, one must also consider the case where $i = j$. Before we consider this case, it is helpful to more clearly describe these two different types of two-electron integrals.

The two-electron integrals, $(ii|jj)$ and $(ij|ji)$, are known as the Coulomb and exchange integrals, respectively. this expression indicates that there are two separate terms for the two electron integrals. Using the chemists' notation, these integrals over spatial orbitals are

$$(ii|jj) = \int \psi_i^*(\boldsymbol{r_1}) \psi_i(\boldsymbol{r_1}) \frac{1}{r_{12}} \psi_j^*(\boldsymbol{r_2}) \psi_j(\boldsymbol{r_2}) \mathrm{d}\boldsymbol{r_1} \mathrm{d}\boldsymbol{r_2} = J_{ij} \tag{1.47}$$

$$(ij|ji) = \int \psi_i^*(\boldsymbol{r_1}) \psi_j(\boldsymbol{r_1}) \frac{1}{r_{12}} \psi_j^*(\boldsymbol{r_2}) \psi_i(\boldsymbol{r_2}) \mathrm{d}\boldsymbol{r_1} \mathrm{d}\boldsymbol{r_2} = K_{ij} \tag{1.48}$$

where J_{ij} and K_{ij} are the notations for the Coulomb and exchange integrals.[1,5] One gains a better understanding of the physical meaning of the Coulomb integrals by rewriting (1.47)

in the following way:

$$J_{ij} = \int |\psi_i(\boldsymbol{r_1})|^2 \frac{1}{r_{12}} |\psi_j(\boldsymbol{r_2})|^2 \mathrm{d}\boldsymbol{r_1}\mathrm{d}\boldsymbol{r_2} \tag{1.49}$$

The squared modulus of an orbital (or wavefunction), $|\psi_i(\boldsymbol{r_1})|^2$, defines the probability density of said orbital; hence, these Coulomb integrals describe the interaction between the electron density of one orbital with that of another orbital. Therefore, these Coulomb integrals are used to approximate electron repulsions in HF theory. However, this is the cause of the major source of error in the HF method. An individual electron in the HF model does not feel the repulsion from each individual electron, but instead experiences average field of smeared out electron charge from all of the remaining electrons in the system.[5] This method of estimating repulsion energies is known as the mean field approximation. Calculating electron repulsions using mean field theory leads to the omission of Coulombic electron correlation (or simply electron correlation). The concept of electron correlation will be discussed in more detail later in this chapter.

As for the exchange integrals, there is no true physical interpretation of these terms. They are effectively a result of having an antisymmetric wave function and only occur between electrons of the same spin. Nonetheless, they are essential for an accurate description of a quantum mechanical system and are calculated according to (1.48).

Returning to the evaluation of the two-electron integrals when $i = j$, exchange is not possible because two electrons of the same spin cannot occupy the same spin orbital and exchange only occurs between same spin electrons. Electron repulsion however, is possible between electrons with different spins within the same orbital. Thus equation (1.44) can be modified for the use of spatial orbitals as follows

$$\sum_{i=1}^{N-1}\sum_{j>i}^{N}\Big([ii|jj]-\delta_{m_{si},m_{sj}}[ij|ji]\Big)=\sum_{i=1}^{N/2}\sum_{j>i}^{N/2}\Big(4(ii|jj)-2(ij|ji)\Big)+\sum_{i=1}^{N/2}(ii|ii)$$
$$=\sum_{i=1}^{N/2}\sum_{j>i}^{N/2}\Big(4J_{ij}-2K_{ij}\Big)+\sum_{i=1}^{N/2}J_{ii} \tag{1.50}$$

In order to simplify this equation, one can remove the restriction that $j > i$ from the double summation and avoid double counting all interactions by dividing by 2. In this process, we effectively include the interaction between electrons in the same orbital twice, $2J_{ii}$, but we also include the interaction K_{ii}. In theory, K_{ii} is equal to zero, but without the spin component, it has the same value as J_{ii} as one can note by setting $j = i$ in expressions (1.47) and (1.48). Including K_{ii} compensates for double counting the repulsion between the two electrons in the same orbital. We can thus reduce the expectation value of the two-electron operator to

$$\langle\Psi^{HF}|\hat{v}_{12}|\Psi^{HF}\rangle=\sum_{i=1}^{N/2}\sum_{j=1}^{N/2}\Big(2J_{ij}-K_{ij}\Big) \tag{1.51}$$

We now have complete expressions for the expectation values of the one- and two-electron operators in terms of spatial orbitals. Referring back to equations (1.33) and (1.34) we can write the expectation value of the electronic Hamiltonian operator under the HF model as

$$E_{elec}=\langle\Psi^{HF}|\hat{H}|\Psi^{HF}\rangle=2\sum_{i=1}^{N/2}(i|\hat{h}|i)+\sum_{i=1}^{N/2}\sum_{j=1}^{N/2}\Big(2(ii|jj)-(ij|ji)\Big)$$
$$=2\sum_{i=1}^{N/2}H_{ii}+\sum_{i=1}^{N/2}\sum_{j=1}^{N/2}\Big(2J_{ij}-K_{ij}\Big) \tag{1.52}$$

Here, we have used H_{ii} as a short hand notation for the expectation value of the one-electron operators.[5] In this expression, we have a complete equation to calculate the electronic energy of a system with respect to its spatial orbitals while the total energy is given by (1.12).

However, we have yet to describe how to determine these orbital functions.

1.5.1 The Hartree-Fock Equations

As the variational theorem states, the expectation value of any normalized trial wave function will always be greater than or equal to that of the true ground state wave function.[5] Therefore, our goal is to obtain the best guess and thus the most accurate energy possible. Under the HF approximation, this best guess is obtained by minimizing the energy expression with respect to the spatial orbitals all the while ensuring that the determined orbital functions are orthonormal. This minimization problem where a set of constraints can be involved is solved using the Lagrange method of undetermined multipliers.[5] The Lagrange function, $\mathscr{L}$, is defined as the difference between a function and any constraints on said function scaled by a Lagrange multiplier, λ. For the HF method, this is given by

$$\mathscr{L} = E - \sum_{i=1}^{N}\sum_{j=1}^{N} \lambda_{ij}(\langle \chi_i | \chi_j \rangle - \delta_{ij}) \tag{1.53}$$

Since the second term in this equation (the constraint) is equal to zero, the Lagrange function has the same minima as the energy expression. Therefore the goal is to minimize the Lagrange function with respect to the orbitals which in turn would minimize the energy of the system. When minimizing a function, one often thinks first of derivatives. In theory, this is very similar to what is done to solve for the molecular orbitals. However, the energy expression is not a function, but a functional. Unlike a *function* which inputs a *variable* and returns a value, a *functional* inputs a *function* to return a value. In this case, the energy expression is a functional of the molecular orbitals, which we denote as $E[\chi(\boldsymbol{x})]$ or $E[\psi(\boldsymbol{r})]$. When minimizing a functional, one takes a variation instead of a derivative; however, many of the rules such as the product rule and chain rules are similar for both methods. To locate a minimum, the roots of the first variation, δ (not to be confused with the Kronecker delta,

δ_{ij}) of the Lagrange function must be determined. Mathematically this is

$$\delta\mathscr{L} = \delta E - \sum_{i=1}^{N}\sum_{j=1}^{N}\lambda_{ij}(\langle\delta\chi_i|\chi_j\rangle + \langle\chi_i|\delta\chi_j\rangle) = 0 \tag{1.54}$$

where the δ_{ij} term vanishes as the variation of a constant is zero.

The first variation of the energy, δE, can be obtained by performing said operation on equation (1.43). This yields

$$\delta E = \sum_{i=1}^{N}\langle\delta\chi_i|\hat{h}|\chi_i\rangle + \langle\chi_i|\hat{h}|\delta\chi_i\rangle + \frac{1}{2}\sum_{i=1}^{N}\sum_{j=1}^{N}\Big([\delta\chi_i\chi_i|\chi_j\chi_j] + [\chi_i\delta\chi_i|\chi_j\chi_j] + [\chi_i\chi_i|\delta\chi_j\chi_j]$$
$$+ [\chi_i\chi_i|\chi_j\delta\chi_j] - [\delta\chi_i\chi_j|\chi_j\chi_i] - [\chi_i\delta\chi_j|\chi_j\chi_i] - [\chi_i\chi_j|\delta\chi_j\chi_i] - [\chi_i\chi_j|\chi_j\delta\chi_i]\Big) \tag{1.55}$$

where the factor of 1/2 is used to remove the restriction ($j > i$) from the double summation. To simplify this expression we can define the Coulomb, $\hat{J}$, and exchange operators, $\hat{K}$, as follows:

$$\hat{J}_j(\boldsymbol{x_1})|\chi_i(\boldsymbol{x_1})\rangle = \langle\chi_j(\boldsymbol{x_2})|r_{12}^{-1}|\chi_j(\boldsymbol{x_2})\rangle|\chi_i(\boldsymbol{x_1})\rangle \tag{1.56}$$

$$\hat{K}_j(\boldsymbol{x_1})|\chi_i(\boldsymbol{x_1})\rangle = \langle\chi_j(\boldsymbol{x_2})|r_{12}^{-1}|\chi_i(\boldsymbol{x_2})\rangle|\chi_j(\boldsymbol{x_1})\rangle \tag{1.57}$$

The operators are shown acting on a molecular orbital, χ_i, as it is impossible to show the exchange operator alone since it involves the interchange of the orbital it is acting on with one contained in the operator itself. Using these definitions and the fact that $[\delta\chi_i\chi_i|\chi_j\chi_j] = [\chi_i\delta\chi_i|\chi_j\chi_j]$ we can express (1.55) as

$$\delta E = \sum_{i=1}^{N}\langle\delta\chi_i|\hat{h}|\chi_i\rangle + \langle\chi_i|\hat{h}|\delta\chi_i\rangle) + \sum_{i,j}^{N}\langle\delta\chi_i|\hat{J}_j|\chi_i\rangle - \langle\delta\chi_i|\hat{K}_j|\chi_i\rangle + \langle\chi_i|\hat{J}_j|\delta\chi_i\rangle - \langle\chi_i|\hat{K}_j|\delta\chi_i\rangle \tag{1.58}$$

This simplifies to

$$\delta E = \sum_{i=1}^{N}\Big(\langle\delta\chi_i|\hat{f}_i|\chi_i\rangle + \langle\chi_i|\hat{f}_i|\delta\chi_i\rangle\Big) \tag{1.59}$$

where the Fock operator, $\hat{f}$, has been introduced.[5] This form of this operator is given by $\hat{f}_i = \hat{h}_i + \sum_{j=1}^{N} \hat{J}_j - \hat{K}_j$. By substituting (1.59) into (1.54), one then obtains

$$\delta\mathscr{L} = \sum_{i=1}^{N} \left(\langle \delta\chi_i | \hat{f}_i | \chi_i \rangle + \langle \chi_i | \hat{f}_i | \delta\chi_i \rangle \right) - \sum_{i=1}^{N} \sum_{j=1}^{N} \left(\lambda_{ij} \langle \delta\chi_i | \chi_j \rangle + \langle \chi_i | \delta\chi_j \rangle) \right) = 0 \quad (1.60)$$

Based on the properties of complex numbers, it is known that $\langle \chi_i | \hat{f}_i | \delta\chi_i \rangle = \langle \delta\chi_i | \hat{f}_i | \chi_i \rangle^*$ and $\langle \chi_i | \delta\chi_j \rangle = \langle \delta\chi_j | \chi_i \rangle^*$, and thus the variation of the Lagrange function can be written

$$\begin{aligned} \delta\mathscr{L} &= \sum_{i=1}^{N} \langle \delta\chi_i | \hat{f}_i | \chi_i \rangle - \sum_{i=1}^{N} \sum_{j=1}^{N} \lambda_{ij} (\langle \delta\chi_i | \chi_j \rangle + \text{ complex conjugate} = 0 \\ &= \sum_{i=1}^{N} \langle \delta\chi_i | \left(\hat{f}_i | \chi_i \rangle - \sum_{j=1}^{N} \lambda_{ij} | \chi_j \rangle \right) + \text{ complex conjugate} = 0 \end{aligned} \quad (1.61)$$

As this must be true for all χ_i and thus all $\delta\chi_i$, the terms enclosed in round brackets must equal zero, which leads to the following relationship

$$\hat{f}_i | \chi_i \rangle = \sum_{j=1}^{N} \lambda_{ij} | \chi_i \rangle \quad (1.62)$$

There are various sets of λ_{ij} which minimize the energy of different state functions; however, it can be shown that one such set of the Lagrange multipliers are given by $\lambda_{ij} = \varepsilon_i \delta_{ij}$. This reduces the HF equations to[5]

$$\hat{f}_i | \chi_i \rangle = \varepsilon_i | \chi_i \rangle \quad (1.63)$$

where ε_i is the energy of the i^{th} molecular orbital.

To convert the HF equations for use with spatial orbitals, we use the definition of a spin orbital ($\chi_i(\boldsymbol{x_1}) = \psi_j(\boldsymbol{r_1})\alpha(\omega_1)$ or $\psi_j(\boldsymbol{r_1})\beta(\omega_1)$), to write the HF equations as

$$\hat{f}_i(\boldsymbol{x_1})\psi_i(\boldsymbol{r_1})\alpha(\omega_1) = \varepsilon_i \psi_i(\boldsymbol{r_1})\alpha(\omega_1) \quad (1.64)$$

Multiplying both sides of (1.64) on the left by $\alpha^*(\omega_1)$ and integrating over the spin component yields

$$\left[\int \alpha^*(\omega_1)\hat{f}(\boldsymbol{x_1})\alpha(\omega_1)\mathrm{d}\omega_1\right]\psi_i(\boldsymbol{r_1}) = \varepsilon_i\psi_i(\boldsymbol{r_1}) \tag{1.65}$$

An alternative to the previous definition of the Fock operator is the following:

$$\hat{f}(\boldsymbol{x_1}) = \hat{h}(\boldsymbol{r_1}) + \sum_{j=1}^{N}\int \chi_j^*(\boldsymbol{x_2})\frac{1}{r_{12}}(1-\mathscr{P}_{12})\chi_j(\boldsymbol{x_2})\mathrm{d}\boldsymbol{x_2} \tag{1.66}$$

where $\mathscr{P}_{12}$ is the permutation operator which acts to interchange the positions of electrons 1 and 2. Substituting this definition into the left hand side of (1.65) gives

$$\begin{aligned}\left[\int \alpha^*(\omega_1)\hat{f}(\boldsymbol{x_1})\alpha(\omega_1)\mathrm{d}\omega_1\right]\psi_i(\boldsymbol{r_1}) &= \left[\int \alpha^*(\omega_1)\hat{h}(\boldsymbol{r_1})\alpha(\omega_1)\mathrm{d}\omega_1\right]\psi_i(\boldsymbol{r_1}) \\ &+ \left[\sum_{j=1}^{N}\int \alpha^*(\omega_1)\chi_j^*(\boldsymbol{x_2})\frac{1}{r_{12}}(1-\mathscr{P}_{12})\chi_j(\boldsymbol{x_2})\alpha(\omega_1)\mathrm{d}\boldsymbol{x_2}\mathrm{d}\omega_1\right]\psi_i(\boldsymbol{r_1})\end{aligned} \tag{1.67}$$

Using the permutation operator, $\mathscr{P}_{12}$, to expand the final integral into two separate integrals and by defining the closed-shell Fock operator as

$$\hat{f}(\boldsymbol{r_1}) = \int \alpha^*(\omega_1)\hat{f}(\boldsymbol{x_1})\alpha(\omega_1)\mathrm{d}\omega_1 \tag{1.68}$$

we can rewrite the equation as

$$\begin{aligned}\hat{f}(\boldsymbol{r_1})\psi_i(\boldsymbol{r_1}) = \hat{h}(\boldsymbol{r_1})\psi_i(\boldsymbol{r_1}) &+ \sum_{j=1}^{N}\int \alpha^*(\omega_1)\chi_j^*(\boldsymbol{x_2})\frac{1}{r_{12}}\chi_j(\boldsymbol{x_2})\alpha(\omega_1)\psi_i(\boldsymbol{r_1})\mathrm{d}\boldsymbol{x_2}\mathrm{d}\omega_1 \\ &- \sum_{j=1}^{N}\int \alpha^*(\omega_1)\chi_j^*(\boldsymbol{x_2})\frac{1}{r_{12}}\chi_j(\boldsymbol{x_1})\alpha(\omega_2)\psi_i(\boldsymbol{r_2})\mathrm{d}\boldsymbol{x_2}\mathrm{d}\omega_1\end{aligned} \tag{1.69}$$

where we have used the orthogonality of the spin functions to simplify the first term on the right-hand side. The remaining spin orbitals must now be substituted with the appropriate spatial orbitals. Therefore, both sums over all spin orbitals, $\sum_j^N$, need to be replaced with

two separate sums, one for α-spin, $\sum_{j}^{N_\alpha=N/2}$, and one for β-spin electrons, $\sum_{j}^{N_\beta=N/2}$, where each sum runs over $N/2$ terms. This substitution converts (1.73) to

$$\begin{aligned}\hat{f}(\boldsymbol{r_1})\psi_i(\boldsymbol{r_1}) &= \hat{h}(\boldsymbol{r_1})\psi_i(\boldsymbol{r_1}) \\ &+\sum_{j=1}^{N/2}\int \alpha^*(\omega_1)\left[\psi_j^*(\boldsymbol{r_2})\alpha^*(\omega_2)\right]\frac{1}{r_{12}}\left[\psi_j(\boldsymbol{r_2})\alpha(\omega_2)\right]\alpha(\omega_1)\psi_i(\boldsymbol{r_1})\mathrm{d}\omega_1\mathrm{d}\omega_2\mathrm{d}\boldsymbol{r_2} \\ &+\sum_{j=1}^{N/2}\int \alpha^*(\omega_1)\left[\psi_j^*(\boldsymbol{r_2})\beta^*(\omega_2)\right]\frac{1}{r_{12}}\left[\psi_j(\boldsymbol{r_2})\beta(\omega_2)\right]\alpha(\omega_1)\psi_i(\boldsymbol{r_1})\mathrm{d}\omega_1\mathrm{d}\omega_2\mathrm{d}\boldsymbol{r_2} \\ &-\sum_{j=1}^{N/2}\int \alpha^*(\omega_1)\left[\psi_j^*(\boldsymbol{r_2})\alpha^*(\omega_2)\right]\frac{1}{r_{12}}\left[\psi_j(\boldsymbol{r_1})\alpha(\omega_1)\right]\alpha(\omega_2)\psi_i(\boldsymbol{r_2})\mathrm{d}\omega_1\mathrm{d}\omega_2\mathrm{d}\boldsymbol{r_2} \\ &-\sum_{j=1}^{N/2}\int \alpha^*(\omega_1)\left[\psi_j^*(\boldsymbol{r_2})\beta^*(\omega_2)\right]\frac{1}{r_{12}}\left[\psi_j(\boldsymbol{r_1})\beta(\omega_1)\right]\alpha(\omega_2)\psi_i(\boldsymbol{r_2})\mathrm{d}\omega_1\mathrm{d}\omega_2\mathrm{d}\boldsymbol{r_2} \quad (1.70)\end{aligned}$$

where the terms enclosed in square brackets are those that were substituted for the spin orbitals. The subsequent integration over the spin components of the expression gives

$$\begin{aligned}\hat{f}(\boldsymbol{r_1})\psi_i(\boldsymbol{r_1}) = \hat{h}(\boldsymbol{r_1})\psi_i(\boldsymbol{r_1}) &+ \left[2\sum_{j=1}^{N/2}\int \psi_j^*(\boldsymbol{r_2})\frac{1}{r_{12}}\psi_j(\boldsymbol{r_2})\mathrm{d}\boldsymbol{r_2}\right]\psi_i(\boldsymbol{r_1}) \\ &- \left[\sum_{j=1}^{N/2}\int \psi_j^*(\boldsymbol{r_2})\frac{1}{r_{12}}\psi_i(\boldsymbol{r_2})\mathrm{d}\boldsymbol{r_2}\right]\psi_j(\boldsymbol{r_1}) \quad (1.71)\end{aligned}$$

Using the definitions for the Coulomb and exchange operators given by (1.56) and (1.57) and modified for spatial orbitals by replacing all occurrences of χ and $\boldsymbol{x_i}$ with ψ and $\boldsymbol{r_i}$, respectively, we can reduce the spatial HF equations to

$$\hat{f}(\boldsymbol{r_1})\psi_i(\boldsymbol{r_1}) = \left[\hat{h}(\boldsymbol{r_1}) + \sum_{j=1}^{N/2}\left(2\hat{J}_j(\boldsymbol{r_1}) - \hat{K}_j(\boldsymbol{r_1})\right)\right]\psi_i(\boldsymbol{r_1}) = \varepsilon_i\psi_i(\boldsymbol{r_1}) \quad (1.72)$$

and subsequently to the most common form

$$\hat{f}(\boldsymbol{r_1})\psi_i(\boldsymbol{r_1}) = \varepsilon_i\psi_i(\boldsymbol{r_1}) \quad (1.73)$$

1.5.2 The Roothaan-Hall Equations

It is possible to solve the Hartree-Fock equations using approximate numerical methods for atomic systems;[1] however, this is uncommon in recent times due to the development of highly efficient algorithms to solve these equations for any type of system. Most commonly, these equations are solved using the Roothaan-Hall equations, which were developed independently by Roothaan[12] and Hall[13] in 1951. These equations require the introduction of a basis set $\{\phi_\nu\}$. Instead of directly solving for the best possible functions to represent the molecular orbitals, we instead express the molecular orbitals, ψ_i, as a linear combination of atomic orbitals (LCAO) by

$$\psi_i = \sum_{\nu=1}^{K} c_{\nu i}\phi_\nu \tag{1.74}$$

where $c_{\nu i}$ are scaling coefficients indicating what portion of each basis function, ϕ_ν is used in the composition of a given molecular orbital and K is the number of basis functions in the basis set. These coefficients are optimized to produce the lowest possible energy for the given system as will be discussed shortly. There are a number of predefined basis sets which are commonly used in quantum chemistry. The details concerning these basis sets and how they are composed will be discussed in a subsequent section of this chapter.

Using the LCAO method to define the molecular orbitals in the spatial HF equations of (1.73) yields

$$\hat{f}|\sum_{\nu=1}^{K} c_{\nu i}\phi_\nu\rangle = \varepsilon_i|\sum_{\nu=1}^{K} c_{\nu i}\phi_\nu\rangle \tag{1.75}$$

The subsequent combination of these new equations with $\langle\phi_\mu|$ on the left gives

$$\langle\phi_\mu|\hat{f}|\sum_{\nu=1}^{K} c_{\nu i}\phi_\nu\rangle = \varepsilon_i\langle\phi_\mu|\sum_{\nu=1}^{K} c_{\nu i}\phi_\nu\rangle \tag{1.76}$$

$$\sum_{\nu=1}^{K} c_{\nu i}\int \phi_\mu^*(\boldsymbol{r_1})\hat{f}(\boldsymbol{r_1})\phi_\nu(\boldsymbol{r_1})\mathrm{d}\boldsymbol{r_1} = \varepsilon_i\sum_{\nu=1}^{K} c_{\nu i}\int \phi_\mu^*(\boldsymbol{r_1})\phi_\nu(\boldsymbol{r_1})\mathrm{d}\boldsymbol{r_1} \tag{1.77}$$

This last expression is informally the Roothaan-Hall equations; however, they are more

often presented in matrix form. To do this, we must first define a set of new matrices, the Fock matrix, $\boldsymbol{F}$, the overlap matrix, $\boldsymbol{S}$, the coefficient matrix, $\boldsymbol{C}$, and the energy matrix, $\boldsymbol{E}$.[5] The elements of the first two matrices are given by

$$F_{\mu\nu} = \int \phi_\mu^*(\boldsymbol{r_1}) \hat{f}(\boldsymbol{r_1}) \phi_\nu(\boldsymbol{r_1}) \mathrm{d}\boldsymbol{r_1} \tag{1.78}$$

$$S_{\mu\nu} = \int \phi_\mu^*(\boldsymbol{r_1}) \phi_\nu(\boldsymbol{r_1}) \mathrm{d}\boldsymbol{r_1} \tag{1.79}$$

while $\boldsymbol{C}$ is simply a $K \times K$ matrix consisting of the coefficients, $c_{\nu i}$, and $\boldsymbol{E}$ is a diagonal matrix with elements that correspond to the orbital energies, ε_i. Using these new definitions, we can express the Roothaan-Hall equations in their most common form as

$$\boldsymbol{FC} = \boldsymbol{SCE} \tag{1.80}$$

This appears to be a simple eigenvalue problem; however, from (1.78), it can be noted that the Fock matrix is dependent on its own eigenfunctions, $\{\psi_i\}$; therefore, this problem must be solved using an iterative procedure. This process is known as a self-consistent field method (SCF) as the iterations are continued until the molecular orbital coefficients or energies converge (i.e. become self-consistent).[1,5]

Due to the dependence of the Fock matrix on the molecular orbitals, solving this problem is not trivial. However, in recent years, highly efficient algorithms have been developed to rapidly perform this SCF routine. To discuss this procedure, we first introduce the electron density, $\rho(\boldsymbol{r})$, which describes the distribution of electron charge throughout a system as a function of the spatial vector, $\boldsymbol{r}$.[5] This density is given by

$$\rho(\boldsymbol{r}) = 2 \sum_{a=1}^{N/2} \psi_a^*(\boldsymbol{r}) \psi_a(\boldsymbol{r}) \tag{1.81}$$

Expanding this expression in terms of the basis introduced for the molecular orbitals yields

$$\rho(\boldsymbol{r}) = 2\sum_{a=1}^{N/2}\sum_{\mu} c_{\mu a}^{*}\phi_{\mu}^{*}(\boldsymbol{r})\sum_{\nu} c_{\nu a}\phi_{\nu}(\boldsymbol{r}) = \sum_{\mu}\sum_{\nu} P_{\mu\nu}\phi_{\mu}^{*}(\boldsymbol{r})\phi_{\nu}(\boldsymbol{r}) \tag{1.82}$$

where we have introduced an element of the density matrix, $\boldsymbol{P}$, which is given by

$$P_{\mu\nu} = 2\sum_{a=1}^{N} c_{\mu a}^{*} c_{\nu a} \tag{1.83}$$

Returning to the definition of the Fock matrix given in (1.78), a more direct expression can be written by using the definition of the Fock operator from (1.73). With the Fock operator consisting of one- and two-electron components, the Fock matrix can be split into analogous parts defined by $H_{\mu\nu}^{core}$ and $G_{\mu\nu}$, respectively. The matrix elements are given by the following expressions

$$H_{\mu\nu}^{core} = \langle\phi_{\mu}|\hat{h}|\phi_{\nu}\rangle = -\frac{1}{2}\int \phi_{\mu}^{*}(\boldsymbol{r_1})\nabla_1^2\phi_{\nu}(\boldsymbol{r_1})\mathrm{d}\boldsymbol{r_1} + \int \phi_{\mu}^{*}(\boldsymbol{r_1})\sum_{A=1}^{M}\frac{Z_A}{r_{1A}}\phi_{\nu}(\boldsymbol{r_1})\mathrm{d}\boldsymbol{r_1} \tag{1.84}$$

$$\begin{aligned} G_{\mu\nu} &= 2\langle\phi_{\mu}|\hat{J}_j|\phi_{\nu}\rangle - \langle\phi_{\mu}|\hat{K}_j|\phi_{\nu}\rangle \\ &= 2\int \phi_{\mu}^{*}(\boldsymbol{r_1})\sum_{\lambda} c_{\lambda i}^{*}\phi_{\lambda}^{*}(\boldsymbol{r_2})r_{12}^{-1}\sum_{\sigma} c_{\sigma i}\phi_{\sigma}(\boldsymbol{r_2})\phi_{\nu}(\boldsymbol{r_1})\mathrm{d}\boldsymbol{r_1}\mathrm{d}\boldsymbol{r_2} \\ &\quad - \int \phi_{\mu}^{*}(\boldsymbol{r_1})\sum_{\lambda} c_{\lambda i}^{*}\phi_{\lambda}^{*}(\boldsymbol{r_2})r_{12}^{-1}\phi_{\nu}(\boldsymbol{r_2})\sum_{\sigma} c_{\sigma i}\phi_{\sigma}(\boldsymbol{r_1})\mathrm{d}\boldsymbol{r_1}\mathrm{d}\boldsymbol{r_2} \end{aligned} \tag{1.85}$$

Using the definition of the charge density matrix element, P_{ij}, the expression for $G_{\mu\nu}$ can be simplified as follows:

$$G_{\mu\nu} = \sum_{\lambda}\sum_{\sigma} P_{\lambda\sigma}[(\mu\nu|\lambda\sigma) - \tfrac{1}{2}(\mu\sigma|\lambda\nu)] \tag{1.86}$$

where we have used the chemists' notation to write the two-electron integrals in short form over basis functions denoted by μ, ν, λ, and σ. The Fock matrix elements can then be computed from

$$F_{\mu\nu} = H_{\mu\nu} + \sum_{\lambda=1}^{K}\sum_{\sigma=1}^{K} P_{\lambda\sigma}[(\mu\nu|\lambda\sigma) - \tfrac{1}{2}(\mu\sigma|\lambda\nu)] \tag{1.87}$$

while the overlap matrix elements, $S_{\mu\nu}$, are determined from (1.79). Although in the derivation of the HF equations, we restricted the molecular orbitals to be orthonormal, there is no such requirement for the basis functions used in the LCAO procedure. Thus, the overlap matrix is not equivalent to the identity matrix, which would greatly simplify this eigenvalue problem. However, this is the approach that is employed in order to solve the problem.

The first step in the SCF method is transforming the overlap matrix, $\boldsymbol{S}$, to the identity matrix. There are a few different ways of doing this but one method, known as symmetrical orthogonalization, involves the calculation of the inverse square root of the $\boldsymbol{S}$ matrix. This matrix can be denoted as $\boldsymbol{S}^{-1/2}$, but can simply be referred to as $\boldsymbol{X}$.[5] The properties of this matrix are such that

$$\boldsymbol{X}^{\dagger}\boldsymbol{S}\boldsymbol{X} = \mathbf{1} \tag{1.88}$$

where $\boldsymbol{X}^{\dagger}$ is the conjugate transpose of $\boldsymbol{X}$ and $\mathbf{1}$ is the identity matrix. One must remember that for matrix multiplication, the order of the multiplication matters. One cannot simply rearrange the matrices in a multiplication as one can with variables. Thus to obtain such a sequence in the Roothaan-Hall equations, we first multiply by $\boldsymbol{X}^{\dagger}$ on the left to give

$$\boldsymbol{X}^{\dagger}\boldsymbol{F}\boldsymbol{C} = \boldsymbol{X}^{\dagger}\boldsymbol{S}\boldsymbol{C}\boldsymbol{E} \tag{1.89}$$

Since $\boldsymbol{X}\boldsymbol{X}^{-1} = \mathbf{1}$, we can insert this term anywhere in the expression since a matrix multiplied by the identity matrix returns the original matrix. Multiplying $\boldsymbol{F}$ and $\boldsymbol{S}$ by this term yields

$$[\boldsymbol{X}^{\dagger}\boldsymbol{F}\boldsymbol{X}](\boldsymbol{X}^{-1}\boldsymbol{C}) = \boldsymbol{X}^{\dagger}\boldsymbol{S}\boldsymbol{X}(\boldsymbol{X}^{-1}\boldsymbol{C})\boldsymbol{E} \tag{1.90}$$

$$\boldsymbol{F}'\boldsymbol{C}' = \boldsymbol{C}'\boldsymbol{E} \tag{1.91}$$

where the identity in (1.88) was used to reduce the first three matrices on the right-hand side to $\mathbf{1}$. We have also defined two new matrices, $\boldsymbol{F}'$ and $\boldsymbol{C}'$, given by the terms enclosed in square and round brackets, respectively. Obtaining the new coefficient matrix, $\boldsymbol{C}'$, and

the orbital energies, ε_i, of the energy matrix can be achieved by diagonalizing $\boldsymbol{F}'$. These coefficients and energies are given by the eigenvectors and the eigenvalues, respectively, of this diagonalized matrix. In order to obtain the true coefficients, $c_{\mu\nu}$, one must consider the definition of the $\boldsymbol{C}'$ matrix. As it is given by $\boldsymbol{C}' = \boldsymbol{X}^{-1}\boldsymbol{C}$, $\boldsymbol{C}$ can be obtained by multiplying both sides on the left by $\boldsymbol{X}$ to give

$$\boldsymbol{X}\boldsymbol{C}' = \boldsymbol{C} \tag{1.92}$$

The new set of coefficients is then used to calculate a new $\boldsymbol{F}$ matrix and the process is repeated as many times as necessary to obtain results that are converged to a satisfactory level. One can then use the final set of coefficients to construct the HF wave function from the Slater determinant. With this wave function, one can determine any quantum mechanical observable or manipulate the wave function for electronic structure studies.

1.5.3 Open-Shell Systems

The derivation of the HF method in the previous section was for the closed-shell restricted HF method (RHF).[5] This method is commonly used for systems in the ground state at equilibrium geometries that contain an even number of electrons. However, for molecules with odd numbers of electrons, or other open-shell systems (e.g. diradicals, excited states), the RHF model lacks accuracy. As you may recall, in the RHF model two electrons are confined to a single spatial orbital. However, consider the H_2 molecule with a bond length such that the two hydrogen atoms are becoming non-interacting bodies. In this case, confining the electrons in the system to the same orbital is not an ideal definition. For systems such as this, or for any open-shell system, the Unrestricted Hartree-Fock (UHF) method provides a more accurate description of the wave function.

In the UHF method, one does not restrict the α and β electrons to be in the same spatial

orbital.[5] Thus, the spin orbital, $\chi(\boldsymbol{x})$, is represented by

$$\chi(\boldsymbol{x}) = \begin{cases} \psi^{\alpha}(\boldsymbol{r})\alpha(\omega) \\ \psi^{\beta}(\boldsymbol{r})\beta(\omega) \end{cases} \tag{1.93}$$

RHF theory requires that $\psi^{\alpha} = \psi^{\beta} = \psi$, however, this restriction is not present under the UHF model. When we expand these molecular orbitals in a basis of one-electron functions, the basis functions must be the same for the ψ^{α} and ψ^{β} orbitals; however the contributions of each basis function to the MO ($c_{\nu i}$ in (1.74)) need not be the same. It should be noted, though, that for closed-shell systems at equilibrium geometries, the UHF solution will be equivalent to the RHF solution as the assumption that the pair of electrons reside in the same spatial orbital is completely valid.

In a similar fashion to the derivation of the HF equations for RHF theory, we can derive a set of HF equations for the UHF method given by[5]

$$\hat{f}^{\alpha}(\boldsymbol{r_1})\psi_i^{\alpha}(\boldsymbol{r_1}) = \varepsilon_i^{\alpha}\psi_i^{\alpha}(\boldsymbol{r_1}) \tag{1.94}$$

$$\hat{f}^{\beta}(\boldsymbol{r_1})\psi_i^{\beta}(\boldsymbol{r_1}) = \varepsilon_i^{\beta}\psi_i^{\beta}(\boldsymbol{r_1}) \tag{1.95}$$

where the Fock operator in this case is given by

$$\hat{f}^{\alpha}(\boldsymbol{r_1}) = \hat{h}(\boldsymbol{r_1}) + \sum_{a=1}^{N^{\alpha}}[\hat{J}_a^{\alpha}(\boldsymbol{r_1}) - \hat{K}_a^{\alpha}(\boldsymbol{r_1})] + \sum_{a=1}^{N^{\beta}}\hat{J}_a^{\beta}(\boldsymbol{r_1}) \tag{1.96}$$

where N^{α} and N^{β} are the numbers of α and β electrons, respectively (an analogous expression can be obtained for $\hat{f}^{\beta}$ by interchanging all occurrences of α and β). One can note that the first sum involves both Coulomb and exchange components as both are possible for electrons of the same spin, while the second sum only involves the Coulomb operator as exchange does not occur between electrons with different spins.

Much like the Roothaan-Hall equations which are used to obtain the molecular orbitals

and energies for the RHF method, one can derive similar expressions for the UHF method which are known as the Pople-Nesbet equations.[14] These are a set of two matrix equations given by

$$\boldsymbol{F}^{\alpha}\boldsymbol{C}^{\alpha} = \boldsymbol{S}^{\alpha}\boldsymbol{C}^{\alpha}\boldsymbol{E}^{\alpha} \qquad \boldsymbol{F}^{\beta}\boldsymbol{C}^{\beta} = \boldsymbol{S}^{\beta}\boldsymbol{C}^{\beta}\boldsymbol{E}^{\beta} \tag{1.97}$$

Recall that the α-Fock operator contains terms involving the β electrons and orbitals, and thus these two matrix equations are codependent. Thus, one must solve these two equations simultaneously in order to obtain the UHF molecular orbitals and energy.

In addition to the UHF method, for open-shell systems, one can also use the restricted open-shell HF method (ROHF).[15] This approach uses doubly occupied spatial orbitals where possible and then singly occupied orbitals wherever necessary. This approach is not as common as the UHF method as it is more difficult to implement as well as the fact that the UHF is also used for some closed-shell systems.

1.6 Basis Sets

It was discussed earlier that to solve the HF equations, one often expands the molecular orbitals in a linear combination of atomic orbitals. These atomic orbitals comprise the basis set for the system. In theory, one can use any type of basis function that satisfies the boundary conditions of the problem; however, some are more appropriate than others.

There are many basis sets that are predefined in the literature that are most often comprised of Gaussian type orbitals (GTO). These are of the form $\eta x^i y^j z^k e^{-\alpha r^2}$ where $i + j + k = \ell$, the angular momentum quantum number, η is a normalization constant, and α is the exponent controlling the radial distribution of the function. In some cases, Slater type orbitals (STO) of the form $\eta x^i y^j z^k e^{-\alpha r}$, are used; however, GTOs are preferable as integration over these functions is far easier. In a minimal basis set, a single basis function is used to represent every orbital for a given atom. For example, when dealing with a hydrogen or helium atom, the basis set would consist of a single basis function repre-

senting the 1s orbital, whereas for the atoms lithium through neon, one has a total of five basis functions (1s, 2s, $2p_x$, $2p_y$, and $2p_z$). The electronic configuration is ignored when considering the number of orbitals for a specific atom. Thus, although Be has an electronic configuration of $1s^2\ 2s^2$, a minimal basis set for the Be atom would still contain functions for the three 2p orbitals. The most commonly used minimal bases are those of the STO-nG set developed by Pople. These basis sets consist of a set of n contracted Gaussian functions which are used to approximate an STO. For example, a 1s orbital, ϕ^{1s}, in an STO-3G basis set is given by

$$\phi^{1s}(\boldsymbol{r}) = d_1\phi_1(\boldsymbol{r}) + d_2\phi_2(\boldsymbol{r}) + d_3\phi_3(\boldsymbol{r}) \qquad \text{where } \phi_i(\boldsymbol{r}) = \eta e^{-\alpha_i r^2} \tag{1.98}$$

where d_i is a contraction coefficient defining the contribution of each Gaussian to the full basis function, ϕ^{1s}. When contracted basis sets are used, the contraction coefficients are predefined and the contribution of ϕ^{1s} is controlled entirely by a single coefficient, c. Therefore, to represent a molecular orbital for a beryllium atom using an STO-3G basis set, one would have the following:

$$\psi_{Be} = c_1\phi^{1s} + c_2\phi^{2s} + c_3\phi^{2p_x} + c_4\phi^{2p_y} + c_5\phi^{2p_z} \tag{1.99}$$

where the coefficients c_i would be determined through an SCF procedure for each molecular orbital and each ϕ^a is given by a form analogous to (1.98).

As valence orbitals are often those that participate in the bonding of molecules, these orbitals are often represented by more than a single orbital. Such basis sets are referred to as split-valence. Bases employing two basis functions to describe each orbital are referred to as split valence double-zeta (DZ), those employing three functions per valence orbital are split valence triple zeta (TZ) basis sets, *etc.*[5] In these cases, the core orbitals are still represented by a single basis function but as in the STO-nG bases, they are often comprised of a linear combination of contracted Gaussians. However, one can have a case where the

core is also split into the same number of functions as each valence orbital. In these cases, the basis sets are simply denoted as double-zeta, triple-zeta, etc.

Two of the most common types of bases are split valence and are known as the Pople basis sets and the Dunning's correlation consistent basis sets.[5,16,17] We will denote the Pople basis sets as k-lmG (DZ) or k-lmnG (TZ) where k denotes the contraction of the core orbitals, while the indices l, m, and n, denote the contraction of each basis function for the split valence, and G simply indicates that Gaussian functions are employed. For instance, the 3-21G basis set uses a contraction of 3 Gaussians to describe each core orbital, and is a split valence DZ basis where the first basis function describing the valence is given by a contraction of two Gaussians, and the second basis function is described by a single Gaussian primitive. Similarly, the 6-311G basis is a split valence TZ basis with a set of 3, 1, and 1 Gaussians for the three basis functions describing each valence orbital and a contraction of 6 functions for the basis functions describing the core orbitals.

For different types of systems, one might prefer to add different types of Gaussians to obtain a more accurate description. For example, in anionic systems, where electron densities tend to be more dispersed, it is common to add diffuse functions to improve accuracy. These diffuse functions account for electron density in far out regions and are denoted by + symbols. Thus, the 6-311G basis set with diffuse functions on heavy atoms (all but H and He, which are the light atoms) would be denoted 6-311+G while the same basis with diffuse functions on both heavy and light atoms is given by 6-311++G.

Similarly, it is common to use functions of higher angular momenta, ℓ, than are normally associated with a particular atom. For example, one could add a set of d-orbitals to a carbon atom to more effectively describe the system. These higher angular momenta functions are referred to as polarization functions and their notation is similar to that of the diffuse functions. For polarization functions on heavy atoms, one can write 6-311G(d) which indicates the addition of a set of d-orbitals to each heavy atom, or 6-311G(d,p) refers to the addition of a set of d-orbitals to heavy atoms and a set of p-orbitals to the light atoms.

In older literature one might see these notations given by 6-311G* and 6-311G**, respectively. However, one can add any type of polarization functions such as 6-311G(3df,pd) where 3 sets of d-orbitals and 1 set of f-orbitals are added to the heavy atoms while 1 set of both p- and d-orbitals are added to hydrogen and helium atoms. Thus, the first number in brackets refers to the polarization functions added to the heavy atoms and the number after the comma (if present) refers to those added to the light atoms. It is quite common to use both diffuse and polarization functions in a basis set and this can be indicated by 6-311++G(d,p).

We previously mentioned the Dunning's correlation consistent (cc) basis sets. These bases are denoted by cc-pVXZ where pV refers to polarization of valence orbitals, and XZ refers to the level of valence splitting (i.e. DZ, TZ, etc).[16] These basis sets are often used in extrapolation schemes as they were designed to converge to the complete (infinite) basis set limit. There are also augmented versions of these bases which are denoted by aug-cc-pVXZ where the augmentation refers to the addition of diffuse functions.[17]

Any type of basis set can be used in a quantum chemical calculation; however, the quality of the basis is reflected in the accuracy of the results. Nonetheless, when performing a calculation, one can define their own basis set, modify an existing basis set, or simply use one of the many predefined basis sets that are included in the many programs that perform quantum mechanical calculations.[1,18]

1.7 Correlation and Correlated Methods

It was mentioned in a previous section that the Hartree-Fock method does not account for Coulombic electron correlation. Instead, it considers repulsions between electrons in an average way rather than accounting for interactions between individual electrons. The HF method does, however, include what is known as Fermi correlation which is neglected in the Hartree method.[1] This correlation is included as the Pauli exclusion principle prohibits two electrons with the same spin from occupying the same spatial orbital. Thus, as the HF

method satisfies the Pauli principle, there is a small region of space, known as the Fermi hole, surrounding an electron where there is zero probability of finding another electron of the same spin.

However, when most theoreticians refer to electron correlation, they are referring to the Coulombic type. For this reason, we will simply refer to Coulombic correlation as correlation for the remainder of this thesis. The omission of this correlation between electrons in the HF model leads to erroneous results that represent approximately 0.5-1.0% of the total electronic energy of the system.[1] One might scoff at an error of only 1%; however, it has been noted that this error is often on the same order of magnitude as reaction energies. Consider the example of the dissociation of Cl_2. The true bond dissociation energy is 239.3 kJ/mol; however, at the HF/6-311+G(d) level of theory, this energy is predicted to be 50.27 kJ/mol. This represents an error of nearly 80%. Thus, although the correlation energy may only be as low as 1.0% of the total system energy, this error causes major problems in determining the energies of chemical reactions.

To overcome the deficiencies in the HF model, methods which include electron correlation have been developed and due to the expanding capabilities of modern technologies, such calculations are becoming feasible for increasingly large systems. Many of the traditional correlated methods are not employed in this study due to the availability of simpler models with equivalent accuracy; however, we will give a brief mention of these theories to show how correlation is included.

Hartree-Fock theory is considered the standard for a non-correlated method. Thus, Löwdin defined the correlation energy, E_{corr}, for a system as the difference between the exact non-relativistic energy, E_{exact}, and the energy at the HF limit, E_{HF}.[19] This is expressed by

$$E_{corr} = E_{exact} - E_{HF} \tag{1.100}$$

Many correlated models are known as post-Hartree-Fock methods as they incorporate the HF wave function but add corrections at the end to account for the electron correlation.

These methods include the commonly used Moller-Plesset perturbative theory (MPPT: MP2, MP3, MP4, etc.),[20] configuration interaction (CI),[21] and coupled cluster (CC)[22] techniques. Each of these methods accounts for correlation in different ways; however, they all incorporate excited state determinants in addition to the HF ground state wave function to include correlation effects. It has long been noted that correlation often pushes electrons farther apart and thus the inclusion of these excited states accounts for this by allowing electrons to increase their separations.

Density functional theory (DFT) is becoming one of the most popular correlated methods today due to its lower computational cost compared to the aforementioned theories.[1] Unlike MPPT, CI, and CC, as well as HF, DFT is not a wave function based theory. Instead, it uses the electron density, $\rho(\boldsymbol{r})$, to determine the energy of a system.[23–25] DFT, as the name suggests, employs functionals to determine each of the energy components. The functionals for the kinetic energy, electron nuclear attraction energy and electron repulsions in a mean field are used for all types of DFT methods; however, the functional that accounts for exchange and correlation takes many different forms.[26–29] This functional often contains empirical parameters obtained by fitting results to extensive sets of experimental data. Nonetheless, with careful parameterization, one can obtain highly accurate results from DFT. Finally, since DFT simplifies a wave function problem which contains $3N$ coordinates to one involving the density and thus only 3 coordinates, this simplification greatly reduces computational times and is one of the major reasons that its use is so widespread today.

MPPT, CI, CC, and DFT all have one thing in common: they account for correlation implicitly. A separate class of correlated methods are those that are explicitly correlated and these are the methods that have been employed throughout this research project. These explicitly correlated methods were first described in the seminal paper by Hylleraas in 1929.[30] In this paper, Hylleraas included a linear r_{12} term in the wave function of the helium atom. In 1957, Kinoshita reported the development of a similar wave function with this

same form of explicit correlation.[31] Each of these methods will be discussed in more detail in the results and discussion chapters of this thesis. In recent years, explicit correlation has been developed further and is often combined with the previously mentioned implicitly correlated methods to improve the results. These combined methods are referred to as the R12 methods (e.g. MPPT-R12).[32,33]

1.8 Two-Electron Probability Distributions

From the solution of the Schrödinger equation, whether it is through exact or approximate methods, one obtains the wave function. The wave function contains all of the information required to physically describe a system, but one cannot visualize such a function. It simply requires too many dimensions to be plotted in any discernible form. Therefore, the function is often manipulated to a form which can be displayed.

1.8.1 The Electron and Pair Densities

In the discussion of the Roothaan-Hall equations, the electron density, $\rho(\boldsymbol{r})$, was briefly introduced. It is one of the most common probability densities as it provides information regarding the distribution of electrons within a system. A more rigorous definition of the electron density is given by

$$\rho(\boldsymbol{r}) = N \int \dots \int \Psi^*(\boldsymbol{r}, \boldsymbol{r_2}, \dots, \boldsymbol{r_N}) \Psi(\boldsymbol{r}, \boldsymbol{r_2}, \dots, \boldsymbol{r_N}) \mathrm{d}\boldsymbol{r_2} \dots \mathrm{d}\boldsymbol{r_N} \tag{1.101}$$

One can see that this density is obtained by integrating the squared modulus of the wave function over all but one of the electronic coordinates. Integration of the resulting density over the angular components of $\boldsymbol{r}$

$$\rho(r) = \int \rho(\boldsymbol{r}) \mathrm{d}\Omega_r \tag{1.102}$$

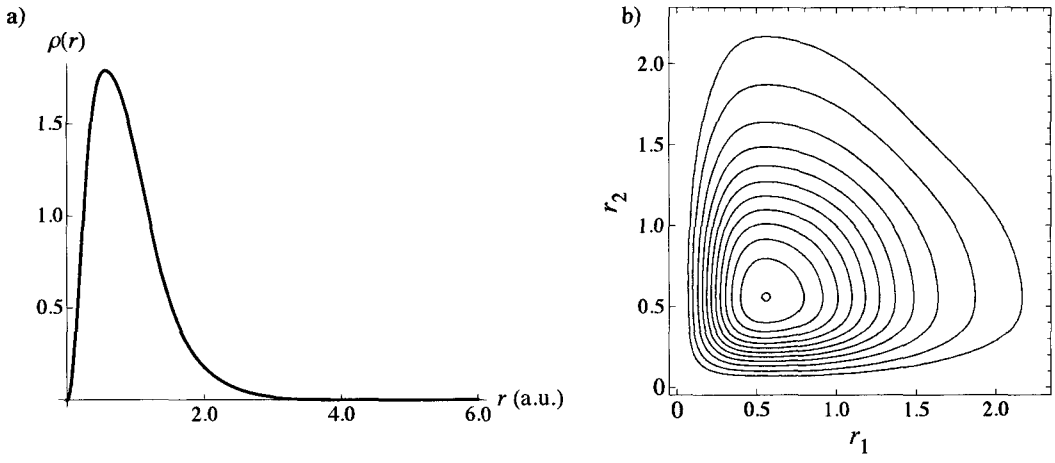

Figure 1.1: Spherically averaged a) electron density, and b) pair density, for the ground state of He.

where $d\Omega_r$ denotes the integration over the angular components of $\boldsymbol{u}$, yields the spherically averaged electron density, $\rho(r)$, which is easily represented in two-dimensions. An example of this density is provided in Figure 1.1 along with the spherically averaged pair density, $\rho(r_1, r_2)$, which will be discussed shortly. In some instances, $\rho(\boldsymbol{r})$ is plotted despite the requirement for four-dimensions. This fourth dimension is obtained either through the use of colours to denote different values of the density, as in electrostatic potential maps, or by plotting specific values (slices) of the density as a function of the three spatial coordinates. The latter method will be employed in Chapter 5 when exploring electron densities of molecules in an analysis of the effects of adding polarization functions to basis sets.

More useful than the electron density is the pair density, $\rho(\boldsymbol{r_1}, \boldsymbol{r_2})$. Similar in nature to the electron density, it is obtained from the squared modulus of the wave function while integrating over all but the first two electronic coordinate vectors as shown below.[1]

$$\rho(\boldsymbol{r_1}, \boldsymbol{r_2}) = \frac{N(N-1)}{2} \int \cdots \int \Psi^*(\boldsymbol{r_1}, \boldsymbol{r_2}, \boldsymbol{r_3}, \ldots, \boldsymbol{r_N}) \times \Psi(\boldsymbol{r_1}, \boldsymbol{r_2}, \boldsymbol{r_3}, \ldots, \boldsymbol{r_N}) d\boldsymbol{r_3} \ldots d\boldsymbol{r_N} \qquad (1.103)$$

As this density depends on the coordinates of two electrons, the pair density requires seven dimensions for graphical representation. As this is not possible, the most common sim-

plification is to integrate over all angular components of the $\boldsymbol{r_1}$ and $\boldsymbol{r_2}$ vectors to obtain $\rho(r_1, r_2)$. This density is highly useful as, unlike the electron density, it provides information regarding the simultaneous distances of two electrons from a reference point. Since the majority of chemistry is dependent on interactions between pairs of electrons, this density provides useful insight into electronic behaviour. However, ideally one would like to explore the full pair density including angular components to not only know how far electrons are from the nucleus, but also where they are in position space. This deficiency has led to the development of many probability densities, which are obtained by manipulating $\rho(\boldsymbol{r_1}, \boldsymbol{r_2})$ in order to obtain different pieces of information regarding electronic structure. Some of these densities will be discussed in this chapter, while development of new densities will be detailed throughout the results and discussion chapters of this thesis.

1.8.2 Intracule Densities

Although the spherically averaged pair density, $\rho(r_1, r_2)$, provides positional information regarding two electrons simultaneously, due to the required integration of the angular components, no information is obtained regarding the distance between the two electrons. However, as previously mentioned, this information is contained in the full pair density $\rho(\boldsymbol{r_1}, \boldsymbol{r_2})$; the only question is how to manipulate the function in order to obtain it.

The variable describing the separation of electrons is the interelectronic coordinate vector $\boldsymbol{u}$. This vector is given by

$$\boldsymbol{u} = \boldsymbol{r_{12}} = \boldsymbol{r_1} - \boldsymbol{r_2} \tag{1.104}$$

while the scalar u is simply the length of the $\boldsymbol{u}$ vector (i.e. $u = |\boldsymbol{r_1} - \boldsymbol{r_2}|$. Using this information, a probability density containing $\boldsymbol{u}$ can be obtained from the pair density by

$$I(\boldsymbol{u}) = \int\int \rho(\boldsymbol{r_1}, \boldsymbol{r_2}) \delta(\boldsymbol{u} - (\boldsymbol{r_1} - \boldsymbol{r_2})) \mathrm{d}\boldsymbol{r_1} \mathrm{d}\boldsymbol{r_2} \tag{1.105}$$

where $\delta(\boldsymbol{x})$ is a three-dimensional Dirac delta function. This function acts by substituting

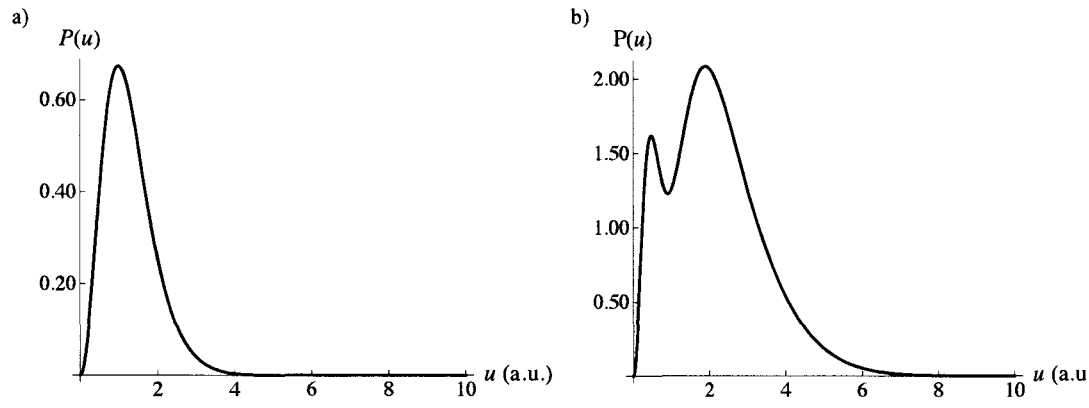

Figure 1.2: The intracule density, $P(u)$, of the ground states of the a) He atom, and b) Be atom.

u for r_1 in this expression through the equality, $\boldsymbol{u} - (\boldsymbol{r_1} - \boldsymbol{r_2}) = 0$. This yields

$$I(\boldsymbol{u}) = \int \rho(\boldsymbol{r} + \boldsymbol{u}, \boldsymbol{r}) \mathrm{d}\boldsymbol{r} \tag{1.106}$$

As this expression contains a single electron position vector, $\boldsymbol{r_2}$, this variable is replaced by a general position vector, $\boldsymbol{r}$. In each of these expressions, $I(\boldsymbol{u})$ is the position intracule density, which describes the probability of finding two electrons separated by the vector $\boldsymbol{u}$.[34,35] Most often, the position intracule is integrated over the angular coordinates to obtain the spherically averaged position intracule, $P(u)$. This spherically averaged density is often calculated directly from the pair density or equivalently from the squared modulus of the wave function by

$$\begin{aligned} P(u) &= \int\int \rho(\boldsymbol{r_1}, \boldsymbol{r_2}) \delta(u - |\boldsymbol{r_1} - \boldsymbol{r_2}|) \mathrm{d}\boldsymbol{r_1} \mathrm{d}\boldsymbol{r_2} \mathrm{d}\Omega_u \\ &= \int |\Psi(\boldsymbol{r_1}, \boldsymbol{r_2}, \ldots, \boldsymbol{r_N})|^2 \delta(u - |\boldsymbol{r_1} - \boldsymbol{r_2}|) \mathrm{d}\boldsymbol{r_1} \mathrm{d}\boldsymbol{r_2} \ldots \mathrm{d}\boldsymbol{r_N} \mathrm{d}\Omega_u \end{aligned} \tag{1.107}$$

As we will only be dealing with $P(u)$ throughout this thesis, it will simply be referred to as the position intracule, or in some cases, the intracule, unless specification is required. This density, as shown in Figure 1.2, is highly informative as it provides information regarding the separation of electrons in chemical systems. The intracule has been studied intensively

Table 1.2: Variously commonly studied intracules

Intracule	Notation	Description of Probability
Wigner[48–52]	$W(u,v)$	Electrons having separation of, u and relative momenta, v
Position[37–49]	$P(u)$	Electrons being separated by a distance, u.
Momentum[49,53]	$M(v)$	Electrons having relative momenta, v
Dot[54,55]	$D(x)$	Electron pair with $x = \boldsymbol{u} \cdot \boldsymbol{v} = u\,v\,\cos[\theta]$
Action[49,51,55]	$A(w)$	Electrons having scalar product $w = u\,v$

since its development in 1961 by Coulson and Neilson.[36–48] These intracules are often compared for different chemical systems or in systems treated with and without correlated models to determine the effects of electron correlation on interelectronic distances.

There are a number of other types of intracules that have been studied over the years. These include densities describing the relative momentum variable, $v \equiv |\boldsymbol{\rho_1} - \boldsymbol{\rho_2}|$ (where $\boldsymbol{\rho_i}$ is the momentum vector for electron i), and others which combine position (u) and momentum variables. A list of commonly studied intracules is given in Table 1.2.

It should be noted that the Wigner intracule is a quasi probability density. This density provides information regarding both the momentum and position of electrons despite the fact that the Heisenberg uncertainty principle states that we cannot know both parameters simultaneously with high accuracy. Each of the intracules listed here provides valuable information for comparing properties of electrons simultaneously and they continue to be studied today.

1.8.3 The Extracule Density

The position intracule provides information regarding the separation of electrons; hence, it provides *relative* position information; but the question remains, where in space do these electrons reside? This question can be answered by the extracule density which is a function of the centre-of-mass vector, $\boldsymbol{R}$.[56,57] The centre-of-mass vector ($\boldsymbol{R}$) and scalar (R) of two

electrons with position vectors $\boldsymbol{r_1}$ and $\boldsymbol{r_2}$ with the nucleus fixed at the origin are defined as

$$\boldsymbol{R} = \frac{\boldsymbol{r_1} + \boldsymbol{r_2}}{2} \qquad\qquad R = \frac{|\boldsymbol{r_1} + \boldsymbol{r_2}|}{2} \tag{1.108}$$

Unlike the intracule where the position of electrons in space is unknown, the extracule does provide information as to where they reside by providing the *absolute* position information through the centre-of-mass coordinate. The determination of the spherically averaged extracule, $E(R)$, is similar to that of the position intracule and can be given by

$$E(R) = \int\int \rho(\boldsymbol{r_1}, \boldsymbol{r_2}) \delta(R - \frac{1}{2}|\boldsymbol{r_1} + \boldsymbol{r_2}|) \mathrm{d}\boldsymbol{r_1} \mathrm{d}\boldsymbol{r_2} \mathrm{d}\Omega_R \tag{1.109}$$

where the only difference lies in the different form of the one-dimensional Dirac delta function. One can also derive a form dependent on the vector $\boldsymbol{R}$ as shown previously with the intracule, but again, these forms are generally not used in analyses.

Extracules are not investigated as often as intracules; nonetheless, they do provide another unique way of studying electron pairs (Figure 1.3). Neither the intracule, the extracule, nor any of the other densities that have been discussed thus far are complete in nature. Due to the complexity of a problem involving two electrons, there will always be some information which is averaged over (through integration) in order to provide a graphical

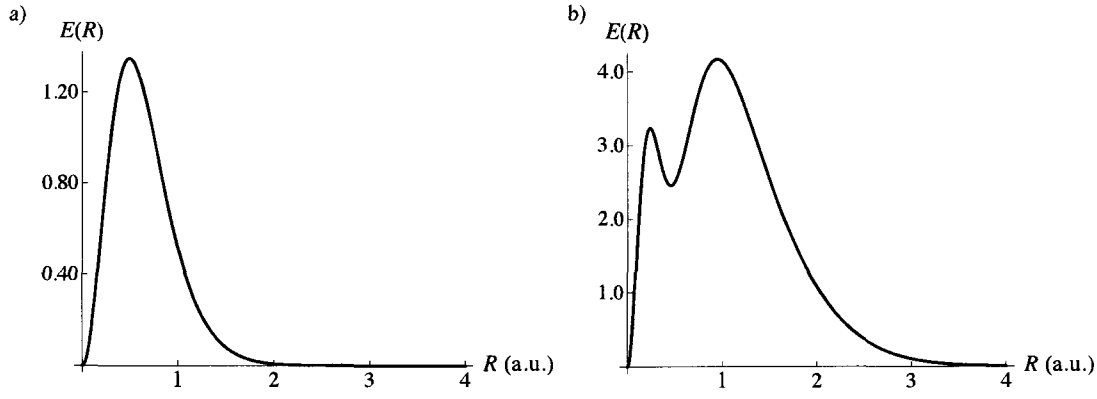

Figure 1.3: The extracule density, $E(R)$, of the ground states of the a) He atom, and b) Be atom.

representation of the information. Nonetheless, by manipulating the wave function and pair densities in specific ways, one can gain valuable information regarding electron structure. The discussion of this thesis will involve the development of new densities in order to provide different perspectives of the information contained in the wave function.

1.8.4 The Coulomb Hole

As previously noted, due to the use of the mean-field approximation in the Hartree-Fock method, the effects of electron correlation are neglected. In 1961, Coulson and Neilson published a now famous paper[36] detailing not only the previously described, position intracule, $P(u)$, but also the Coulomb or correlation hole. This Coulomb hole is the result of the difference between position intracules obtained from exact (i.e. correlated) and HF wave functions as given by

$$\Delta P(u) = P^{Exact}(u) - P^{HF}(u) \tag{1.110}$$

The Coulomb hole demonstrates the effect that correlation has on interelectronic separations in a system. From the figure of the Coulomb hole (Figure 1.4), the initial negative region followed by the positive region indicate that correlation decreases the probability that electrons will be close together.[36,37,41,48] Therefore, it is concluded that by allowing individual electrons to "see" one another, they are pushed further apart. This suggests that the mean field approximation underestimates electron repulsion energies in chemical systems.

1.8.5 The Secondary Coulomb Hole

It was long believed that the effects of correlation on interelectronic separations were accurately described by a universal contraction of electrons. However, in 2009, Pearson *et al.* described a new phenomenon that they referred to as the secondary Coulomb hole.[58] In this work, the correlation hole was analyzed at large values of u (i.e. where the function

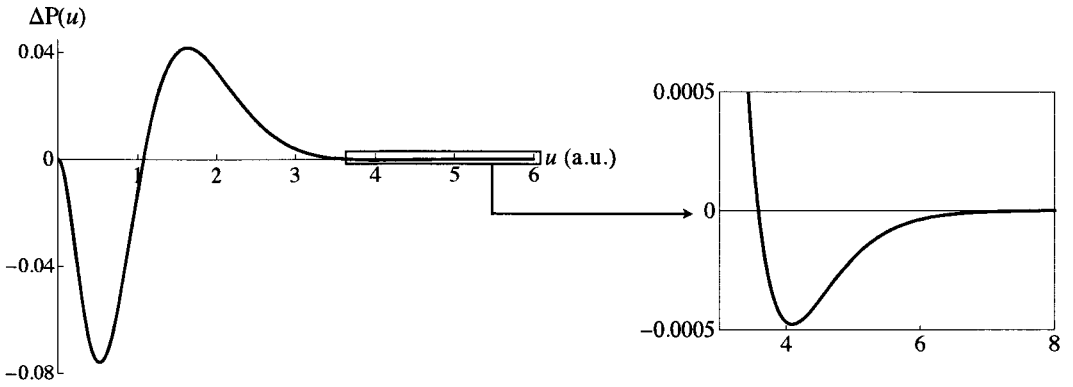

Figure 1.4: The Coulomb hole and the secondary Coulomb hole (inset) for the ground state of He atom.

approached zero) through the use of highly accurate HF and correlated wave functions. They detected the presence of a secondary negative region in the correlation hole (Figure 1.4). This phenomenon had been noted before but it had been considered to be an artefact of inaccurate wave functions.[48,59,60] However, these researchers demonstrated that the secondary Coulomb hole did not occur with the less accurate HF wave functions, but instead only became evident as the accuracy of the wave functions increased.

The occurrence of this secondary Coulomb hole suggests that correlation decreases the probability that electrons will be far apart. This is counterintuitive as previous evidence suggested that correlation universally pushed electrons further apart. This idea has been behind the development of correlation methods such as configuration interaction (CI) which incorporates higher energy orbitals to allow for the electrons to separate further than a HF treatment would allow. Furthermore, it is commonly stated in introductory text books describing quantum chemistry that correlation increases interelectronic separations.[61]

Since the seminal paper on this topic, there have been reports detailing the secondary Coulomb hole in different systems including the H_2 molecule[35] and the fictional system describing two electrons confined to the surface of a sphere (spherium).[62] These systems will be discussed in more detail throughout this thesis as we provide more evidence regarding this newly discovered effect.

1.9 Project Goals

The focus of the first half of this research project is two-fold. First of all, we aimed to develop new tools for the analysis of electronic structure. The motivation for the development of these tools was to gain a further understanding of the secondary Coulomb Hole with the hopes of determining its exact origin. We examined various methods in an attempt to explain the source of this phenomenon including the development of a new probability density, the study of fictional two-electron systems with varying differences from real two-electron systems, and finally the study of the relationship between the size of the secondary hole and the properties of the particular system.

As previously mentioned, the intracule density provides *relative* position information. Thus, it contains information concerning how far apart two electrons are within a system, but it affords no details regarding where the electrons are in the system with respect to the nucleus. The extracule density does provide this *absolute* position information but is lacking in terms of interelectronic separation data. Thus, it is obvious that a probability density that could provide both *relative* (**int**racule) and *absolute* (**ex**tracule) position information would be highly beneficial. This novel probability density, which we have coined the intex distribution, was to be determined for a series of atomic systems in order to provide a greater understanding of the secondary Coulomb hole.

There are a number of fictional systems that have been studied through the use of quantum mechanics to determine how they relate to real systems. Two such systems, are the Hooke's Law atom, or hookium, and ballium. Hookium is analogous to the helium atom being a two-electron system; however, the two electrons are bound to the nucleus by a harmonic potential instead of the more physical Coulombic potential. Ballium, on the other hand, has a constant or zero potential inside the sphere. By modifying the state of existence of these nuclear potentials, we can determine what role, if any, the nucleus plays in the existence of the secondary hole.

Finally, we examined the size, or strength, of the secondary hole to determine whether it could be related to a measurable property of the HF intracule. This relationship was studied for the helium isoelectronic series with respect to properties related to the diffuseness of the electron density.

In a related electronic structure study, we analyzed the effects of polarization functions on interelectronic separations. Much like the recently observed secondary Coulomb hole, it had been noted in a recent paper[54] that the introduction of polarization functions into a basis set led to an overall contraction of electron pairs. We aimed to determine the origin of this effect by conducting more thorough analyses involving intracules, energy components, and electron densities.

Deviating from electronic structure studies, the second part of this research project focussed on the development of a reaction optimization program. This introductory chapter did not contain information directly aimed at this project; however, all of the discussion regarding QM methods and calculations is pertinent. A more detailed description of the theory will be discussed in the chapter describing the project which should be more than sufficient for the required understanding of the reader.

The idea behind this project was to create a program with the capability to optimize any chemical or biochemical process. The concept was to target a functional site within a reactant complex such as a drug or drug precursor, which could be optimized to make the drug work more efficiently or make it easier to synthesize. The foundation for the optimization is to superimpose a large series of functional groups at this one site in the molecule. The algorithm would then sort through this set of functional groups to determine which one would be best in order to optimize the specific reaction process with respect to reaction or activation energies. The goal of this program is not to be a stand-alone system, but to work in conjunction with experimental chemistry to streamline these types of processes.

2 A Simultaneous Probability Density for the Intracule and Extracule Coordinates

2.1 Introduction

In the previous chapter, we discussed the intracule, $P(u)$, and extracule, $E(R)$, densities which describe the distribution of electrons within a system with respect to the interlectronic separation variable, u, and the centre of mass radius, R. These densities, especially the intracule, are highly useful in the study of electronic structure and in determining the effects of electron correlation. The previously mentioned Coulomb hole, which again is given by

$$\Delta P(u) = P^{\text{Exact}}(u) - P^{\text{HF}}(u) \tag{2.1}$$

was initially used to show that correlation causes electrons to separate; however, the secondary Coulomb hole that was discovered by Pearson *et al.* elucidates a richer behaviour of electronic structure differences between the HF and correlated models. This secondary hole indicates that at large interelectronic separations, correlation actually leads to a contraction of the electron pairs. This counterintuitive effect requires further study to be properly understood and in the present chapter as well as the following two chapters, data will be presented which sheds more light on the origins of the secondary Coulomb hole as well as

evidence suggesting the potential cause of the effect.

It would be invaluable to know more about the spatial distribution of electrons in the case that correlation causes a contraction of their distribution. This information is impossible to obtain from the spherically averaged intracule density alone, as it only measures *relative* distances between electrons and not their *absolute* location.[37–40] The location of an electron pair however may be probed using its centre of mass vector $\boldsymbol{R} = \frac{1}{2}(\boldsymbol{r}_1 + \boldsymbol{r}_2)$ described by the extracule density,[56,57] and thus it would be advantageous to develop a simultaneous probability density for both of these coordinates. In the current work, we will be concerned with deriving such a density for the ground state of the helium atom and helium-like ions. Thus, we need only consider the radial component of the extracule coordinate $R = \frac{1}{2}|\boldsymbol{r}_1 + \boldsymbol{r}_2|$ due to the spherical symmetry of such systems.

The simultaneous probability of finding two electrons separated by a distance u and with their centre of mass located at R is described by

$$X(R,u) = \langle\Psi|\delta(R - \tfrac{1}{2}|\boldsymbol{r}_1 + \boldsymbol{r}_2|)\delta(u - |\boldsymbol{r}_1 - \boldsymbol{r}_2|)|\Psi\rangle, \tag{2.2}$$

where Ψ is the wave function and $\delta(x)$ is a one-dimensional Dirac delta function. Because this density combines both relative (intracular) and absolute (extracular) position information to more completely describe the spatial distribution of electron pairs, we refer to $X(R,u)$ as the intex density.

As this chapter will involve a great deal of interpretation with regards to the $\boldsymbol{R}$ and $\boldsymbol{u}$ coordinates, these vectors as well as those describing the positions of electrons 1 and 2 are represented graphically in Figure 2.1.

The purpose of this chapter is to introduce the intex density and subsequently determine the intex correlation holes of the ground states of the helium atom and helium-like ions, defined as the difference between the exact and HF intex densities. This provides the opportunity to obtain a deeper understanding of the phenomenon of electron correlation;

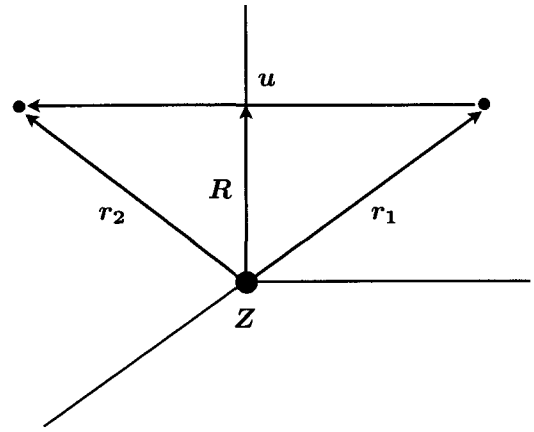

Figure 2.1: Schematic representation of a two-electron atom with electronic coordinate vectors $\boldsymbol{r}_1$, $\boldsymbol{r}_2$, $\boldsymbol{R}$. Z indicates the nuclear charge at the origin.

more specifically, it will allow for a more complete description of the secondary Coulomb hole,[35,58] which demonstrates the high utility of this novel probability density. Atomic units are used throughout.

2.2 Hartree-Fock Intex Density

For an N-electron ($N \geq 2$) system, the pair density

$$\rho(\boldsymbol{r}_1, \boldsymbol{r}_2) = \frac{N(N-1)}{2} \langle \Psi | \delta(\boldsymbol{r}_1' - \boldsymbol{r}_1) \delta(\boldsymbol{r}_2' - \boldsymbol{r}_2) | \Psi \rangle \tag{2.3}$$

gives the probability that one electron will be found at $\boldsymbol{r}_1$ and another at $\boldsymbol{r}_2$ simultaneously. As mentioned in the previous chapter, one can obtain the intracule and extracule densities from $\rho(\boldsymbol{r}_1, \boldsymbol{r}_2)$ by

$$P(u) = \int\int\int \rho(\boldsymbol{r}_1, \boldsymbol{r}_2) \delta(\boldsymbol{u} - [\boldsymbol{r}_1 - \boldsymbol{r}_2]) \, \mathrm{d}\boldsymbol{r}_1 \, \mathrm{d}\boldsymbol{r}_2 \, \mathrm{d}\Omega_{\boldsymbol{u}} \tag{2.4}$$

and

$$E(R) = \int\int\int \rho(\boldsymbol{r}_1, \boldsymbol{r}_2) \delta(\boldsymbol{R} - \tfrac{1}{2}[\boldsymbol{r}_1 + \boldsymbol{r}_2]) \, \mathrm{d}\boldsymbol{r}_1 \, \mathrm{d}\boldsymbol{r}_2 \, \mathrm{d}\Omega_{\boldsymbol{R}} \tag{2.5}$$

respectively, where $\mathrm{d}\Omega_{\boldsymbol{i}}$ denotes integration over the angular components of vector $\boldsymbol{i}$.

Similarly, one can also obtain an expression for the intex distribution directly from the pair density by

$$X(R,u) = \int\int\int\int \rho(\boldsymbol{r}_1,\boldsymbol{r}_2)\delta(\boldsymbol{R}-\tfrac{1}{2}[\boldsymbol{r}_1+\boldsymbol{r}_2])\delta(\boldsymbol{u}-[\boldsymbol{r}_1-\boldsymbol{r}_2])\,\mathrm{d}\boldsymbol{r}_1\,\mathrm{d}\boldsymbol{r}_2\,\mathrm{d}\Omega_{\boldsymbol{u}}\,\mathrm{d}\Omega_{\boldsymbol{R}}. \quad (2.6)$$

and subsequent integration over the R and u variables will yield the intracule or extracule density, respectively, as shown below

$$\int_0^\infty X(R,u)\,\mathrm{d}R = P(u) \quad (2.7)$$

$$\int_0^\infty X(R,u)\,\mathrm{d}u = E(R) \quad (2.8)$$

If the two-particle density is obtained from a restricted HF wave function for a closed shell system, the intex density may be expanded as

$$X^{\mathrm{HF}}(R,u) = \sum_{\mu\nu\lambda\sigma}^{K} \Gamma^{\mathrm{HF}}_{\mu\nu\lambda\sigma}\,(\mu\nu\lambda\sigma)_X, \quad (2.9)$$

where $\Gamma^{\mathrm{HF}}_{\mu\nu\lambda\sigma}$ represents the usual HF two-particle density matrix element,[1] which is obtained from the density matrix elements, $P_{\mu\nu}$ of (1.83), by

$$\Gamma_{\mu\nu\lambda\sigma} = \frac{1}{4}\left(2P_{\mu\nu}P_{\lambda\sigma} - P_{\mu\sigma}P_{\lambda\nu}\right) \quad (2.10)$$

and $(\mu\nu\lambda\sigma)_X$ are the intex integrals over atomic orbital basis functions denoted by μ, ν, λ, and σ. These integrals are given by

$$(\mu\nu\lambda\sigma)_X = \int\int \phi^*_\mu(\boldsymbol{R}-\frac{\boldsymbol{u}}{2})\,\phi_\nu(\boldsymbol{R}-\frac{\boldsymbol{u}}{2})\phi^*_\lambda(\boldsymbol{R}+\frac{\boldsymbol{u}}{2})\,\phi_\sigma(\boldsymbol{R}+\frac{\boldsymbol{u}}{2})\,\mathrm{d}\Omega_{\boldsymbol{u}}\,\mathrm{d}\Omega_{\boldsymbol{R}} \quad (2.11)$$

For the concentric cases of two-electron systems where all of the basis functions are

Gaussians of s-type symmetry, equation (2.11) may be integrated analytically as

$$(\text{ssss})_X = 16\pi^2 R^2 u^2 e^{[(\alpha+\beta+\gamma+\delta)(R^2+u^2/4)]} \frac{\sinh[Ru(\alpha+\beta-\gamma-\delta)]}{Ru(\alpha+\beta-\gamma-\delta)}, \tag{2.12}$$

where α, β, γ, and δ represent the exponents of the Gaussian functions and $\sinh(x)$ is the hyperbolic sine function. Alternatively, one may pursue other forms for ϕ such as Slater functions to enforce the nuclear-electronic cusp conditions; however, these are significantly more difficult to implement and have been shown to have a minimal effect on intracules when compared to an appropriately chosen set of Gaussians.[63,64] Thus far, only calculations of intracules involving s-type Gaussians have been performed; however, determining these intex integrals for p- and d-orbitals would be of great interest to be able to calculate intracules for larger atoms and molecules. Although, this chapter will highlight the use of the intex distribution to develop a greater understanding about the features of the Coulomb hole, it must be stressed that this probability density presents a novel way of describing electron pairs in atomic and molecular systems.

In order to construct accurate HF intex distributions, we employed a series of even-tempered basis sets proposed by Schmidt and Ruedenberg,[65] which utilize Gaussian primitives with exponents given by

$$\zeta_k = \alpha\beta^k, (k = 1, 2, \ldots, K), \tag{2.13}$$

where,

$$\ln\ln\beta = b\ln K + b', \tag{2.14}$$

and

$$\ln\alpha = a\ln(\beta - 1) + a'. \tag{2.15}$$

The coefficients (a, a', b, b') for all atoms from helium through argon are available in the literature[65] and thus, it is straightforward to construct a basis set containing any number of

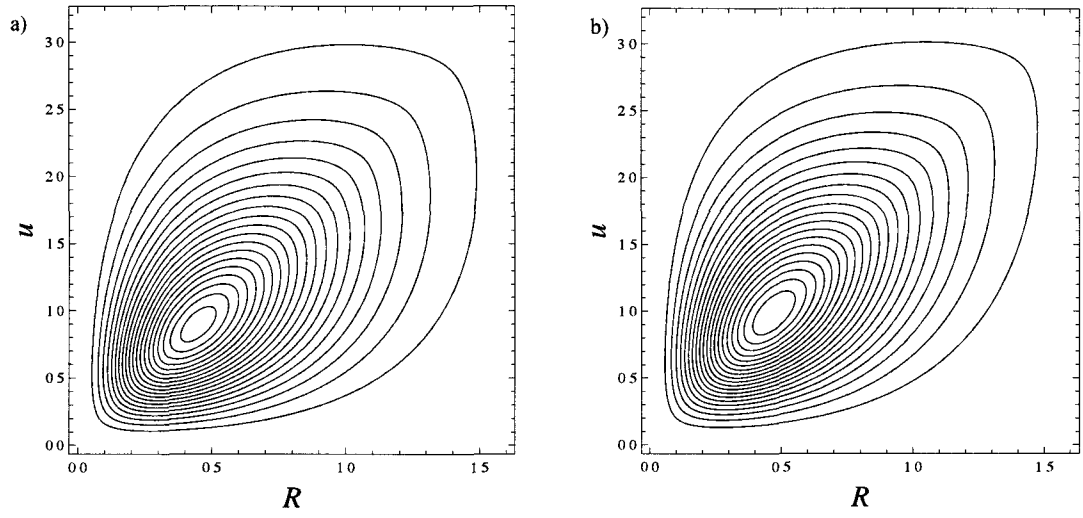

Figure 2.2: a) HF intex density of the helium atom, b) Correlated intex density of the helium atom. Contours have magnitudes of $5n$ x 10^{-2}, where n=1,2,3,...,20.

Gaussian functions, K. Coefficients for the atomic orbitals were then determined using the Q-CHEM package.[18]

We have calculated $X^{\mathrm{HF}}(R,u)$ with basis sets up to $K = 40$ and found that the largest of these is satisfactorily converged for the purposes of this investigation. This is demonstrated by comparing the $K = 39$ and $K = 40$ intex densities and calculating the maximum difference between the two as $\max_{u>0,\, R>0} |X^{\mathrm{HF}}_{40}(R,u) - X^{\mathrm{HF}}_{39}(R,u)| = 1.0 \times 10^{-7}$, which we interpret as a measure of the maximum basis set incompleteness error (BSIE) in the $K = 40$ intex density. This level of accuracy is more than sufficient to study fine correlation effects at large values of u.[58]

The HF intex density for the ground-state of the helium atom is shown in Figure 2.2a. The distribution has a global maximum at $u = 0.891$ and $R = 0.446$ and monotonically decays in all directions away from it. Interestingly, one can see that the distribution is symmetric about the $u = 2R$ line.

Inspection of equation (2.12) reveals that $X^{\mathrm{HF}}(R,u) = X^{\mathrm{HF}}(u/2, 2R)$, confirming that the distribution is *exactly* symmetric. This demonstrates a rigorous relationship between the HF intracule and extracule densities for spherically symmetric systems in ac-

Table 2.1: Coordinates (R_{max}, u_{max}) and magnitude of the maxima in the HF and correlated intex densities for the helium isoelectronic series.

		HF		Exact	
Ion	Z	(R_{max}, u_{max})	$X(R_{max}, u_{max})$	(R_{max}, u_{max})	$X(R_{max}, u_{max})$
He	2	(0.446, 0.891)	1.031	(0.468, 0.978)	1.045
Li^{+}	3	(0.282, 0.564)	2.680	(0.290, 0.598)	2.711
Be^{2+}	4	(0.206, 0.413)	5.099	(0.210, 0.430)	5.147
B^{3+}	5	(0.163, 0.325)	8.291	(0.165, 0.336)	8.355
C^{4+}	6	(0.134, 0.268)	12.253	(0.136, 0.275)	12.334
N^{5+}	7	(0.114, 0.228)	16.987	(0.115, 0.234)	17.084
O^{6+}	8	(0.099, 0.199)	22.492	(0.100, 0.203)	22.605
F^{7+}	9	(0.088, 0.176)	28.769	(0.089, 0.179)	28.898
Ne^{8+}	10	(0.079, 0.158)	35.817	(0.079, 0.160)	35.962

cordance with the isomorphisms for intracule and extracule densities reported in the literature.[66–71] From an empirical relation, Koga found the approximate isomorphism $d(R) \cong 8h(2R)$ for the spherically averaged extracule and intracule densities,[66–70] where $d(R) = E^{HF}(R)(4\pi R^2)^{-1}$ and $h(u) = P^{HF}(u)(4\pi u^2)^{-1}$. Romera later confirmed that this expression was exact for systems with two-electron densities of even parity.[71] Integrating our intex distribution (2.12) appropriately (equations (2.7) and (2.8)) provides a simple alternative derivation for this isomorphism.

In addition to the ground state of the helium atom, we have computed the HF intex densities for the ground states of the helium-like ions with atomic numbers $Z = 3$ to 10. As in several previous studies of this series,[58,72] the hydride ion, H^{-}, was omitted due to the difficulty in obtaining adequately converged results. As expected, the maxima in the intex densities shift to lower values of R and u as the charge on the ions increased. The coordinates and magnitude of the maxima in the intex densities are listed in Table 2.1. Despite the contraction towards the origin, the intex density for each ion of the He isoelectronic series is qualitatively similar.

2.3 Correlated Wave Function/Intex Density

In a previous paper,[58] Pearson *et al.* employed explicitly correlated wave functions of the Hylleraas type[73] to produce correlated intracules and the corresponding Coulomb holes. Unfortunately however, variationally optimized exponents and coefficients of the Hylleraas expansions are not available in the literature[74] for all of the ions in the isoelectronic series presented here and thus we have also explored a series of explicitly correlated wave functions based on those first described by Kinoshita in 1957:[31]

$$\Psi^{\mathrm{Kin}}(\boldsymbol{r}_1, \boldsymbol{r}_2) = e^{-\zeta s} \sum_{i=1}^{K} c_i \, s^{l_i/2} \left(\frac{t}{u}\right)^{m_i} \left(\frac{u}{s}\right)^{n_i/2} . \tag{2.16}$$

where s, t, and u are the Hylleraas coordinates defined as

$$s = |\boldsymbol{r}_1| + |\boldsymbol{r}_2| \qquad t = |\boldsymbol{r}_1| - |\boldsymbol{r}_2| \qquad u = |\boldsymbol{r}_1 - \boldsymbol{r}_2| \tag{2.17}$$

and the exponents, l_i, m_i, and n_i are non-negative integers. These exponents, along with the nonlinear parameter ζ, and the linear parameters c_i may be variationally optimized and this has been reported previously[75] for a variety of expansion sizes, K. The Kinoshita wave function employed here uses half-integer powers, which was demonstrated to significantly improve the accuracy of the expansion.[75] Using an expansion of $K = 100$ terms, the wave function reproduces an energy for the ground-state of the helium atom to within 1 picohartree (pE_h) of the exact value[75] which exceeds the accuracy of the previously reported Hylleraas wave functions.[74]

With the u variable already incorporated into the wave function, the extracule variable, R, may be related to these expressions by the equality

$$4R^2 = s^2 + t^2 - u^2. \tag{2.18}$$

Switching from Cartesian coordinates to Hylleraas coordinates and integrating over the three external angles $(\theta_R, \phi_R, \phi_u)$ requires the inclusion of the Jacobian resulting in the following

$$\mathrm{d}\boldsymbol{r}_1\,\mathrm{d}\boldsymbol{r}_2 \rightarrow \frac{4\pi^2 R\,u(4R^2+u^2-2t^2)}{\sqrt{4R^2+u^2-t^2}}\mathrm{d}t\,\mathrm{d}R\,\mathrm{d}u \tag{2.19}$$

Substituting this equality into (2.6) where the pair density is obtained from the Kinoshita wavefunction (expressed in terms of R, t, and u) and integration of the resultant expression over t affords the intex density. These expressions were integrated numerically using the built-in numerical integrator in the Mathematica package.[76]

Figure 2.2b illustrates the intex density obtained using the 100-term Kinoshita wave function. Although, as in the case of HF, the correlated intex density appears symmetric about the $u = 2R$ line, close inspection of (2.16) shows that the intex density obtained from these correlated functions will not possess this exact symmetry. This asymmetry is more clearly evident in the intex correlation hole (*vide infra*) and in the data provided in Table 2.1. From this data, it is clearly seen that, in addition to other effects, correlation causes a deviation in the maxima from this line of symmetry.

2.4 Intex Correlation Hole

The intex density is a valuable quantity to describe correlation effects in atomic and molecular systems due to its inherent relative (intracule density) and absolute (extracule density) position information. Figure 2.3 displays the intex correlation hole for the ground state of the helium atom, $\Delta X(R,u)$, which is given by

$$\Delta X(R,u) = X^{\mathrm{Exact}}(R,u) - X^{\mathrm{HF}}(R,u), \tag{2.20}$$

As previously noted, the intracule can be derived from the intex density by integrating over the R variable. Similarly, the usual Coulomb hole, $\Delta P(u)$, can be calculated by

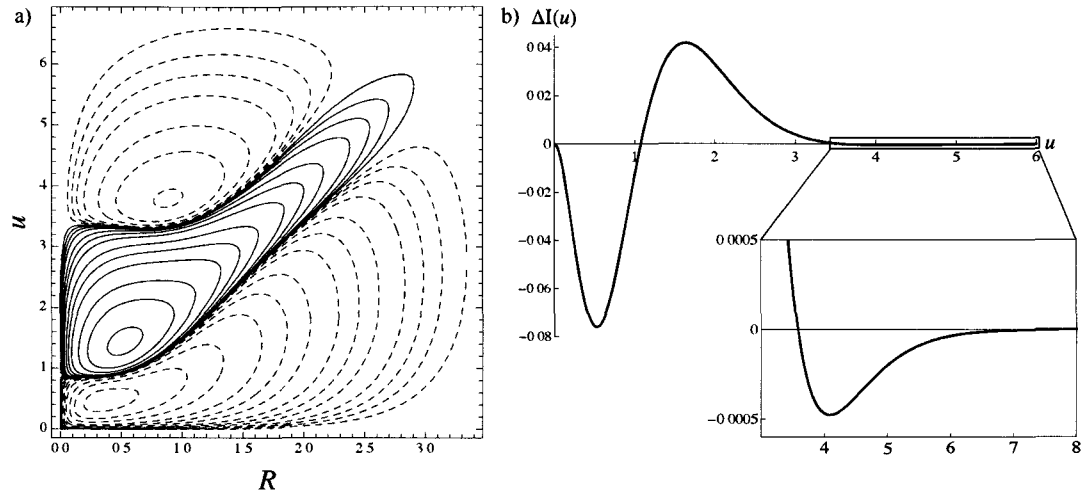

Figure 2.3: a) The intex correlation hole, $\Delta X(R,u)$, for the ground state of the helium atom. Contours have values of ± 2 x 10^{-n}, ± 4 x 10^{-n}, and ± 8 x 10^{-m} where n=2,3,4,5 and m=2,3,4,5,6. Positive contours are denoted by solid lines whereas negative contours are denoted by dashed lines. b) The Coulomb hole, $\Delta P(u)$ for the ground state of the helium atom.

$$\int_0^\infty \Delta X(R,u)\,\mathrm{d}R = \Delta P(u) \tag{2.21}$$

From Figure 2.3 we observe two negative regions intersected by a positive region in the correlation hole. A negative value of $\Delta X(R,u)$ indicates a *decrease* in probability due to the effects of electron correlation whereas a positive value of $\Delta X(R,u)$ indicates an *increase* in probability. Because each intex density is normalized to the number of electron pairs, the integral

$$\int\int \Delta X(R,u)\,\mathrm{d}R\,\mathrm{d}u = 0 \tag{2.22}$$

vanishes and thus the size of both negative regions is exactly proportional to that of the positive one. The positive region reaches a maximum value of 0.092 at $R = 0.520$ and $u = 1.417$ and this area extends along the $u = 2R$ line, creating a ridge. The first negative region, which mainly occurs at small u, reaches a minimum value of 0.109 at $R = 0.344$ and $u = 0.562$ (Min I) . The second negative region is far more shallow than the first and reaches a minimum value of 0.0008 at $R = 0.886$ and $u = 3.786$ (Min II).

The correlation hole for the helium atom[58] (see Figure 2.3) has roots at $u = 1.1$ and $u = 3.6$ and the conclusion is that the effects of correlation make it less favorable for electrons to be closer than 1.1 atomic units or farther apart than 3.6 atomic units. While the former is more intuitive than the latter, the results are clear and the intex density offers additional insight into this phenomenon. However, from the intex correlation hole, it would appear as though the relative separation of an electron pair does not *universally* indicate whether correlation will act to separate or contract the pair. The absolute position (R) of the electron pair is an important quantity, as is evidenced by the rich topology of the intex correlation hole in both the u and R dimensions. Evidently, correlation *can* increase the probability of finding electrons separated by large distances ($u > 3.6$) so long as their centre of mass is close to $\frac{1}{2}u$. Additionally, when $u < R$, which implies that the electron pair is on the same side of the nucleus, the intex correlation hole is always negative. This feature indicates that in such cases correlation will always act to either separate the electrons or move their centre of mass closer to the origin (or both).

The intex correlation holes were also determined for the helium isoelectronic series up to Ne^{8+} and as expected, the features of $\Delta X(R,u)$ contract toward the origin as the atomic number and nuclear charge increase. As with the case of the Coulomb holes of this series,[58] the intex correlation holes are all qualitatively similar and each system bears the same topological features. Table 2.2 summarizes the extrema of the correlation holes and lists the strengths of the secondary Coulomb holes defined by

$$S = \int_{\bar{u}_2}^{\infty} |\Delta P(u)| \mathrm{d}u \tag{2.23}$$

where $\bar{u}_2$ is the second root of $\Delta P(u)$. S is well defined for all of the systems under investigation in the current work because all exhibit a second root $\bar{u}_2$ and it appears as though such secondary Coulomb holes may be ubiquitous in two-electron systems.[35,58,77] S has been reported previously for Z-scaled intracules[58] for He, Li^+, Be^{2+}, B^{3+}, and Ne^{8+} and all are in exact agreement with those in Table 2.2 upon introduction of the scaling

Table 2.2: Coordinates (R, u) of the extrema in intex correlation holes and secondary hole strength for the helium isoelectronic series.

Ion	Z	Min I (R, u)	Max (R, u)	Min II (R, u)	S
He	2	(0.344, 0.562)	(0.520, 1.417)	(0.886, 3.786)	6.30 x 10^{-4}
Li^{+}	3	(0.227, 0.286)	(0.316, 0.873)	(0.570, 2.399)	3.54 x 10^{-4}
Be^{2+}	4	(0.170, 0.207)	(0.227, 0.632)	(0.421, 1.759)	2.33 x 10^{-4}
B^{3+}	5	(0.136, 0.162)	(0.177, 0.495)	(0.333, 1.389)	1.71 x 10^{-4}
C^{4+}	6	(0.113, 0.134)	(0.146, 0.407)	(0.276, 1.149)	1.34 x 10^{-4}
N^{5+}	7	(0.097, 0.114)	(0.123, 0.346)	(0.235, 0.979)	1.09 x 10^{-4}
O^{6+}	8	(0.085, 0.099)	(0.107, 0.300)	(0.205, 0.852)	9.20 x 10^{-5}
F^{7+}	9	(0.076, 0.087)	(0.095, 0.265)	(0.182, 0.756)	7.94 x 10^{-5}
Ne^{8+}	10	(0.068, 0.078)	(0.085, 0.238)	(0.163, 0.677)	6.97 x 10^{-5}

factor, Z. The additional data for C^{4+}, N^{5+}, O^{6+} and F^{7+} confirms the trend that the proportion of the secondary Coulomb hole diminishes with increasing Z.

2.5 Z-Scaling

It was mentioned earlier that the intex density for each of the ions in the helium isoelectronic series is qualitatively similar. However, it would be interesting to have a quantitative assessment of the similarities between each of the densities. In various reports, Coulson, Curl and Boyd detailed the scaling of intracule densities by a factor, $Z - \delta$, where Z is the atomic number of the ion and δ is a screening constant.[78–80] This approach was also employed by Pearson *et al.* in their paper detailing the secondary Coulomb hole. We employ an analogous approach here for the intex density. These screening factors are introduced to demonstrate that the distribution of electrons in different systems can be correlated with respect to the effective nuclear charge that is approximated by $Z - \delta$. In the past, these factors have also been useful in comparing the effects of screening between the ground and excited states of atoms.[78–80]

These new functions, $X'(R', u')$ are obtained by first scaling the R and u coordinates

by $Z-\delta$ to give $R' = (Z-\delta)R$ and $u' = (Z-\delta)u$. Using these scaled coordinates in the intex distribution, $X(R', u')$, and dividing by the square of the scaling constant yields the Z-scaled intex density, $X'(R', u')$ as follows:

$$X'(R', u') = \frac{X(R', u')}{(Z-\delta)^2} \tag{2.24}$$

In order to determine the optimal value for the screening constant, δ, we minimized the following expression with respect to δ

$$\Delta_{Ion}^{X'}(\delta) = \int\int \left[X_{Ion}'^{HF}(R', u') - X_{He}'^{HF}(R', u')\right] \mathrm{d}R\, \mathrm{d}u \tag{2.25}$$

through brute force analysis using numerical integration methods. As we were looking for a single screening constant for each tested system of the helium isoelectronic series, the ion that was used in this minimization scheme was Ne^{8+} as it represented the greatest difference from the intex density of the reference Helium atom. Through this process, the optimal value was determined to be $\delta = 0.339$. Using this value, we also determined $\Delta_{Ion}^{X'}(0.339)$ for the remaining ions in the isoelectronic series as a quantitative assessment of the differences between the scaled densities. These values as well as other measures including the coordinates of the extrema and scaled hole strengths are tabulated in Table 2.3. In the determination of the optimal value of δ, we also looked at the use of different values of screening constants for the R, δ_R, and u ,δ_u, coordinates, but it was determined that the best correlation between the He and Ne^{8+} intex densities was obtained when $\delta_R = \delta_u = 0.339$. Figure 2.4 displays the scaled intex correlation holes for each of the systems studied here. One can note that the correlation holes are very similar and each show the same type of trend in terms of configurations where correlated or HF treatments are favoured. The values of S that are given in the table indicate that even when multiplied by the scaling constant, $Z-\delta$, the size of the hole decreases suggesting that the effect is more complex than simply being related to the distance of the electrons from the nucleus.

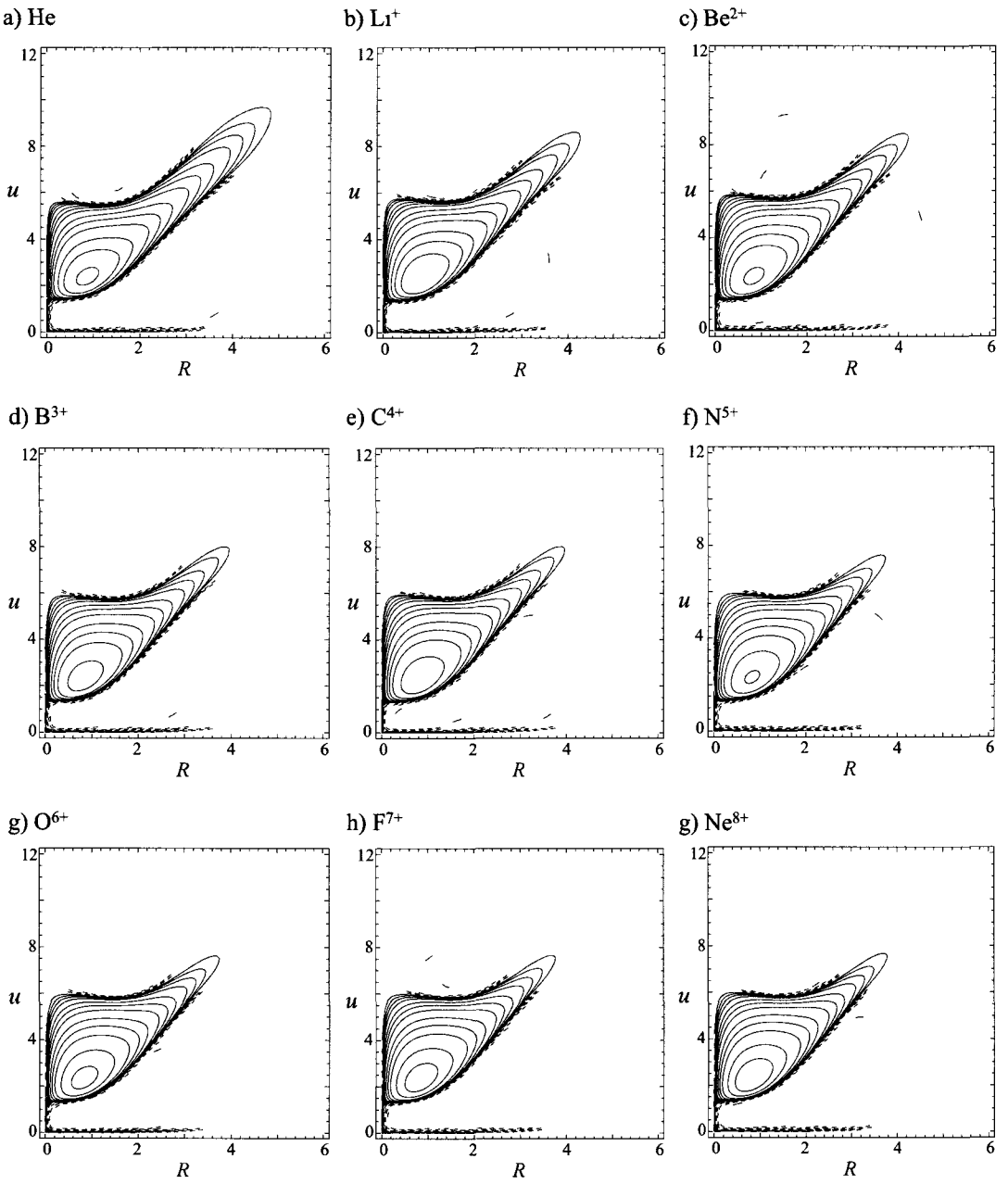

Figure 2.4: The Z-scaled intex densities, $\Delta X(R', u')/(Z-\delta)^2$, for the ground states of the He isoelectronic series ($Z = 2$ to 10) Contours have values of $\pm 2 \times 10^{-n}$, $\pm 2 \times 10^{-n}$, and $\pm 2 \times 10^{-n}$ where $n = 2, 3, 4, 5, 6$ and $m = 3, 4, 5, 6$ As Z increases the following contours are excluded c) to i)$\rightarrow \pm 2 \times 10^{-2}$ and g) to i)$\rightarrow \pm 8 \times 10^{-3}$ Positive contours are denoted by solid lines whereas negative contours are denoted by dashed lines

In Chapter 4, we will explore the strength of the secondary Coulomb hole with respect to other properties of the position intracule, but for now, we note that we can obtain reason-

Table 2.3: Assessments of the similarities between the Z-scaled intex densities and correlation holes.

Ion	Δ^X_{Ion}	Min I (R', u')	Max (R', u')	Min II (R', u')	$(Z-\delta)S$
He	- - - -	(0.572, 0.768)	(0.865, 2.354)	(1.471, 6.288)	1.01 x 10^{-3}
Li^+	0.0303	(0.605, 0.760)	(0.840, 2.323)	(1.518, 6.383)	9.41 x 10^{-4}
Be^{2+}	0.0433	(0.622, 0.758)	(0.831, 2.315)	(1.540, 6.438)	8.54 x 10^{-4}
B^{3+}	0.0505	(0.634, 0.757)	(0.827, 2.309)	(1.553, 6.472)	7.96 x 10^{-4}
C^{4+}	0.0551	(0.642, 0.756)	(0.824, 2.306)	(1.562, 6.502)	7.56 x 10^{-4}
N^{5+}	0.0583	(0.647, 0.756)	(0.822, 2.303)	(1.568, 6.521)	7.27 x 10^{-4}
O^{6+}	0.0606	(0.651, 0.756)	(0.821, 2.301)	(1.571, 6.525)	7.05 x 10^{-4}
F^{7+}	0.0624	(0.655, 0.756)	(0.819, 2.297)	(1.575, 6.543)	6.88 x 10^{-4}
Ne^{8+}	0.0638	(0.657, 0.756)	(0.819, 2.300)	(1.577, 6.543)	6.73 x 10^{-4}

ably overlapped functions by scaling the position intracules of each of the ions by a factor involving the atomic number and a screening constant.

2.6 Concluding Remarks

In this chapter, we have introduced the development of a novel electron pair distribution, the intex density, which is defined by (2.2). This new density employs both the intracular and extracular coordinates to more completely describe the probability distributions of electron pairs in position space. Using even-tempered basis sets of 40 s-type Gaussians, we have calculated the HF intex distribution of the ground state helium-like ions from He to Ne^{8+}. In all of these cases we note that the intex distribution is symmetrical about the line $u = 2R$, implying the previously described[66–71] relation $2P(2R) = E(R)$.

A correlated treatment of the intex density was performed using Kinoshita type wave functions. Unlike the HF intex density, the correlated intex density is not symmetric about the $u = 2R$ line. Using the correlated intex densities, we were able to determine the intex correlation hole for the ground state of the helium atom and the helium isoelectronic

series. The intex correlation hole provides a more complete picture of the effects of electron correlation on the spatial distribution of electron pairs in an atomic system. Specifically, we observe that the secondary Coulomb hole is not universal; it does not occur at all large values of u, but instead is dependent on the centre of mass of the electron pair. We conclude that the probability of observing an electron pair with a very large interelectronic separation increases with the inclusion of correlation *only* when their centre of mass radius is close to half of their separation. It would be reasonable to conjecture that in such cases, one electron remains close to the nucleus while the second is far away as such configurations would lead to favourable interactions between the electron and the nucleus. However, to accurately determine the most probable configurations, one must consider the probability distribution of the angle between the interelectronic separation and centre-of-mass vectors. This can be achieved through selective integration over the angular components of the two vectors and will be explored in detail in the ensuing chapter. Additionally, it has been shown that part of the effects of correlation in these systems are to decrease the probability of observing $u < R$ (i.e. both electrons on the same side of the nucleus).

3 Angular Dependence of the Two-Electron Intex Distribution

3.1 Introduction

Two-electron atoms have been the focus of a wide range of theoretical research.[81,82] There is value in understanding the pair-wise interactions of electrons in such simple systems as this can usually be extrapolated to better understand even the most subtle correlation effects in arbitrarily large systems.[81] Even the correlation energy of the helium atom still garners attention from the chemical physics community.[83–86] Furthermore, the subtle (and counterintuitive) correlation effects that have been observed within the context of the Coulomb hole[35,58,87,88] have yet to be satisfactorily explained (i.e. the secondary Coulomb hole).

In the previous chapter, we introduced the intex density to describe the spatial distribution of electron pairs in terms of the intracular (u) and extracular (R) coordinates simultaneously. The intex density is, as previously mentioned, given by

$$X(R,u) = \langle \Psi(\boldsymbol{r}_1,\boldsymbol{r}_2) | \delta(R - \tfrac{1}{2}|\boldsymbol{r}_1 + \boldsymbol{r}_2|)\, \delta(u - |\boldsymbol{r}_1 - \boldsymbol{r}_2|) | \Psi(\boldsymbol{r}_1,\boldsymbol{r}_2) \rangle \qquad (3.1)$$

and describes the probability that a pair of electrons will be separated by a distance u and simultaneously have their centre of mass located at a distance R from a reference point.

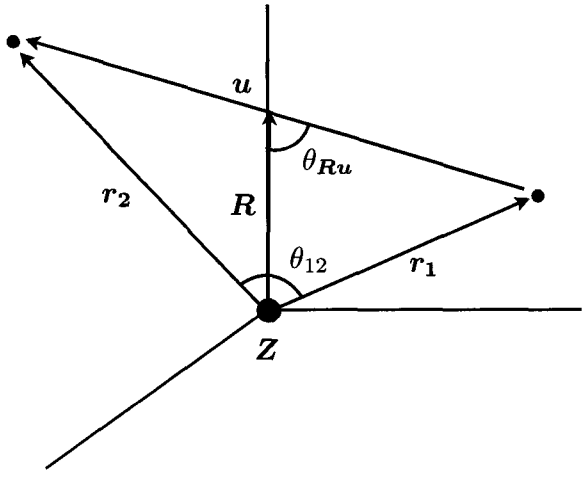

Figure 3.1: Schematic representation of a two-electron atom with electronic coordinate vectors $\boldsymbol{r}_1$, $\boldsymbol{r}_2$, $\boldsymbol{R}$, $\boldsymbol{u}$, and the angular coordinates θ_{Ru}, and θ_{12}. Z indicates the nuclear charge at the origin.

The intex density has proven to be quite useful in providing a clearer picture of the effects of electron correlation and the spatial distribution of electron pairs owing to the fact that it contains information regarding the relative separation of electrons *and* their absolute position in space. In the present chapter, we aim to expand the development of the intex density by studying its dependence on the angle, θ_{Ru}, between the coordinate vectors $\boldsymbol{R}$ and $\boldsymbol{u}$. Figure 3.1 is an expansion of Figure 2.1 illustrating the angular separation of the $\boldsymbol{R}$ and $\boldsymbol{u}$ vectors as well as that between the electron position vectors, $\boldsymbol{r}_1$ and $\boldsymbol{r}_2$. In spherically symmetric systems such as the ground states of two-electron atoms, the set of scalar coordinates r_1, r_2, and θ_{12} represent a complete description. Analogously, the scalar intracular coordinate, u, extracular coordinate, R, and angle θ_{Ru} also represent a complete set. As such, we will focus on the ground states of the helium isoelectronic sequence in this work for the purposes of simplifying the initial implementation of this new probability density.

Probability densities of interelectronic angles have been studied extensively[89–107] and are intimately related to angular correlation, which is the result of electrons increasing their angle of separation (θ_{12}) in order to avoid one another. This differs from radial correlation, which is the result of electrons avoiding one another by adopting different radii with re-

spect to the nucleus. Such probability distributions still garner much attention today from well-respected theoreticians as evidenced by the recent work by Koga *et al.*[108] The inter-electronic angle density describes the probability of finding two electrons with an angle of θ_{12} separating their respective position vectors and are generally of the form

$$A(\theta_{12}) = \int \frac{\rho(\boldsymbol{r_1}, \boldsymbol{r_2})}{\sin(\theta_{12})} \frac{\mathrm{d}\boldsymbol{r_1}\, \mathrm{d}\boldsymbol{r_2}}{\mathrm{d}\theta_{12}} \tag{3.2}$$

where $\mathrm{d}\boldsymbol{r_1}\, \mathrm{d}\boldsymbol{r_2}/\mathrm{d}\theta_{12}$ denotes the integration over all spatial and angular components of $\boldsymbol{r_1}$ and $\boldsymbol{r_2}$ with the exception of θ_{12}. Here, $\rho(\boldsymbol{r_1}, \boldsymbol{r_2})$ is the previously mentioned pair density function given by

$$\rho(\boldsymbol{r_1}, \boldsymbol{r_2}) = \frac{N(N-1)}{2} \int |\Psi(\boldsymbol{r_1}, \ldots, \boldsymbol{r_N})|^2 \, \mathrm{d}\boldsymbol{r_3} \cdots \mathrm{d}\boldsymbol{r_N} \tag{3.3}$$

In an alternative approach to studying angular correlation phenomena, we have calculated the contributions of the angle θ_{Ru} to the intex density and observe what effects correlation has on the optimal angle between the $\boldsymbol{R}$ and $\boldsymbol{u}$ vectors. This probability distribution may also be obtained from the two-electron density by

$$X(R, u, \theta_{Ru}) = \int\int\int\int \rho(\boldsymbol{r}_1, \boldsymbol{r}_2) \delta \left[\boldsymbol{R} - \frac{1}{2}(\boldsymbol{r}_1 + \boldsymbol{r}_2) \right] \delta[\boldsymbol{u} - (\boldsymbol{r}_1 - \boldsymbol{r}_2)] \, \mathrm{d}\boldsymbol{r}_1 \, \mathrm{d}\boldsymbol{r}_2 \, \frac{\mathrm{d}\Omega_R \, \mathrm{d}\Omega_u}{\mathrm{d}\theta_{Ru}} \tag{3.4}$$

where θ_{Ru} is an angular component of the vector $\boldsymbol{u}$ with the $\boldsymbol{R}$ vector acting as the principal axis and again, $\mathrm{d}\Omega_u \mathrm{d}\Omega_R/\mathrm{d}\theta_{Ru}$ denotes integration over all angular components of the $\boldsymbol{R}$ and $\boldsymbol{u}$ vectors with the exception of θ_{Ru}. The angular component may then be isolated by integrating over the radial R and u components as follows

$$A(\theta_{Ru}) = \int\int X(R, u, \theta_{Ru}) \, \mathrm{d}R \, \mathrm{d}u \, . \tag{3.5}$$

Throughout this chapter we will refer to $X(R, u, \theta_{Ru})$ as the angular-dependent intex

density and to $A(\theta_{Ru})$ simply as the angular intex density. The form of our expression differs slightly from that in equation (3.2) in that we retain the $\sin(\theta)$ factor of the Jacobian so that we may maintain the normalization of the probability distribution, which in the case of such two-electron densities is the number of electron pairs, or $N(N-1)/2$. This resembles the approach of Boyd and co-workers for interelectronic angle densities.[93–95]

A primary and immediate application of these angular densities is to better understand the spatial distributions of electron pairs and how this gives rise to the anomalous secondary Coulomb hole. These quantities are also important for the fundamental understanding of electron-electron interactions in our test systems because for probable configurations of u and R, there exists two very different extremes whereby $\theta_{Ru} = \pi/2$ or $\theta_{Ru} = (0, \pi)$ and these represent cases where the electrons are equidistant from the nucleus and where the pair of electrons and the nucleus are colinear, respectively. Therefore the influence of the nuclear potential may be probed using this technique. Also, $X(R, u, \theta_{Ru})$ allows one to understand the distribution of θ_{Ru} for specific values of u and R. For a more general application to larger atoms and molecules, the vectorized extracular coordinate may be considered, $\boldsymbol{R}$, which will allow for the localization of such an analysis.

In the present chapter, we study the features of these probability distributions and consequently learn about the restrictions that correlation imposes upon the spatial distribution of electron pairs. Along with the intex density, it is shown that this novel density provides a clearer picture of the effects of electron correlation and more details concerning the nature of the secondary Coulomb hole. Once again, atomic units are used throughout the chapter.

3.2 Theory

3.2.1 Hartree-Fock Wave Function

The angular and angular-dependent intex densities may be obtained from equations 3.5 and 3.4, respectively. If one uses a HF wave function to generate the two-particle density, the

angular dependence function may be expressed as an expansion

$$X(R,u,\theta_{Ru}) = \sum_{\mu\nu\lambda\sigma}^{K} \Gamma^{\mathrm{HF}}_{\mu\nu\lambda\sigma}(\mu\nu\lambda\sigma)_{X_A}\,, \tag{3.6}$$

where $\Gamma^{\mathrm{HF}}_{\mu\nu\lambda\sigma}$ is the usual HF two-particle density matrix described in Chapter 2, while $(\mu\nu\lambda\sigma)_{X_A}$ are the angular intex integrals over the set of K atomic orbital basis functions denoted by μ, ν, λ, and σ. One can note the similarities between the present expression and that given by (2.9) for the intex distribution where the intex integrals, $(\mu\nu\lambda\sigma)_X$, are replaced by the angular intex integrals, $(\mu\nu\lambda\sigma)_{X_A}$. These new integrals are given by

$$(\mu\nu\lambda\sigma)_{X_A} = \int\int \phi^*_\mu(\boldsymbol{R}-\frac{\boldsymbol{u}}{2})\,\phi_\nu(\boldsymbol{R}-\frac{\boldsymbol{u}}{2})\,\phi^*_\lambda(\boldsymbol{R}+\frac{\boldsymbol{u}}{2})\,\phi_\sigma(\boldsymbol{R}+\frac{\boldsymbol{u}}{2})\,\frac{\mathrm{d}\Omega_u\,\mathrm{d}\Omega_R}{\mathrm{d}\theta_{Ru}}\,, \tag{3.7}$$

and for spherically concentric systems utilizing Gaussian basis functions of s-type symmetry, these integrals may be expressed analytically as

$$(\mathrm{ssss})_{X_A} = 8\,\pi^2 R^2\,u^2\sin(\theta_{Ru})\,e^{-(R^2+u^2/4)(\alpha+\beta+\gamma+\delta)-Ru(\alpha+\beta-\gamma-\delta)\cos(\theta_{Ru})}\,, \tag{3.8}$$

where the exponents of the Gaussian primitives are denoted by α, β, γ, and δ. From expressions (3.8) and (3.5), it is straightforward to obtain $A(\theta_{Ru})$ through numerical integration over R and u and we have employed the numerical integrator implemented in the Mathematica package[76] for this purpose.

For the purposes of constructing accurate HF wave functions, we employed the same set of even-tempered basis sets proposed by Schmidt and Ruedenberg that were used for the study of the intex distribution in the previous chapter. Thus, the K exponents of the Gaussian primitives can be determined from expressions (2.13)-(2.15). The atomic orbital coefficients were once again determined using the Q-CHEM package.[18]

We have determined that basis sets consisting of $K = 30$ Gaussians produce intex densities that are more than adequately converged for the current work. This determination

is based on a calculation of the maximum BSIE for the $K = 30$ Gaussian helium-like ion basis set as $\max_{u>0,R>0} |X^{\mathrm{HF}}_{K=30}(R,u) - X^{\mathrm{HF}}_{K=29}(R,u)| = 2.3 \times 10^{-7}$.

3.2.2 Kinoshita Wave Function

Kinoshita wave functions have long been considered as high-accuracy benchmarks for calculations on atomic systems.[31,73–75] For the construction of our exact wave functions we have once again chosen a series of Kinoshita expansions given by

$$\Psi^{\mathrm{Kin}}(\boldsymbol{r}_1, \boldsymbol{r}_2) = e^{-\zeta s} \sum_{i=1}^{N} c_i \, s^{l_i/2} \left(\frac{t}{u}\right)^{m_i} \left(\frac{u}{s}\right)^{n_i/2}, \tag{3.9}$$

The accuracies of these Kinoshita wavefunctions are more than adequate for the purposes of this study as was mentioned in Chapter 2.

To obtain the angular intex density, a function solely dependent on θ_{Ru}, s and t was substituted using the definitions of s ($s = r_1 + r_2$), and t ($t = r_1 - r_2$), containing r_1 and r_2 after which these variables were replaced by the identities

$$r_1 = \sqrt{R^2 + \frac{u^2}{4} - Ru\cos(\theta_{Ru})} \qquad r_2 = \sqrt{R^2 + \frac{u^2}{4} + Ru\cos(\theta_{Ru})}. \tag{3.10}$$

The angular-dependent intex density may then be obtained by using the resultant wave function, dependent on R, u, and θ_{Ru} in equation (3.4).

3.3 Results and Discussion

The HF and Kinoshita angular intex densities for the ground state of the helium atom are shown in Figure 3.2(a). This figure demonstrates that there is very little dependence on the angle between the vectors $\boldsymbol{R}$ and $\boldsymbol{u}$ over most of the range from 0 to π. Due to the inherent symmetry in the definition of θ_{Ru}, $A(\theta_{Ru})$ is symmetric about $\pi/2$. The density displays maxima at $\theta_{Ru} \approx 0.749$ and 2.393 under the HF approximation whereas the maxima occur

at $\theta_{Ru} \approx 0.574$ and 2.568 for the correlated treatment. The local minima for both methods occur at $\theta_{Ru} = \pi/2$. Figure 3.2(b) displays the angular intex correlation hole, $\Delta A(\theta_{Ru})$, which is given by

$$\Delta A(\theta_{Ru}) = A^{\text{Kin}}(\theta_{Ru}) - A^{\text{HF}}(\theta_{Ru}) \tag{3.11}$$

We observe a minimum at $\pi/2$ radians in $\Delta A(\theta_{Ru})$ indicating, as expected, that HF has a preference for configurations where the electrons are equidistant from the nucleus in comparison to exact treatments. This is not to say that systems under the HF approximation are most probable to have configurations where $\theta_{Ru} = \pi/2$, as that would contradict what is shown in Figure 3.2(a). Intead, this angle represents where the HF and correlated treatments differ the greatest in favour of HF. Similarly, the maxima are much closer to 0 and π, which signifies a greater preference in correlated systems for configurations where one electron is closer to the nucleus than the other.

Due to the spherical symmetry of the systems in the helium isoelectronic series, one might expect that the most probable configuration would be that of the electrons being equidistant from the nucleus (i.e. $\theta_{Ru} = \pi/2$). However, with local minima occurring where the $\boldsymbol{R}$ and $\boldsymbol{u}$ vectors are perpendicular to one another (i.e. electrons equidistant from the nucleus), the plot of $A(\theta_{Ru})$ confirms that this is not the case. The angular-dependent intex density may be used to explore this further (*vide infra*).

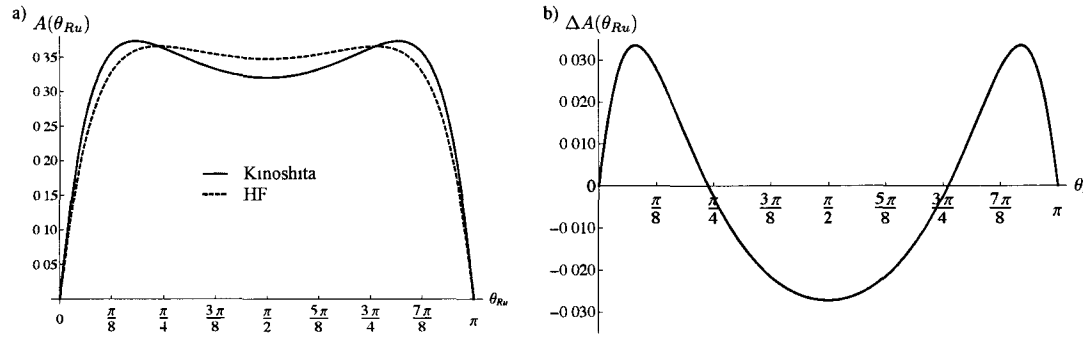

Figure 3.2: a) $A(\theta_{Ru})$ for HF and Kinoshita wave functions of the ground state of the helium atom, b) $\Delta A(\theta_{Ru})$ for the ground state of the helium atom.

Table 3.1: Coordinates of the maxima in the angular intex density ($\theta_{Ru}^{\max}$) in radians and the relative angular dependence of $A(\theta_{Ru})$ for the helium-like ions, Δ_θ (defined in the text).

		HF		Exact	
Ion	Z	$\theta_{Ru}^{\max}$	Δ_θ	$\theta_{Ru}^{\max}$	Δ_θ
He	2	0.749	0.0494	0.574	0.142
Li^{+}	3	0.828	0.0317	0.686	0.0779
Be^{2+}	4	0.868	0.0272	0.748	0.0544
B^{3+}	5	0.891	0.0215	0.789	0.0426
C^{4+}	6	0.907	0.0194	0.818	0.0357
N^{5+}	7	0.919	0.0180	0.840	0.0312
O^{6+}	8	0.928	0.0170	0.856	0.0281
F^{7+}	9	0.934	0.0163	0.869	0.0258
Ne^{8+}	10	0.940	0.0157	0.880	0.0240

The angular intex densities were determined for the series of helium-like ions from He to Ne^{8+} and the coordinates of the maxima are indicated in Table 3.1. Also included in the table is a measure of the relative angular dependence (Δ_θ) of $A(\theta_{Ru})$ for each of the ions defined by

$$\Delta_\theta = \frac{A^{\max}(\theta_{Ru}) - A^{\min}(\theta_{Ru})}{A^{\max}(\theta_{Ru})} \tag{3.12}$$

where $A^{\min}(\theta_{Ru})$ and $A^{\max}(\theta_{Ru})$ correspond to the value of $A(\theta_{Ru})$ at the local minimum and maximum, respectively. The value of Δ_θ demonstrates the relative difference in probabilities of the local minima and maxima in densities where a local minimum is observed and thus provides a measure of how greatly the density of the system is affected by changes in this angle.

Table 3.1 demonstrates that as the nuclear charge increases, the angle of the global maxima steadily increases in addition to an apparent decrease in the relative angular dependence, Δ_θ. With the only difference in these systems being that of the differing nuclear charges, these trends can be attributed to the electrons being drawn closer to the nucleus in

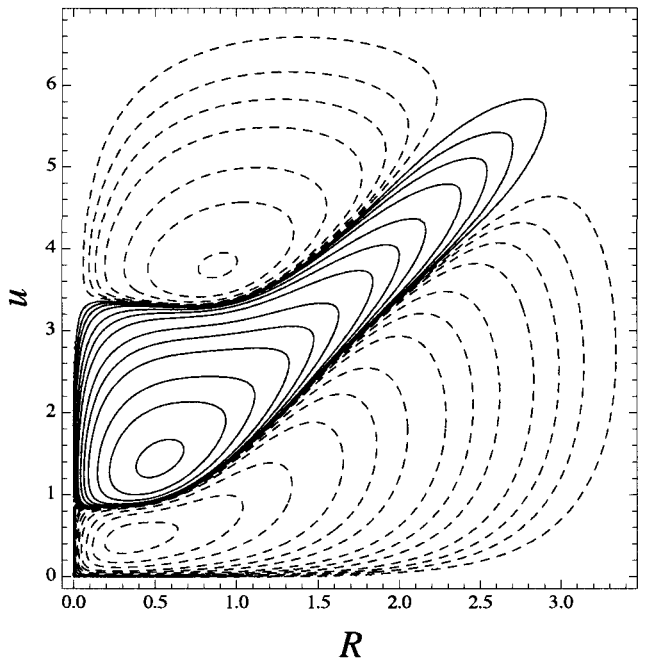

Figure 3.3: Intex correlation hole, $\Delta X(R,u)$, for the ground state of the helium atom. Contours have values of ± 2 x 10^{-n}, ± 4 x 10^{-n}, and ± 8 x 10^{-m} where $n = 2-5$ and $m = 2-6$. Solid lines denote positive contours whereas dashed lines denote negative contours.

the systems containing more protons. Consequently, when the electrons are closer to the nucleus, the positions of the electrons are more limited.

In addition to these trends, which are common to both HF and correlated cases, there are some significant differences between the two approaches, themselves. From the tabulated data, it can be noted that $\theta_{Ru}^{\max}$ is lower in correlated systems suggesting a preference for angles closer to 0 (or π), as discussed previously. Furthermore, the relative angular dependence is significantly greater in correlated systems, especially for the ions with lower nuclear charges. Therefore the data demonstrates that correlated treatments favour configurations where one electron is closer to the nucleus in comparison to HF theory. This idea is neither surprising nor new as correlation causes the position of one electron to be dependent on the positions of the remaining electrons in the system while the motions of opposite-spin electrons under the HF model are statistically independent; however, the angular intex density gives us a brand new way of looking at this effect.

To investigate the properties of the intex correlation hole[87] we can take slices of the angular-dependent intex distribution, $X(R, u, \theta_{Ru})$, at fixed values of R and u. This will afford an analysis of the probability distribution of θ_{Ru} for specific configurations of the electron pair relevant to the Coulomb and secondary Coulomb holes. To try and yield more information regarding these holes, we have chosen to examine the extrema of the intex correlation hole ($\Delta X(R, u) = X^{\text{Kin}}(R, u) - X^{\text{HF}}(R, u)$) and these are shown in Figure 3.3. There are two minima occurring at $(\check{R}_1, \check{u}_1) = (0.344, 0.562)$ and $(\check{R}_2, \check{u}_2) = (0.886, 3.786)$ and a maximum at $(\hat{R}, \hat{u}) = (0.520, 1.417)$. Appropriate slices of the angular-dependent intex density are then studied using these coordinates.

The HF and Kinoshita angular-dependent intex densities at the coordinates of the extrema of the intex correlation hole are displayed in Figures 3.4(a)-(c) while their respective angular-dependent intex correlation holes, $\Delta X(R, u, \theta_{Ru})$, are represented in Figures 3.4(d)-(f). As expected, the probability for HF systems is greater in (a) and (c) which represent the two minima in the intex correlation hole. Conversely, the correlated density is greater in the system described in (b), which is taken from the coordinates of the maximum in the intex correlation hole. From the plots of $\Delta X(R, u, \theta_{Ru})$, we see that a minimum occurs at $\theta_{Ru} = \pi/2$ in all cases. This again confirms that this configuration is more greatly favoured in relation to other angles for HF systems regardless of the value of R and u.

The main point of interest here is the trend that is observed when we progress from (a) to (c). As we progress from the coordinates of (a) to the coordinates of (c), the values of R and u both increase. From Figure 3.4, we see that in (a), the density reaches a maximum at $\pi/2$ for both HF and correlated systems, whereas in (b) and (c), $\pi/2$ represents a minimum and the level of dependence on θ_{Ru} is increasing. This reveals the explanation behind the overall form of the angular intex density in Figure 3.2. In the case where both R and u are very large values, two extremes would be possible: the first case being that where both electrons are far from the nucleus (and each other) with $\theta_{Ru} = \pi/2$ and the second case being the configuration where one electron is near the nucleus while the other is very far

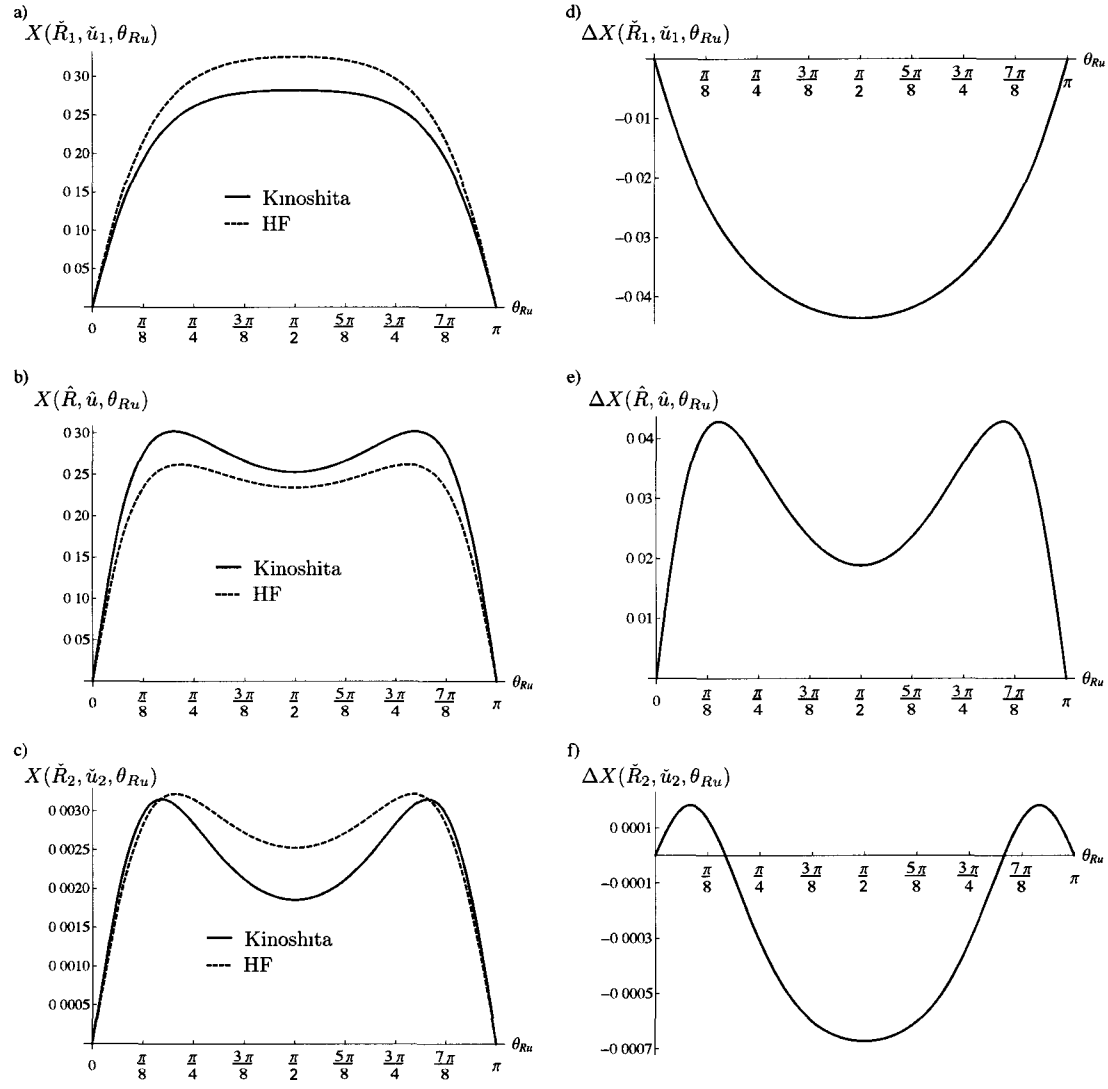

Figure 3.4: HF and Kinoshita angular-dependent intex densities, $X(R, u, \theta_{Ru})$, and the corresponding correlation holes $\Delta X(R, u, \theta_{Ru})$ at values of R and u corresponding to the extrema of the intex correlation hole for the ground state of the helium atom shown in Fig. 3.3. The coordinates (R, u) are as follows: a) and d) $\rightarrow$ $(\check{R}_1, \check{u}_1) = (0.344, 0.562)$; b) and e) $\rightarrow$ $(\hat{R}, \hat{u}) = (0.520, 1.417)$; c) and f) $\rightarrow$ $(\check{R}_2, \check{u}_2) = (0.886, 3.786)$

away corresponding to $\theta_{Ru} \approx 0$ or π. In the first case, we effectively have three separate one-particle systems, where neither electron has significant interaction with the nucleus nor each other, whereas in the second case, one electron is interacting favourably with the nucleus while the other is far enough away to be considered an isolated system. It is obvious that the latter is the more favourable configuration and thus it is expected that as

we increase both R and u, the level of angular dependence will increase and the optimal angle will approach 0 and π with the angular intex density consisting of two sharp peaks in these regions.

The relevant question then becomes, how large must R and u become before we observe such an inflection in the curvature of the angular-dependent intex density with respect to θ_{Ru} (i.e. a local minimum at $\theta_{Ru} = \pi/2$)? From Figure 3.4, we know that a maximum in $X(R, u, \theta_{Ru})$ at $\theta_{Ru} = \pi/2$ does occur for small values of R and u, so by gradually increasing each of these variables until an inflection is observed we are able to isolate the critical values of R and u for which the inflection takes place. These analyses were conducted for both the HF and Kinoshita densities and the results are shown in Figure 3.5. The dashed line in this figure divides the regions where the angular-dependent intex density at fixed R and u is a minimum or a maximum with respect to θ_{Ru} at $\pi/2$. The region below this line (low R and/or u) are the sets of coordinates where a maximum occurs at $\pi/2$, whereas the majority of the density which lies above the line represents the coordinates where a minimum is observed. Figure 3.5(a) demonstrates that the critical coordinate line for the HF system is symmetric about the $u = 2R$ line, as expected from

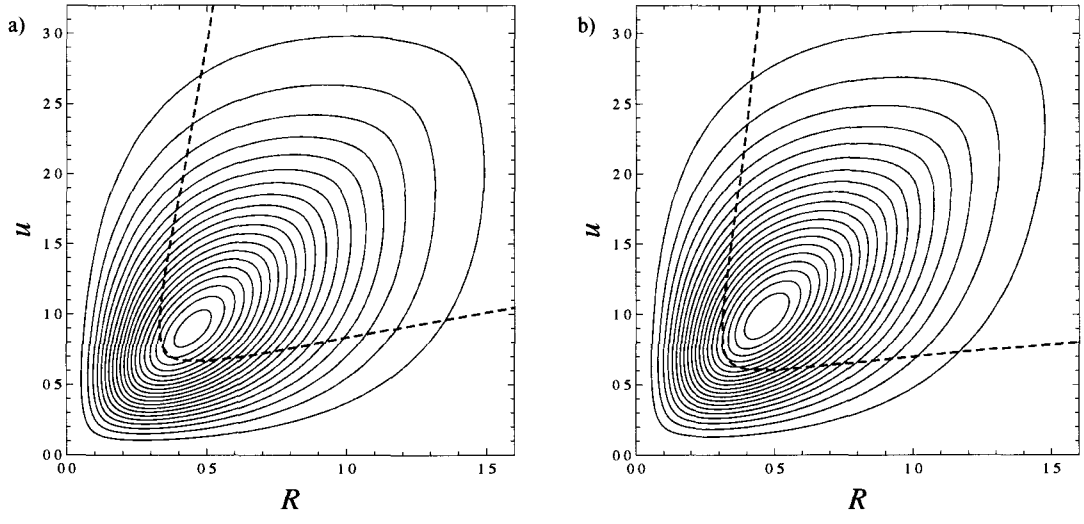

Figure 3.5: Critical coordinate lines for the inflection of the angular-dependent intex density at $\pi/2$ for the ground state of the helium atom with a) HF, and b) Kinoshita wave functions.

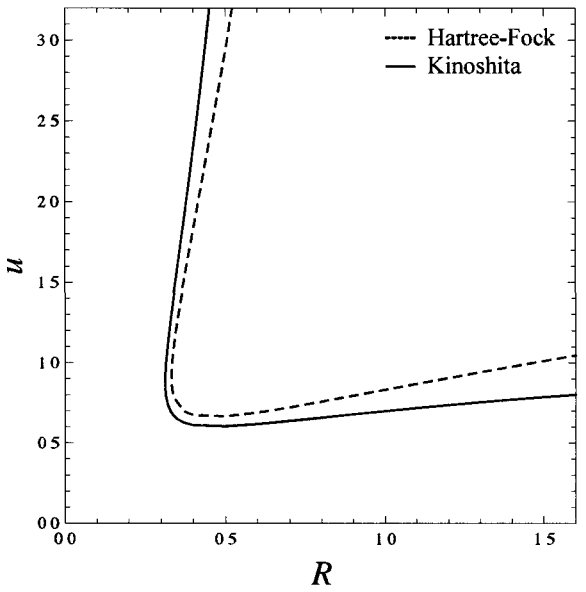

Figure 3.6: Critical coordinate line comparison for HF and correlated treatments for the ground state of the helium atom.

the known symmetry of the intex density for two-electron systems consisting solely of s-type orbitals of even parity.[87] The differences in this critical coordinate line for the HF and Kinoshita densities are fairly minimal but the region corresponding to configurations where the angular-dependent intex density reaches a maximum at $\theta_{Ru} = \pi/2$ is larger in HF systems. This is more evident in Figure 3.6 which displays the critical coordinate lines for both treatments overlaid. Approximate numerical integrations were performed to determine the percentage of the intex density that lies below this critical coordinate line. It was determined that for HF densities, configurations where $\theta = \pi/2$ represents a maximum in probability are roughly 31% of the density whereas this percentage decreases to approximately 23% for Kinoshita densities. This figure highlights some key differences about correlated systems. The critical line for the correlated system is extended towards both the R and u axes. Furthermore, the correlated critical line deviates from the HF line to a greater extent with respect to the u values than for the R values. This result is intuitive as one would expect correlation to have a greater effect on the interelectronic separation variable, u, than on the centre-of-mass variable, R.

With regards to the secondary Coulomb hole, it was noted in the previous chapter that the effects of correlation on the intex density are to increase the probability that electron pairs will be found with $R \approx u/2$ while systems treated with the HF method have greater probabilities for configurations with combined small u and large R values or large u and small R values. But these observations are limited by the fact that they were obtained by integration over the angular components of the $\boldsymbol{R}$ and $\boldsymbol{u}$ vectors. As we stated previously, R, u, and θ_{Ru} represent a complete set of coordinates for spherically symmetric systems; therefore, integrating over this angle leads to a loss of information. For this reason, we have explored the angular-dependent intex density, $X(R, u, \theta_{Ru})$, by taking slices at different values of θ_{Ru} much like we did previously for specific R and u values.

In the previous case, when we observed slices of $X(R, u, \theta_{Ru})$ at predefined R and u values, we chose to study the extrema of the intex correlation hole as there are countless possibilities of R and u coordinates that could have been chosen, but those were the main areas of interest. Here we have chosen to study $X(R, u, \theta_{Ru})$ using slices at every interval of 10° from 10° to 90°. As previously mentioned, the angular density is symmetric about $\theta_{Ru} = \pi/2$ by definition, and thus this range adequately represents all possible orientations of the $\boldsymbol{R}$ and $\boldsymbol{u}$ vectors. Contour plots of each of these slices are provided in Figure 3.7.

The information provided by these slices of the angular-dependent intex density are highly informative. Previously, we noted that correlation favours orientations where the centre of mass radius, R, is roughly twice the value of the interelectronic separation, u. This information was provided by the intex density which was previously unknown due to the limited information of the intracule density. However, from the data in this figure, we can see that this idea is also limited by the omission of the angular component in the intex density. These contour plots demonstrate that correlation only favours configurations where R is twice u at angles less than 30°. In fact, there are very few configurations that are favoured in correlated treatments when θ_{Ru} is greater than 30° which is consistent with electrons trying to avoid one another in correlated treatments. However, in every contour

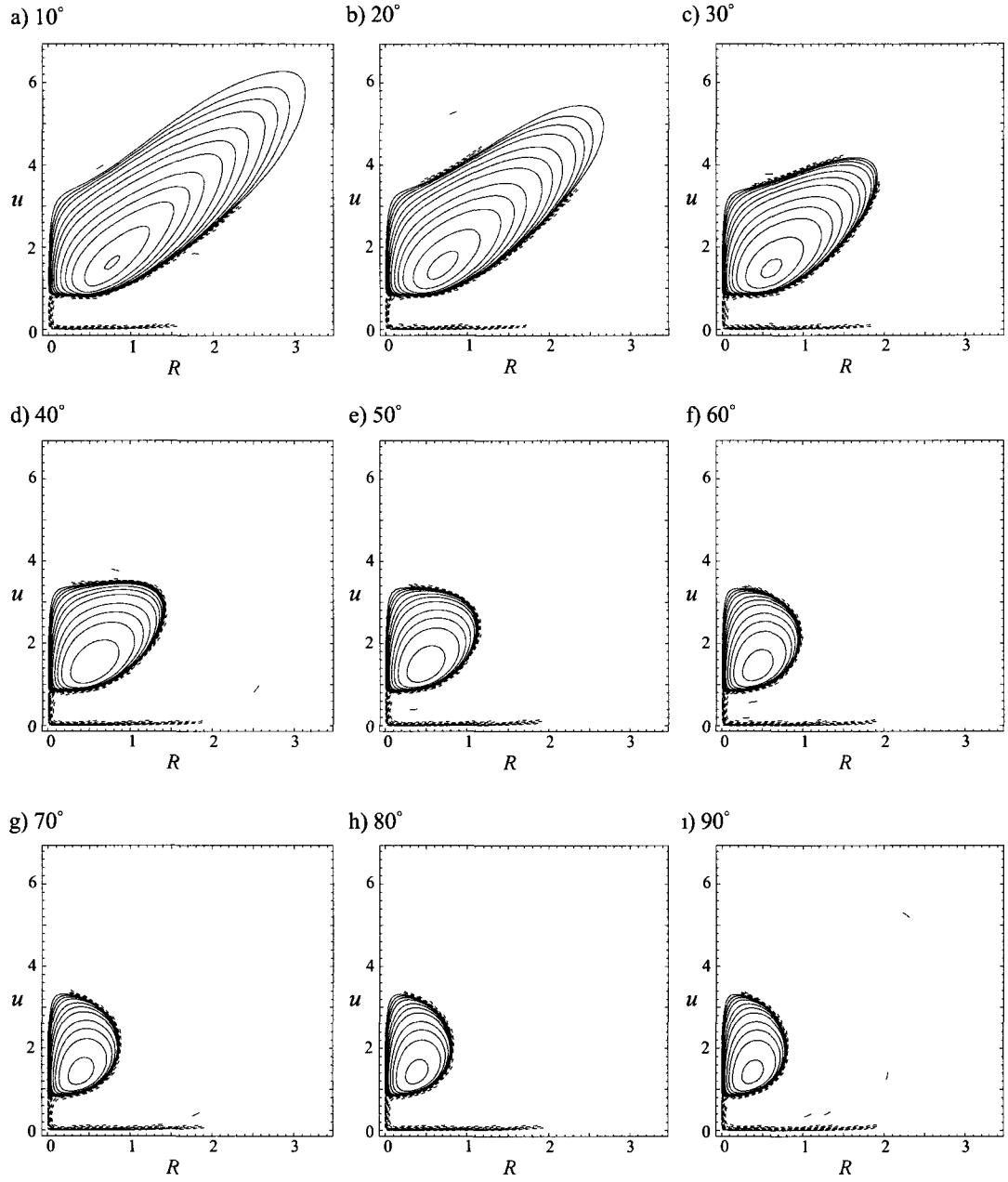

Figure 3.7: Slices of the angular-dependent intex correlation hole, $\Delta X(R, u, \theta_{Ru})$, at specific values of θ_{Ru}) for the ground state of the helium atom. Contours have values of ± 2 x 10^{-n}, ± 4 x 10^{-n}, and ± 8 x 10^{-m} where $n = 2 - 5$ and $m = 2 - 6$ Solid lines denote positive contours whereas dashed lines denote negative contours Slices were chosen in 10° intervals starting at 10° in a) up to 90° in i)

plot, a positive region at moderate u (roughly $0.8 < u < 3.2$) and small R values, indicate a preference for such configurations in correlated treatments. With these relative values of R and u, the electrons would likely be situated on opposite sides of the nucleus regardless of the value of θ_{Ru}, which is consistent with what would be expected in a correlated model due to angular correlation.

The information generated by these slices of the angular-dependent intex density are useful, but can we use it to gain more insight into the secondary Coulomb hole? In the comparison of correlated and HF treatments, the data indicate that under the HF approximation, there is a greater probability of having configurations with large values of u and small values of R regardless of the value of θ_{Ru}. However, at the larger angles (i.e. $\theta_{Ru} > 35°$), systems treated with HF theory demonstrate greater probabilities of having distant electrons at all values of R. Therefore, these configurations appear to contribute more substantially to the occurrence of the secondary Coulomb hole. Nonetheless, all configurations do contribute to some extent to this effect as evidenced by the negative contours at large u in every contour plot presented in Figure 3.7.

3.4 Conclusion

We have introduced the angular-dependent intex density $X(R, u, \theta_{Ru})$, isolated the angular component of this distribution, $A(\theta_{Ru})$, and used it to explore correlation effects in two-electron atoms. We have determined that exact treatments of these quantities favour angles closer to 0 or π between the $\boldsymbol{R}$ and $\boldsymbol{u}$ vectors while a HF treatment favours orientations where the angle is closer to $\pi/2$. Using the angular-dependent intex density to explore areas of interest in the intex correlation hole, it was noted that as R and u increase, the favoured angles for both HF and exact densities approach 0 and π. This reflects the fact that as R and u grow, the electrons and the nucleus can behave like three independent particles and thus θ_{Ru} will approach 0 or π to allow for one of the electrons to approach the nucleus and create a lower-energy configuration. In terms of the secondary Coulomb hole (which exists

at large u), given that correlation favours orientations where $R \approx u/2$ (see Figure 3.3)[87] we may conclude that it is also likely that the intex angle (θ_{Ru}) approaches 0 and π for these configurations and thus one electron remains relatively close to the nucleus while the other is far. We have demonstrated that the most probable angles can depend significantly on the values of R and u. Both the HF and near-exact Kinoshita densities predict that electrons will generally be equidistant from the nucleus at small R and/or u values. The angular intex density has proven to provide a more complete picture of electron-electron interactions and the effects of electron correlation.

4 Correlation Effects on Interelectronic Separations

4.1 Introduction

As mentioned previously, the simplest way to explore electron correlation effects is through the study of two-electron systems. Such systems have been studied extensively in the past and continue to be an area of focus today.[19,36,58,62,81,109–111] Coulson and Neilson's work clearly demonstrated that correlation pushes electrons further apart and this was considered to be an accurate description until the discovery of the secondary Coulomb hole. Prior to the paper by Pearson *et al.*[58] detailing this phenomenon, there were a few reports noting the presence of a secondary negative region in $\Delta P(u)$, but they were considered to be artefacts resulting from inaccurate wavefunctions.[48,59,60] However, the paper detailing this hole clearly indicated that the secondary negative region did not appear until the HF intracules reached a certain level of accuracy.

In Chapter 2, we described the intex density, $X(R,u)$, which again, details the electronic distribution with respect to the centre of mass radius, R, and the interelectronic distance, u.[87] Using this density to analyze the correlation hole, it was noted that correlation does not universally contract distant electron pairs. This contraction with respect to HF treatments was found to be dependent on the R variable (Figure 2.3a). In the previous chapter, we sought to expand our understanding of the secondary hole by studying the dependence of the intex distribution on the angle between the $\boldsymbol{R}$ and $\boldsymbol{u}$ vectors.

Although Chapters 2 and 3 did shed more light on correlation effects and the nature of the secondary Coulomb hole, they did not elucidate the origin of this counter-intuitive

effect. Other studies on systems such as the H_2 molecule[35,112] and spherium (a system where the movements of two electrons are confined to the surface of a hollow sphere)[111] have noted that when you increase the probability that the electrons will be far apart (i.e. lengthening the bond in H_2 or increasing the radius, R, in spherium), one eventually reaches a point where there is a complete reversal in the trend of the Coulomb hole. Thus, the primary and secondary negative regions decrease and increase in size, respectively, until the primary region vanishes entirely. At this point, HF treatments cause electrons to separate at all values of u.

In this chapter, we will discuss our studies regarding the correlation hole, $\Delta P(u)$, in systems containing traditional Coulombic potentials (real systems) and others containing alternative external potentials (fictional systems) to determine what effect, if any, the form of the potential has on the strength and/or existence of the secondary Coulomb hole. For the purposes of the study, HF energy and intracule calculations for the real systems were carried out using the Q-CHEM package[18] while Mathematica[76] was used to develop code for the fictional systems and for the exact real systems. Atomic units are used throughout.

4.2 Results

4.2.1 Real Systems

The study of correlation holes for the helium isoelectronic series has been well documented in the literature[41,58,74,75,80,87,113–116] as well as in the previous two chapters. With only two electrons in the system, the ground state electron configuration is given by $1s^2$ and thus, only s-type orbitals are required to accurately describe these systems. For the construction of the HF wave function, we employ the same set of even-tempered basis sets developed by Schmidt and Ruedenberg that were used in Chapters 2 and 3. Here, we have employed the same basis set consisting of 60 s-type Gaussians as that which was employed by Pearson and coworkers in their seminal paper on the secondary Coulomb hole.[58] The accuracy of

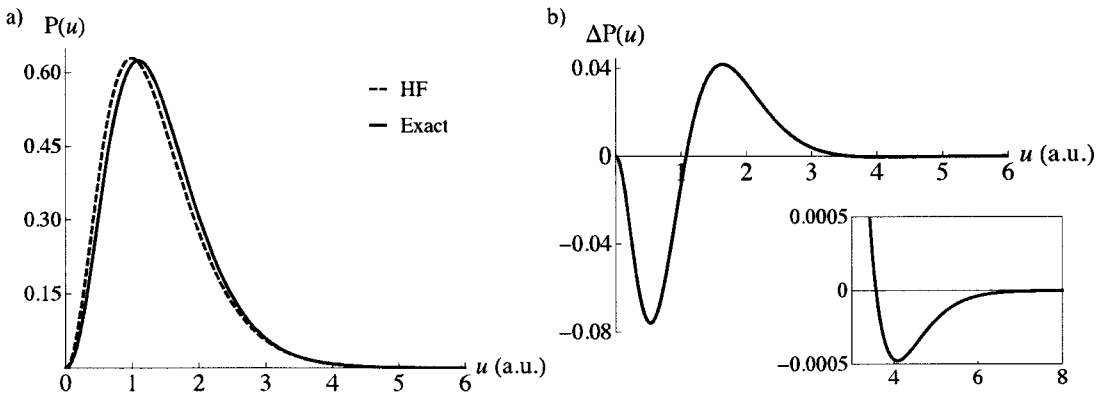

Figure 4.1: a) Exact and HF intracules and b) Coulomb hole, for the ground state of the Helium atom.

the intracules obtained from these basis sets is more than adequate for the requirements of this study. It should be noted that a basis set containing 30 or 40 Gaussian functions would be sufficient for these purposes; however, as intracule calculations can be performed rapidly relative to intex and angular intex calculations, a larger basis set was used to obtain a wave function closer to the HF limit.

Figure 4.1 displays both the Coulomb hole and the secondary Coulomb hole of the ground state of the helium atom. The Coulomb hole was also calculated for each of the ions of the helium isoelectronic series from $Z = 3$ to 10. Table 4.1 lists the strength of the secondary hole for each of these ions as well as three measures used to indicate how diffuse the electrons are within these systems (u_{max},$\langle u \rangle$, and $\langle u^2 \rangle$) in addition to the two-electron energy of the system ($\langle u^{-1} \rangle$). The first measure, u_{max}, is the value of u where the intracule density reaches a maximum. The last three measures are the moments of the position intracule which are given by

$$\langle u^n \rangle = \int_0^\infty u^n P(u)\, \mathrm{d}u \tag{4.1}$$

The three moments listed in the table each have a clear physical interpretation: $\langle u \rangle$ is defined as the average or mean value of u, $\langle u^2 \rangle$ can be related to the standard deviation, σ,

of the probability distribution by

$$\sigma = \sqrt{\langle u^2 \rangle - \langle u \rangle^2} \tag{4.2}$$

while $\langle u^{-1} \rangle$ is exactly equal to the sum of the Coulomb and exchange components of the HF energy. The values for all of these measures were obtained from the HF intracule. From the data listed in the table, it can be noted that as the atomic number increases, the first and second moments decrease indicating contracting electron density while the first negative moment increases which is indicative of stronger electronic repulsions as the electrons are drawn inward. Additionally, the size of the secondary hole decreases concomitantly. These measures provide a more quantitative measure of how the strength of the secondary Coulomb hole is related to the diffuseness of the electrons within the system.

We have attempted to develop a relationship between the size of the secondary Coulomb hole and these tabulated properties of the HF intracule. By developing such an empirical relationship, we can gain insight into what factors lead to the existence of the hole which allows for a more concrete understanding of the deficiencies of the HF model. Displayed

Table 4.1: Extrema/moments of the HF intracule and secondary Coulomb hole strengths for the He isoelectronic series.

Ion	Z	u_{max}	$\langle u \rangle$	$\langle u^2 \rangle$	$\langle u^{-1} \rangle$	Strength (S)
He	2	1.097	1.362	2.370	1.026	6.11 x 10^{-4}
Li^{+}	3	0.664	0.838	0.891	1.652	3.54 x 10^{-4}
Be^{2+}	4	0.475	0.606	0.464	2.277	2.33 x 10^{-4}
B^{3+}	5	0.370	0.474	0.284	2.902	1.71 x 10^{-4}
C^{4+}	6	0.303	0.390	0.191	3.527	1.34 x 10^{-4}
N^{5+}	7	0.256	0.331	0.138	4.153	1.09 x 10^{-4}
O^{6+}	8	0.222	0.287	0.104	4.778	9.20 x 10^{-5}
F^{7+}	9	0.196	0.245	0.0811	5.403	7.94 x 10^{-5}
Ne^{8+}	10	0.176	0.228	0.0651	6.028	6.97 x 10^{-5}

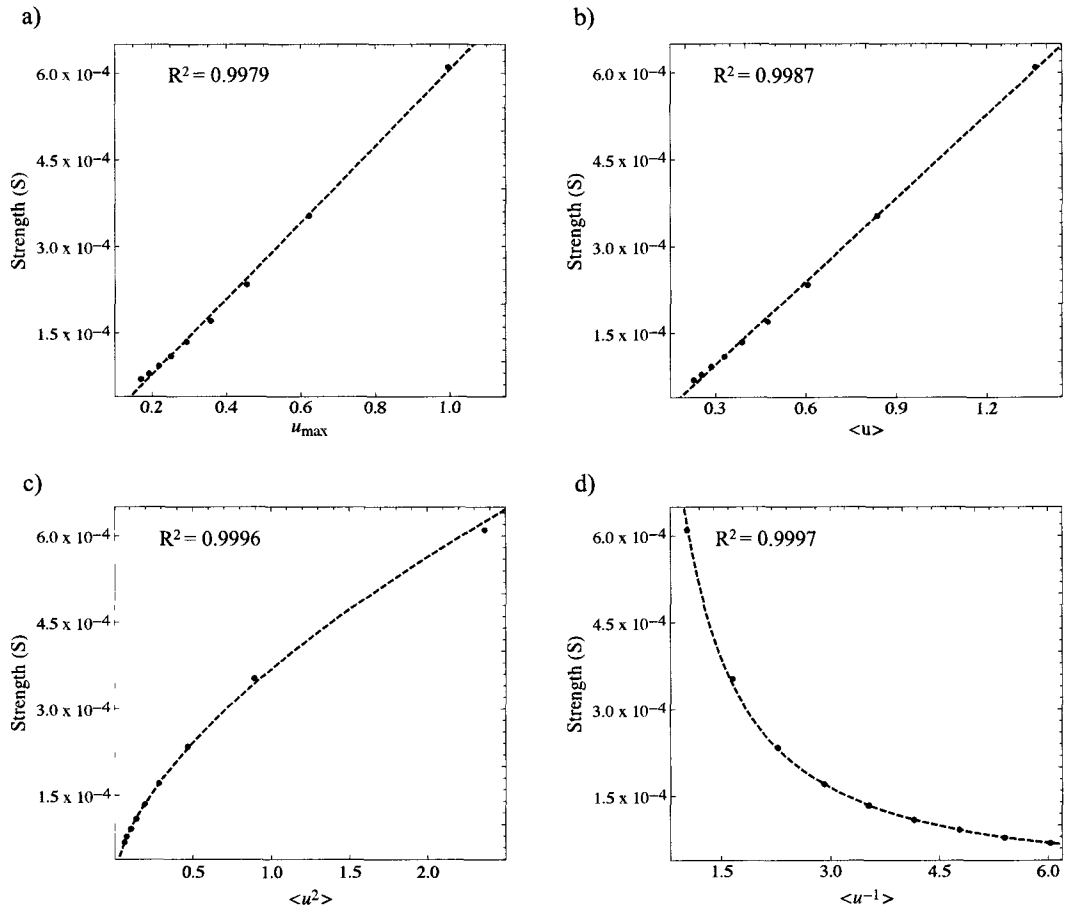

Figure 4.2: Linear (a and b) and power (c and d) function relationships between the strength of the secondary Coulomb hole and a) u_{max}, b) the first moment, $\langle u \rangle$, c) the second moment, $\langle u^2 \rangle$, and d) the first negative moment, $\langle u^{-1} \rangle$.

in Figure 4.2 are four of the relationships that were developed between the strength of the hole and each of the four quantitative measures listed in Table 4.1. There was no theoretical reasoning for choosing the type of trend line to employ for each of these relationships; they were simply chosen on a case by case basis to provide the best possible agreement with the results obtained from the calculations. However, polynomial fits were avoided whenever possible as one can easily fit any curve to a high order polynomial function. In addition to the relationships presented here, others were developed as well and these can be found in Appendix A.

This figure clearly demonstrates a strong correlation between the secondary Coulomb

hole and the properties studied here. Each of the R^2 values indicate very little deviance from the fit line suggesting that these models would be useful in predicting the size of secondary Coulomb holes. For the two linear plots, if one looks closely at the data points nearest the origin, it can be noted that there is a slight curvature of the data suggesting that the relationship is not exactly linear. Nonetheless, for the systems studied here, a linear relationship proves to be an accurate predictive model. However, one must keep in mind that each of these systems are single atoms containing two electrons. To determine the true value of these relationships as predictive models, one would have to include data involving atomic and molecular systems containing varying numbers of electrons.

4.2.2 Hookium

Hookium, Hk, is a well-documented[48,109,117–125] fictional system that is very similar to the He atom. It contains two electrons which are attracted to the centre of the system by an external potential (i.e. the nucleus). However, whereas in He, the two electrons are attracted to the protons contained within the nucleus, in Hk, the two electrons are bound to the "nucleus" by a harmonic potential. Thus one can think of the two electrons as being bound to springs, with force constants k, that emanate from the centred origin. From Hooke's Law,[1] we know that

$$\vec{F} = -k\Delta\vec{r} \tag{4.3}$$

where the negative sign simply indicates that the direction of the force, $\vec{F}$, is opposite that of the displacement, $\Delta\vec{r}$. The potential energy, V, stored in the spring is then given by the integral of the force expression over the distance which gives us

$$V = \frac{1}{2}kr^2 \tag{4.4}$$

In terms of the quantum mechanical representation of Hk and He, the potential energy operator is the only difference between the two systems. The Coulombic potential of He is

replaced by the harmonic potential of hookium. Therefore, the Hamiltonian for Hk is given by

$$\hat{H} = -\frac{1}{2}\nabla_1^2 - \frac{1}{2}\nabla_2^2 + \frac{1}{2}kr_1^2 + \frac{1}{2}kr_2^2 + \frac{1}{r_{12}} \tag{4.5}$$

where the Coulombic potential of He, $V = -\left(2r_1^{-1} + 2r_2^{-1}\right)$, is replaced by the harmonic potential expression given by (4.4).

It has been noted that when $k = 1/4$, the Schrödinger equation for hookium is exactly solvable with an energy of exactly 2 E_h.[117] The exact wave function obtained from this solution is

$$\Psi(\boldsymbol{r}_1, \boldsymbol{r}_2) = \frac{1}{2\sqrt{8\,\pi^{5/2} + 5\,\pi^3}} \left(1 + \frac{r_{12}}{2}\right) \exp\left(-\frac{r_1^2 + r_2^2}{4}\right) \tag{4.6}$$

From this wave function, a simple closed-form expression of the position intracule, $P(u)$, can be derived which is given by

$$P(u) = \frac{1}{8 + 5\,\pi^{1/2}}\, u^2 \left(1 + \frac{u}{2}\right)^2 \exp\left(-\frac{u^2}{4}\right) \tag{4.7}$$

There have been a number of methods reported in the literature of different types of basis functions used to construct the HF wave function.[48,119,122] The most accurate HF energy to date was reported by Ragot[119] who proposed the use of a HF orbital expansion of the form

$$\psi^{HF}(r) = \eta_n \sum_{i=0}^{n} c_i (-1)^i \frac{\partial^i}{\partial \alpha^i} \exp(-\alpha r^2) \tag{4.8}$$

where c_i is the scaling orbital coefficient for each term of the expansion and η_n is the normalization constant given by

$$\frac{1}{\eta_n^2} = \sum_{i=0}^{n} \sum_{j=0}^{n} c_i c_j (-1)^{i+j} \frac{\partial^i}{\partial \alpha^i} \frac{\partial^j}{\partial \beta^j} \left(\frac{\pi}{\alpha + \beta}\right)^{3/2}. \tag{4.9}$$

In the previous two expressions, α and β are the Gaussian exponents. In this case, both α and β were chosen to be $\frac{1}{4}$. Using this expansion with $n = 11$, the author noted a HF energy

of 2.0384388718 E_h with a convergence on the order of 10^{-10}. The problem remains to calculate a HF intracule from this expansion which is not trivial; however, the author also suggested a closed form approximation to the previous expansion. This proposed HF orbital was given by

$$\psi^{HF} = \eta_{HF} \exp(-\alpha r^2) \sqrt{r^2 + \beta^2} \tag{4.10}$$

where α and β are both parameters to be optimized and the normalization constant η_{HF} is

$$\eta_{HF} = \frac{2(2/\pi)^{3/4} \alpha^{5/4}}{\sqrt{3 + 4\alpha\beta^2}} \tag{4.11}$$

By optimizing the energy with respect to the two parameters, this HF orbital led to an energy of 2.0384394491 E_h where the parameters were optimized at $\alpha = 0.251117376$ and $\beta = 2.711087898$.[119] This energy value is only 5.8×10^{-7} E_h greater than the HF limiting energy given by the aforementioned orbital expansion.

With no definitive way of determining the accuracy of the intracule obtained from the latter method employed by Ragot, we also explored the approach used by O'Neill and Gill in their study of Hookium.[48] This group considered two different types of basis functions to develop accurate HF wave functions. The first method involved the use of harmonic-oscillator eigenfunctions which are comprised of Hermite polynomials.[126]

$$\phi_k(r) = \frac{H_{2k-1}(r/\sqrt{2})}{2^k \sqrt{(2k-1)!}\, r/\sqrt{2}} \frac{\exp(-r^2/4)}{(2\pi)^{3/4}} \tag{4.12}$$

Here, $H_k(x)$ is the kth Hermite polynomial given by

$$H_k(x) \equiv \frac{k!}{2\,\pi\,i} \oint \exp(-t^2 + 2\,t\,x)\, t^{-k-1}\, \mathrm{d}t = (-1)^k \exp(x^2) \frac{d^k}{d\,x^k} \exp(-x^2) \tag{4.13}$$

where $\oint$ is a contour integral, i is the imaginary unit ($i = \sqrt{-1}$), and $k!$ denotes the factorial

of k. Using this set of basis functions, the HF orbital is given by the expansion

$$\psi(r) = \sum_{k=1}^{N} c_k \, \phi_k(r) \tag{4.14}$$

With a basis set comprised of $N = 7$ basis functions, the authors determined that the energy of hookium was $E = 2.03843887\ E_h$ with the determined convergence of the energy to be on the order of 10^{-8}. However, due to the relatively complicated nature of the basis functions, they instead employed an expansion of Gaussian basis functions to obtain a good approximation for the wave function. The exponents of the Gaussian functions that were used appear to be based on a randomly selected geometric series with a few exponents in the middle of the set optimized to obtain a more accurate energy. The exponents used were the set, {0.0375, 0.0750, 0.23185, 0.30241, 0.37297, 0.6000, 1.2000, 2.4000}, which produced an energy of 2.0384390 E_h.[48]

Here we employ a similar strategy as the latter approach by O'Neill *et al.*[48] Using a method analogous to that developed by Schmidt and Ruedenberg[65] for the development of even-tempered basis sets, we generated lists of K exponents for s-type Gaussian primitives and determined which exponents produced the lowest energy for a given set of K basis functions. The formula used to generate the exponents is that which is given by (2.13). The Gaussian exponents, ζ, were obtained simply by optimizing α and β through brute-force analysis for each different expansion size, K. We initially attempted to determine values for the parameters for a, a', b, and b' as done by Schmidt and Ruedenberg (equations (2.14) and (2.15)); however, this method did not yield good results, and it was abandoned in favour of optimizing the values of α and β for each individual case. Using an expansion of only 7 Gaussians, an energy of $E = 2.03843887175\ E_h$ was obtained with a convergence on the order of 10^{-10}. This energy is of the same accuracy as the most accurate report to date by Ragot[119] but uses a simpler and more conventional basis set. Using the obtained Gaussian exponents, the HF position intracule was then calculated as per normal methods. Expan-

Table 4.2: Optimized parameters for s-type Gaussians of Hookium for basis set size, K.

K	α	β	$E\ (E_h)$
3	0.19436	1.24033	2.038 438 879
4	0.16115	1.20012	2.038 438 875
5	0.15281	1.24221	2.038 438 874
6	0.14990	1.26600	2.038 438 871 76
7	0.15554	1.24550	2.038 438 871 75

sions of $K = 3, 4, 5, 6$ Gaussians were also used to determine the level of convergence of the energy as well as the accuracy of the position intracule. The maximum error associated with the intracule, P_{err} was assessed by the following expression

$$P_{err} = \int_0^\infty |P_7^{HF}(u) - P_6^{HF}(u)| \mathrm{d}u \tag{4.15}$$

where $P_K^{HF}(u)$ is the position intracule obtained from the HF wave function using a basis set consisting of K Gaussian functions and $|x|$ denotes the absolute value of the enclosed functions. It was determined that $P_{err} = 1.65 \times 10^{-9}$ which was deemed sufficient for the purposes of the study. Table 4.2 describes the values of the optimal α and β parameters for each basis set expansion as well as the associated energy.

Figure 4.3 displays the intracules for the exact and HF wave functions in a) while the correlation hole and an inset of the secondary Coulomb hole are shown in b). Relative to the secondary Coulomb holes for the He isoelectronic series, the strength of the hole in Hk is only on the order of 10^{-8}. The reasons for this significantly weaker secondary hole will be explored in the discussion section of this chapter.

4.2.3 Ballium

The particle-in-a-box (PIB) model is well known to both theoreticians and non-theoreticians in the fields of chemistry and physics.[1,5] It effectively restricts the movement of a particle

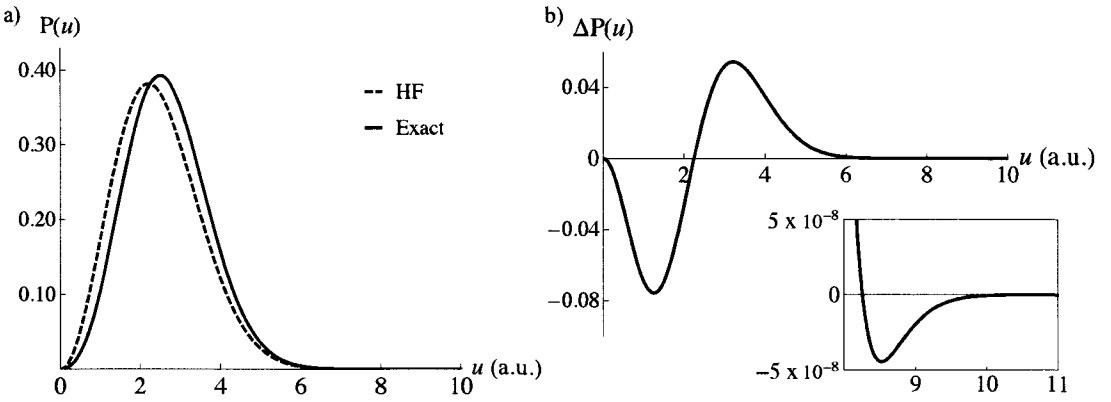

Figure 4.3: a) Exact and HF intracules and b) Coulomb hole, for the ground state of the Hookium atom.

to within the confines of a specific area by imposing an infinite external potential at the walls of this region (box). For a one-dimensional box of length ℓ, the external potential, $V(x)$, can be expressed by

$$V(x) = \begin{cases} 0 & 0 < x < \ell \\ \infty & \text{otherwise} \end{cases} \tag{4.16}$$

where x is the position coordinate of the electron along the length of the box. From this expression, it is clear that there is a zero or constant potential exerted on the particle within the box, unlike the cases with Coulombic potentials in real systems or the harmonic potential in the case of Hookium. Therefore, the electron or electrons move freely within the boxed area.

For the simple case of a single particle in a box, there is a very well known solution.[1,5] However, in recent years, there has been a focus on systems of interacting particles (i.e. two electrons) in boxes of varying shapes and numbers of dimensions. Such systems are far more complicated as they involve the interelectronic interaction term which makes the Schrödinger equation inseparable. The two-particle systems studied to date include cylindrical boxes,[127] 2-D rectangular (or 3-D cuboidal) boxes,[128,129] and spherical boxes[110,130–135] to name a few. For the purposes of this study, we have focussed on the

spherical boxes which are commonly referred to as D-ballium, where D represents the dimensionality of the system. For the sake of comparison with the He and Hk cases, 3-ballium was analyzed in this study.

The Hamiltonian operator for the 3-ballium system[110] is defined as

$$\hat{H} = -\frac{1}{2}\nabla_1^2 - \frac{1}{2}\nabla_2^2 + V(r_1) + V(r_2) + \frac{1}{r_{12}} \tag{4.17}$$

where the one-electron potential energy operators, $V(r_i)$, much like those defined for the PIB model are given by

$$V(r_i) = \begin{cases} 0 & 0 < r_i < R \\ \infty & \text{otherwise} \end{cases} \tag{4.18}$$

When dealing with ballium, it is convenient to define the wave function in terms of a scaled coordinate vector $\boldsymbol{t} = \boldsymbol{r}/R$ in order to effectively scale all radii to unity.[110] For the HF wave function, the chosen basis functions must obey the condition that $\Psi(\boldsymbol{r_1}, R) = \Psi(R, \boldsymbol{r_2}) = 0$ where R is the radius of the ball, and the wave function should vanish for any electronic scalar coordinates greater than R. The two most accurate results to date for this system have been published by Thompson and Alavi[135] who used a basis set consisting of spherical Bessel functions and Loos and Gill[110] who employed an even-degree polynomial basis. Here, we employed the basis designed by Loos and Gill as it has demonstrated higher accuracy with greater numbers of basis functions. As we were uncertain what level of accuracy would be required for studies of the secondary Coulomb hole, we opted for the most accurate description that has been published to date.

The basis functions of Loos and Gill are given by[110]

$$\phi(\boldsymbol{t}) = (1 - t^2)\sum_{k=0}^{K-1} c_k \boldsymbol{t}^{2k} \tag{4.19}$$

where K is the number of basis functions in the expansion and $\boldsymbol{t}$ is the aforementioned scaled electronic coordinate. One can note the presence of the $(1 - t^2)$ factor in the expression which forces the function to be equal to zero when $t = 1$ (i.e. $r = R$). In order to account for the piecewise definition of the one-electron potential energy operator, these same restraints were placed on the wave function using the Mathematica package.[76] With a constant (zero) potential acting on the electrons within the sphere, it can be shown that the energy of the system is given as

$$E_{HF} = \frac{\eta^2}{R^2}\langle\hat{T}\rangle + \frac{\eta^4}{R}\langle\hat{J}\rangle \tag{4.20}$$

where $\langle\hat{T}\rangle$ and $\langle\hat{J}\rangle$ are the expectation values of the kinetic energy and Coulomb operators, respectively, and η is the normalization constant given by

$$\frac{1}{\eta^2} = 8\sum_{i=0}^{\omega}\sum_{j=0}^{\omega} c_i c_j \frac{[2(i+j-1)+3]!!}{[2(i+j+2)+3]!!}. \tag{4.21}$$

In the previous equation, the values of 3 represent the number of dimensions of the ball and [x]!! denotes the double factorial[126] of x which is a piecewise function defined as

$$x!! = \begin{cases} x\cdot(x-2)\cdot(x-4)\ldots 5\cdot 3\cdot 1 & \text{if } x > 0 \text{ and odd}\ , \\ x\cdot(x-2)\cdot(x-4)\ldots 6\cdot 4\cdot 2 & \text{if } x > 0 \text{ and even}\ , \\ 1 & \text{if } x = -1 \text{ or } x = 0 \end{cases} \tag{4.22}$$

The scaling coefficients, c_i, for the basis functions were determined variationally through built-in minimization algorithms in the Mathematica[76] package by minimizing (4.20) with respect to the coefficients.

Unlike hookium, there is no exact solution to the Schrödinger equation for 3-Ballium. However, Loos and Gill devised a wave function much like those developed by Hylleraas

in the late 1920s.[30,73] The wave function, which is explicitly correlated, is of the form[110]

$$\Psi(r_1, r_2, u) = \sum_{i=0}^{\omega} \sum_{j=0}^{i} \sum_{k=0}^{\omega} c_{ijk}(1 + \hat{P}_{12})\psi_{ijk}(r_1, r_2, u) \tag{4.23}$$

where $\hat{P}_{12}$ is the previously described permutation operator which ensures antisymmetry of the wave function. The basis functions in this expression, ψ_{ijk}, are defined by

$$\psi_{ijk} = (1 - x^2)(1 - y^2)x^{2i}y^{2j}z^k \tag{4.24}$$

where x, y, and z are scaled coordinates representing respectively, r_1, r_2, and u, as

$$x = \frac{r_1}{R} \qquad y = \frac{r_2}{R} \qquad z = \frac{u}{R} \tag{4.25}$$

Two of the sums in (4.23) are up to ω, which is a value used to control the number of basis functions in the expansion. The relationship between ω and the number of basis functions, K, is[110]

$$K = \frac{(\omega + 1)^2(\omega + 2)}{2} \tag{4.26}$$

Once again, the reader can note that the correlated wave function contains the factor of $(1 - x^2)(1 - y^2)$ which forces the wave function to vanish when either electron is at the boundary of the sphere.

One may recall from the introduction, that the orbital energies in the HF method are given from the eigenvalues of $\boldsymbol{X}^\dagger \boldsymbol{F} \boldsymbol{X}$ where $\boldsymbol{X}$ is as described in the introduction (i.e. $\boldsymbol{X} = \boldsymbol{S}^{-1/2}$). Similarly, for correlated wave functions of this form, the ground state energy of the system is given by the lowest eigenvalue[110] of

$$\boldsymbol{X}^\dagger(\boldsymbol{T} + \boldsymbol{J})\boldsymbol{X} \tag{4.27}$$

where $\boldsymbol{T}$ and $\boldsymbol{J}$ are the kinetic and electron repulsion matrices, respectively. Furthermore,

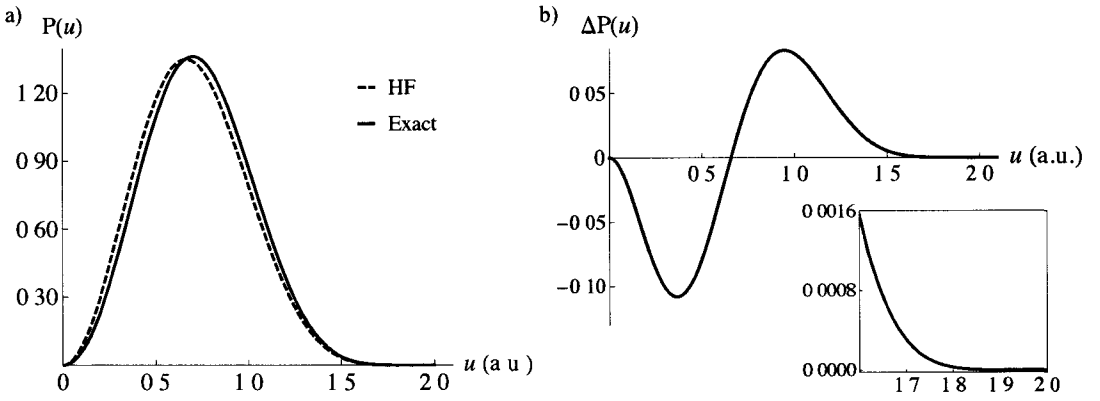

Figure 4.4: a) Exact and HF intracules and b) Coulomb hole, for the ground state of the 3-Ballium atom.

the coefficients of the basis functions, c_{ijk}, are given by the eigenfunctions of this product of matrices.

When determining the position intracule from the correlated wave function, since the u variable is incorporated explicitly, one simply integrates over the x and y coordinates. However, as before, since this is a confined system, one must impose the following restraints on each of the variables:

$$0 \leq x \leq 1 \qquad 0 \leq y \leq 1 \qquad |x-y| \leq z \leq x+y \tag{4.28}$$

Performing such actions would yield the intracule with respect to z, i.e. $P(z)$; however, one can obtain the true intracule, $P(u)$, by simply replacing z with its definition from (4.25).

Using this methodology, and that described for the HF treatment, we obtained the position intracules for a number of 3-ballium systems with varying radii, R (1, 3, 4.5, 5, 10, 20). An example is shown in Figure 4.4 with the Coulomb hole displayed on the right-hand side. As noticed by the magnified inset of the Coulomb hole, there is no detectable secondary negative region for these systems. We also performed analyses with UHF wave functions with the same set of basis functions but these results were identical to those obtained using the RHF wave functions. However, there are issues associated with using the present basis functions for UHF analyses and these will be discussed in the next section.

4.3 Discussion

From the results shown in Figures 4.1-4.3, it is obvious that the type of external potential involved in a system has a significant effect on the strength and/or presence of the secondary Coulomb hole. We explored three distinct two-electron cases in this study: 1) helium with a traditional Coulombic potential, 2) hookium with a harmonic potential, and 3) 3-ballium with a potential of zero inside of the sphere and an infinite potential at the boundaries. The strength of the secondary hole in each of these cases is summarized in Table 4.3 below. Additionally Figure 4.5 details the one-electron external potential for each of the cases and the accompanying secondary Coulomb holes.

The data suggest that as the form of the external potential is modified, there is a noticeable change in the secondary hole. From the Coulombic potential in helium to the harmonic potential in hookium, the secondary hole strength decreases by **four** orders of magnitude. Moreover, employing a potential of zero inside the bounds of the system, the secondary hole ceased to exist.

The results obtained for 3-Ballium at a number of radii suggest that the secondary Coulomb hole may not exist in the absence of a non-zero potential or restoring force. However, for spheres with larger radii, the RHF approximation becomes increasingly inaccurate. Thompson and Alavi[135] have noted that the RHF and UHF solutions begin to differ at $r_s \approx 6$ where r_s is defined as

$$r_s = \frac{R}{2^{1/3}} \tag{4.29}$$

Table 4.3: Relating the strength of the secondary hole to the external potential.

System	Potential	Secondary Hole	Strength (S)
Helium	Coulombic	Yes	6.1×10^{-4}
Hookium	Harmonic	Yes	3.1×10^{-8}
3-Ballium	Constant (Zero)	No	N/A

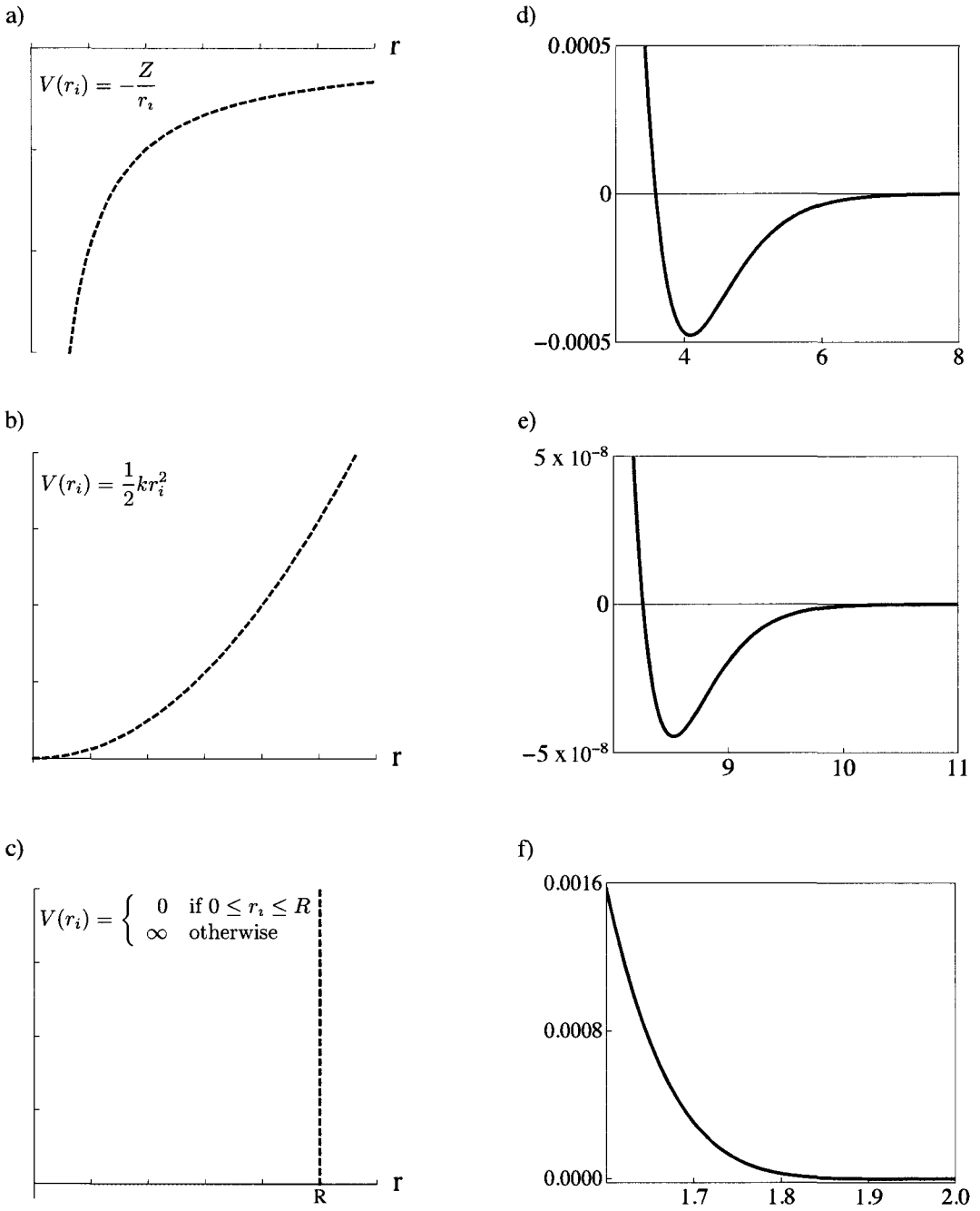

Figure 4.5: Graphical representation of the one-electron external potentials of a) helium, b) hookium, and c) 3-ballium along with their respective secondary Coulomb holes given in d)-f).

Therefore, using the RHF method beyond radii of approximately 4.8 au yields inaccurate descriptions of the wave function, and in turn, the position intracule. However, with a radius of 4.8 au, the electrons can separate by nearly 9.6 au in this system. If we consider ballium to be comparable to the real systems with Coulombic potentials, it would be somewhat analogous to the case when $Z = 0$. Since, the occurrence of the secondary Coulomb hole shifts to higher values of u with lower nuclear charges, the secondary hole in ballium would be furthest out compared to the systems of the helium isoelectronic series studied here. However, the secondary Coulomb hole does begin at 3.4 au in helium, and thus one might expect that it would occur at some point in the ball with a radius of 4.8 au where the RHF model provides an accurate description.

As noted previously, we have used the UHF method to analyze the 3-ballium system but our results did not differ from those obtained using the RHF method at all values of R. This is due to the spherical symmetry of the basis functions employed in the study which prevents the breaking of this form of symmetry required to allow for a different UHF solution. The basis set employed by Thompson and Alavi does allow for symmetry breaking and they noted more accurate (i.e. lower) energies for the UHF systems for $r_s > 6$. Analyses using this same basis set should be performed in the future to determine the true nature of long range correlation effects in ballium.

Regardless, there is still a great deal of information suggesting that the secondary hole will not exist for the ballium system. When considering ballium, there are two extreme scenarios that can be considered. The first is that it follows the series of the helium isoelectronic series. From Table 2.2, it can be noted that the strength of the hole increases with decreasing atomic number Z. In this case, ballium could be considered to be similar to the $Z = 0$ case and one would expect the secondary hole to be the largest of any of the systems studied here. However, this is obviously not observed in this study.

The second extreme is the scenario that we did observe. With no potential drawing these electrons centrally, the secondary Coulomb hole does not exist. This suggests that an

attractive external potential is the origin of the secondary hole and our theory is that it is caused by an inadequate description of screening in the HF method.

Consider the cases which have been studied in the literature thus far. The first report detailed the secondary Coulomb hole in the helium isoelectronic series with the hole strength decreasing as the nuclear charge increased.[58] As we increase the atomic number, the electrons contract towards the nucleus and in order to avoid one another, they are more likely to move to opposite sides of the nuclei even under the HF approximation. Such configurations would minimize the effects of screening since the two electrons would no longer be interfering with the respective attraction to the nucleus or origin.

The second case published in the literature was the study of the H_2 molecule and the effect on the secondary hole as the bond length was stretched.[35] In this case, the size of the secondary negative region actually surpassed that of the primary negative region as the bond length increased beyond 3.0 au. More recently, Hollett *et al.*[112] noted that as the bond length increases past 3.6 au, one observes a complete reversal of the correlation hole, i.e. HF pushes electrons further apart at all values of u. This is indicated by an initial positive region followed by a negative region in the graph of $\Delta P(u)$. The authors claimed that this is due to overlocalization of the molecular orbitals in the UHF approach. However, consider what this could mean in the context of screening. If the HF method overestimates screening on distant electrons, the two electrons will likely reside near their respective nuclei shielding one another strongly from the opposite nucleus. This would likely cause an overlocalization of the UHF orbitals compared to the exact system where the electrons would reside more in the bonding region.

The most recent study that has been published focussed on the fictional atom, spherium.[111] In this system, the motions of the two electrons are confined to the surface of a sphere of radius R. Much like the H_2 molecule, a reversal of the correlation hole was noted at large values of R. As this system does not have a non-zero *attractive* external potential, one can say that this is obviously not the defining factor for the presence of a secondary Coulomb

hole. However, remember that the electrons in this system are confined to move on the surface of the sphere. Therefore, they will always be the same distance from the centre of the system and even if there were a "traditional" nucleus at the origin, the electron nuclear attraction energy would be a constant. Recall from Chapter 1 that the expectation value of a constant operator does not affect the eigenfunctions of the full operator (i.e. nuclear repulsion operator as part of the Hamiltonian operator) but simply adds said constant to each of the eigenvalues. This is effectively the same scenario that we are faced with here. Even if we place a nucleus with protons at the centre of this system, the wave function will not change. The energy of the system will change, but the wave function will remain the same. The spherium system simply differs to much from the other systems to draw significant conclusions from these results. However, it should be noted, that due to the unorthodox nature of this system, the presence of the secondary Coulomb hole in spherium does not necessarily contradict the hypothesis that screening is the cause.

Another piece of evidence suggesting that the secondary Coulomb hole will not exist in the true UHF solution of ballium stems from the fact that **all** other systems which have demonstrated this phenomenon have shown it when studied using the RHF model. For the real atomic/ionic systems in the He isoelectronic series, the RHF solution is the only solution (i.e. UHF is identical), but for H_2 and spherium, at relatively small bond lengths/radii, correlation holes calculated with the RHF solution demonstrate the secondary Coulomb hole and these holes remain at large separations where RHF theory provides an inadequate description. The fact that ballium does not demonstrate this hole even with radii of 4.5 au suggests that even when treated at the UHF level of theory, this effect will not be present.

This idea that HF systems have a greater probability of having distant electrons is not a new one; but it is new for ground states. The Coulomb holes of excited states have been well documented in the literature[136–140] and they all express significant negative regions at large values of u. These systems can be considered an extreme case for shielding of valence electrons by electrons in inner shells, which is much greater than that by electrons in the

same shell. In fact, Thakkar[139] stated the following in a paper detailing the Coulomb hole for excited states of helium:

> *Counter-intuitive effects such as an increase in interelectronic repulsion upon inclusion of electron correlation occur for helium and smoothly disappear as the atomic number increases.*

This quote demonstrates that even in excited states, it was unexpected. But as discussed, as the atomic number increases, the size of the negative region decreases as there would be less shielding as the electrons are drawn closer to the nucleus. In a separate report, Ugalde *et al.*[138] identified the cause of this effect in excited states as shielding as noted below:

> *Electron correlation is shown to reduce the nuclear shielding provided by the K-shell distribution and as a consequence, to lead to a relative shrinking of the outer shell density*

This describes the exact effect that we are observing here. Shielding would not be nearly as great for electrons in the same shell, but it would still be present. This provides a logical explanation as to why the secondary hole is large in excited states and largely unnoticeable in the ground state. To be certain that shielding is the cause of the secondary hole, we must obtain the results using the true UHF intracule for ballium; however, based on the evidence presented here, it is hypothesized that the secondary Coulomb hole is a *nuclear* effect.

4.4 Conclusion

We have analyzed the effect of the external potential on the shape of the Coulomb hole. It has been noted that the secondary Coulomb hole is most strongly expressed in real systems with Coulombic potentials and while it is still present for Hookium with its harmonic potential, the strength of the hole decreases significantly. The results obtained thus far for 3-ballium have indicated that this phenomenon does not occur; however, further studies

need to be conducted for confirmation. Nonetheless, based on the evidence presented here, and past work reported in the literature, it is anticipated that the secondary Coulomb hole will not be present in ballium or any other system lacking an attractive potential.

5 Polarization Effects on Interelectronic Separations in Atoms and Molecules

5.1 Introduction

The previous three chapters focussed on the development of novel tools for the study of electronic structure and their application to the study of correlation effects in two electron systems. In this chapter, we change gears and focus not on correlation effects but the effects of the addition of polarization functions to a basis set.

As discussed in Chapter 1, the variational theorem states that by using a normalized trial wave function, ϕ_G, the ground state energy obtained will always be greater than or equal to the exact ground state energy for a particular system.[5] As it is often impossible to solve the Schrödinger equation exactly, this theorem is highly useful since it acts as a measure of the accuracy for a given ϕ_G, as improvements in the trial wave function would be evidenced by lower ground state energies for the system.

Recently, Pearson *et al.* reported their studies on basis set effects on position, $P(u)$, and dot, $D(x)$, intracules.[54] This report explored the HF intracule, $P^{\text{HF}}(u)$, using wave functions expanded in a variety of basis sets. These intracules were then compared to a large reference basis (in that case 6-311++G$(3df, 3pd)$) to detect any differences between the intracules of the large, highly polarized, reference basis and those obtained from the smaller basis sets. This difference was denoted $\Delta P(u)$, not to be confused with the Coulomb hole[36] which is traditionally defined as $\Delta P(u) = P^{\text{Exact}}(u) - P^{\text{HF}}(u)$. $\Delta P(u)$ in this instance is

given by

$$\Delta P(u) = P^{\text{Ref}}(u) - P^{B_i}(u) \tag{5.1}$$

where $P^{\text{Ref}}(u)$ is the intracule obtained using the reference basis set and $P^{B_i}(u)$ is the intracule obtained from using any of the other basis sets employed in the study. The work indicated that upon the inclusion of polarization functions into the basis sets for the systems of the G1 test set, $\Delta P(u)$ displayed a so-called "basis antihole". This is opposite to the effect that is seen for the Coulomb hole[36,58] as polarization causes electron pairs to contract, whereas correlation often causes electrons to be further apart. This basis antihole implies that incorporating polarization functions leads to an increase in electron repulsion energy (denoted by E_J), by drawing electrons closer together. One might expect that due to the presence of the higher angular momentum orbitals and an increased flexibility in the basis set, the electrons would move more freely and the electron-electron repulsion energy would decrease; however, this is not the case.

Here, we examine why systems studied with polarized basis sets display the basis antihole and greater two-electron energies (E_{ee}) compared to their respective unpolarized counterparts. From the variational theorem, we know that as the basis set improves, the energy must decrease and thus we also explore the other components of the energy to determine which ones compensate for this decrease in E_{ee}. For the purposes of this study, all energy and intracule calculations were performed using Q-CHEM.[18] Atomic units are used throughout this chapter.

5.2 Results and Discussion

5.2.1 Basis Set Dependence in Intracules

Expanding the HF wave function in a one-electron basis set, the position intracule $P(u)$ can be expressed as

$$P(u) = \sum_{\mu\nu\lambda\sigma} \Gamma_{\mu\nu\lambda\sigma} [\mu, \nu, \lambda, \sigma]_P \tag{5.2}$$

where $[\mu, \nu, \lambda, \sigma]_P$ are the intracule integrals and $\Gamma_{\mu\nu\lambda\sigma}$ is the usual two-particle density matrix.[44] The $[ssss]_P$ integrals are well-known, while the integrals containing orbitals of higher angular momenta can be obtained either through differentiation as suggested by Boys,[141] or by using the recurrence relation recently developed by Hollet *et al.*[142] These intracule integrals have also been implemented into the Q-CHEM package[18] for orbitals with angular momenta up to $\ell = 3$.

For the purposes of this study, position intracules were calculated for each of the atoms and molecules of the G1 test set[143] with the exception of the hydrogen atom as it contains only a single electron. These intracules were constructed from HF wave functions expanded from basis sets of increasing complexity. The basis set comparisons employed in this study are as follows:

(1) 6-31G vs 6-31G(d,p)

(2) 6-311G vs 6-311G(d,p)

(3) 6-311++G vs 6-311++G(d,p)

(4) 6-311++G(d,p) vs 6-311++G(3d,3p)

(5) 6-311++G(3d,3p) vs 6-311++G(3df,3pd)

(6) cc-VDZ vs cc-pVDZ

(7) cc-VTZ vs cc-pVTZ

where cc-VDZ and cc-VTZ are the non-polarized parts of the respective Dunning's correlation consistent basis sets.[16,144] From this set of comparisons, with the exception of cases (4) and (5), it can be noted that each set contains basis sets with and without polarization functions. In cases (4) and (5), the comparisons were performed to explore the effects of increasing levels of polarization within the basis sets. Thus, in contrast to the earlier work[54]

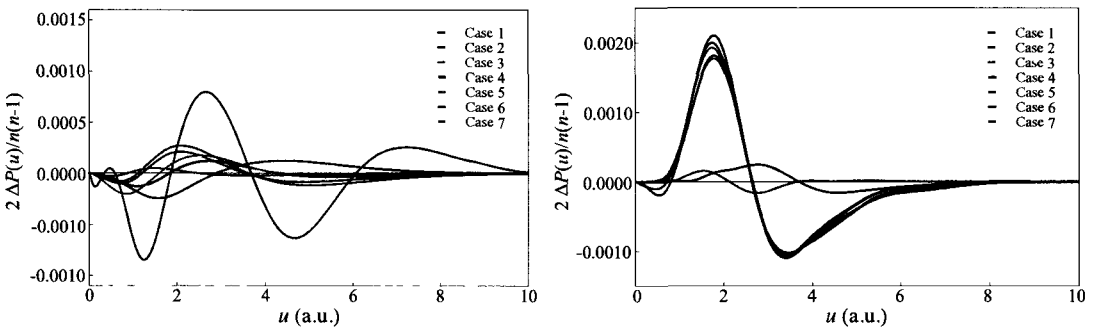

Figure 5.1: (Color) Averaged difference intracules, $\Delta P(u)$ normalized to unity for the atoms (left) and molecules (right) for the G1 test set. The case defined in the legend corresponds to the basis set comparison as described in the text.

where a single reference basis set was used in all cases, here the difference intracule is expressed by

$$\Delta P^{i}(u) = P^{\mathrm{Ref}_i}(u) - P^{B_i}(u) \tag{5.3}$$

where i denotes the comparison case number and the remaining terms are as previously described. From the cases listed above, the second basis set in the list denotes the reference. Results of the averaged difference intracules are shown in Figure 5.1. These intracules represent an average for all of the atoms (left) or molecules (right) in the G1 test set which were all normalized to unity. From the plot of the atomic difference intracules, it is apparent that for the most part, polarization functions have no consistent effect on interelectronic separations in atoms. However, upon looking at the averaged difference intracule for the molecular systems, a basis antihole is clear and the magnitudes of the resulting functions are much greater than those obtained for the atomic systems. This suggests that the differences in atomic systems are essentially noise. Atomic intracules aside, this figure demonstrates that the basis antihole is a property of molecular systems. As previously mentioned both here and in the paper by Pearson *et al.*,[54] the antihole is indicative of electrons being closer together in the reference (i.e. polarized) systems, which is a counterintuitive effect.

5.2.2 Basis Set Dependence on Energy Components

Based on the different results obtained for atomic and molecular systems, all components of the energy were explored for these seven basis set comparisons. Table 5.1 lists the energy differences for the kinetic, $\Delta E_T^{(2)}$, electron nuclear attraction, $\Delta E_{eN}^{(2)}$, and two-electron, $\Delta E_{ee}^{(2)}$, components of the energy as well as the total energy difference, $\Delta E_{tot}^{(2)}$, for basis set comparison (2). For a comprehensive list of the difference in energy components between the basis and its polarized reference, the interested reader is directed to the Supplementary Information. In the final two columns of this table, $\Delta E_{ee}^{(2)}$ is partitioned further into the Coulomb, $\Delta E_J^{(2)}$, and exchange components, $\Delta E_K^{(2)}$. Herein, it can be noted that ΔE_{ee} tends to be positive for molecular systems indicating a decrease in the two-electron energy, while the sign of ΔE_{ee} for atomic systems is dependent on the particular element. This correlates well with the results shown in Figure 5.1 as the basis antihole for molecules corresponds well to the trend for molecular two-electron energy differences. There are some exceptions for these molecular trends within the G1 test set, but these instances represented a small percentage of the total number of test cases. Systems containing the electropositive Li and electronegative F atoms where often those problematic cases that demonstrated a decrease in $\Delta E_{ee}^{(2)}$.

Close observation of the ΔE_{ee}^2 values for atomic systems in Table 5.1 reveals one interesting note. For systems containing filled or half-filled valence shells (He, Li, Be, N, Ne, Na, Mg, P, and Ar), the addition of polarization functions has no effect. This is most likely due to the symmetry of these systems. Having a half-filled or filled shell leads to the incorporation of a single electron or pair of electrons, respectively, into each valence atomic orbital, by Hund's rule. The subsequent addition of one more electron to any of these orbitals would disrupt the symmetry and thus polarization of said orbitals would be beneficial.

Table 5.1: Energy differences for basis set comparison (2)

System	$\Delta E^{(2)}_{tot}$	$\Delta E^{(2)}_{T}$	$\Delta E^{(2)}_{eN}$	$\Delta E^{(2)}_{ee}$	$\Delta E^{(2)}_{J}$	$\Delta E^{(2)}_{K}$
Al	-0.00213	0.00814	-0.03512	0.02485	0.03170	-0.00685
Ar	0.00000	0.00000	0.00000	0.00000	0.00000	0.00000
B	-0.00308	0.00536	-0.00687	-0.00158	0.00658	-0.00816
Be	0.00000	0.00000	0.00000	0.00000	0.00000	0.00000
C	-0.00302	0.00505	-0.00573	-0.00234	0.00496	-0.00731
Cl	-0.00356	0.00847	-0.02004	0.00800	0.01642	-0.00842
F	-0.00272	0.00493	-0.00569	-0.00195	0.00432	-0.00627
He	0.00000	0.00000	0.00000	0.00000	0.00000	0.00000
Li	0.00000	0.00000	0.00000	0.00000	0.00000	0.00000
Mg	0.00000	0.00000	0.00000	0.00000	0.00000	0.00000
N	0.00000	0.00000	0.00000	0.00000	0.00000	0.00000
Na	0.00000	0.00000	0.00000	0.00000	0.00000	0.00000
Ne	0.00000	0.00000	0.00000	0.00000	0.00000	0.00000
O	-0.00272	0.00463	-0.00568	-0.00166	0.00478	-0.00644
P	0.00000	0.00000	0.00000	0.00000	0.00000	0.00000
S	-0.00319	0.00844	-0.02425	0.01262	0.02085	-0.00823
Si	-0.00257	0.00882	-0.02947	0.01808	0.02502	-0.00694
BeH	-0.00403	0.00538	-0.02246	0.01305	0.02072	-0.00767
CH	-0.01540	-0.00319	-0.04260	0.03039	0.04634	-0.01595
$CH_2(^1A_1)$	-0.02333	-0.01322	-0.07093	0.06082	0.07739	-0.01657
$CH_2(^3B_1)$	-0.01410	-0.00990	-0.03552	0.03132	0.04638	-0.01506
CH_3	-0.01817	-0.01469	-0.03934	0.03587	0.05753	-0.02166
CH_3Cl	-0.04320	-0.07913	-0.10776	0.14369	0.17137	-0.02768
CH_3SH	-0.06255	-0.08676	-0.21907	0.24328	0.28666	-0.04338
CH_4	-0.02091	-0.01789	-0.03814	0.03512	0.06121	-0.02609
Cl_2	-0.04678	-0.17659	-0.13461	0.26441	0.26247	0.00194
ClF	-0.03658	-0.13091	-0.06743	0.16176	0.16129	0.00048

Table 5.1: (*Continued.*)

System	$\Delta E_{tot}^{(2)}$	$\Delta E_{T}^{(2)}$	$\Delta E_{eN}^{(2)}$	$\Delta E_{ee}^{(2)}$	$\Delta E_{J}^{(2)}$	$\Delta E_{K}^{(2)}$
ClO	-0.05844	-0.19780	-0.09446	0.23382	0.23591	-0.00210
CN	-0.04257	-0.10480	-0.12726	0.18949	0.18892	0.00056
CO	-0.06857	-0.06952	-0.28497	0.28592	0.31774	-0.03183
CO_2	-0.11849	-0.09924	-0.54085	0.52160	0.58603	-0.06442
CS	-0.06517	-0.11710	-0.35027	0.40220	0.43004	-0.02784
F_2	-0.01817	-0.05463	-0.06147	0.09792	0.09802	-0.00010
H_2	-0.00450	0.00415	-0.01559	0.00694	0.01387	-0.00694
H_2CCH_2	-0.03434	-0.03422	-0.10053	0.09942	0.14077	-0.04135
H_2CO	-0.05882	-0.06940	-0.21199	0.22257	0.26365	-0.04108
H_2NNH_2	-0.05938	-0.06109	-0.17348	0.17519	0.20704	-0.03185
H_2O	-0.03704	-0.02611	-0.10374	0.09282	0.10693	-0.01412
H_2S	-0.04679	-0.03825	-0.21351	0.20498	0.23280	-0.02782
H_3CCH_3	-0.04006	-0.03720	-0.07886	0.07600	0.12301	-0.04700
H_3COH	-0.05583	-0.06351	-0.13564	0.14332	0.17888	-0.03555
HCCH	-0.02955	0.00438	-0.14987	0.11594	0.15077	-0.03482
HCl	-0.02856	-0.02179	-0.12289	0.11612	0.12928	-0.01316
HCN	-0.04916	-0.04086	-0.21345	0.20514	0.24235	-0.03721
HCO	-0.06275	-0.07557	-0.21313	0.22595	0.25967	-0.03373
HF	-0.02477	-0.01730	-0.06472	0.05725	0.06488	-0.00764
HOCl	-0.05408	-0.13372	-0.13917	0.21881	0.22656	-0.00775
HOOH	-0.05983	-0.08140	-0.18122	0.20279	0.21998	-0.01719
Li_2	-0.00018	0.00056	-0.00250	0.00177	0.00213	-0.00036
LiF	-0.00661	-0.02145	0.03261	-0.01777	-0.02358	0.00581
LiH	-0.00113	0.00157	-0.00957	0.00687	0.00910	-0.00223
N_2	-0.07527	-0.07752	-0.31241	0.31466	0.35249	-0.03784
Na_2	-0.00032	0.00087	-0.01123	0.01004	0.01041	-0.00037
NaCl	-0.00723	-0.00405	-0.13930	0.13612	0.13806	-0.00194

Table 5.1: (*Continued.*)

System	$\Delta E^{(2)}_{tot}$	$\Delta E^{(2)}_{T}$	$\Delta E^{(2)}_{eN}$	$\Delta E^{(2)}_{ee}$	$\Delta E^{(2)}_{J}$	$\Delta E^{(2)}_{K}$
NH	-0.01867	-0.01096	-0.05040	0.04268	0.05645	-0.01377
NH_2	-0.03176	-0.01863	-0.09152	0.07838	0.09811	-0.01973
NH_3	-0.03218	-0.02272	-0.09035	0.08089	0.10012	-0.01923
NO	-0.06952	-0.16052	-0.16704	0.25803	0.26098	-0.00294
O_2	-0.05875	-0.13201	-0.14914	0.22240	0.23364	-0.01124
OH	-0.02364	-0.01282	-0.06356	0.05274	0.06762	-0.01499
P_2	-0.06938	-0.13313	-0.59634	0.66010	0.69314	-0.03304
PH_2	-0.04001	-0.01483	-0.23035	0.20517	0.23842	-0.03325
PH_3	-0.05384	-0.02342	-0.30050	0.27008	0.31376	-0.04368
S_2	-0.07515	-0.20359	-0.36533	0.49377	0.51042	-0.01665
Si_2	-0.03514	-0.04325	-0.37625	0.38436	0.41286	-0.02850
Si_2H_6	-0.09221	-0.00722	-0.63157	0.54658	0.65622	-0.10963
$SiH_2(^1A_1)$	-0.03042	-0.00879	-0.20851	0.18688	0.21151	-0.02463
$SiH_2(^3B_1)$	-0.02605	-0.00019	-0.15941	0.13355	0.16402	-0.03047
SiH_3	-0.04064	0.00290	-0.24702	0.20348	0.25265	-0.04917
SiH_4	-0.05288	-0.00324	-0.31094	0.26130	0.32346	-0.06216
SiO	-0.06417	-0.08018	-0.48996	0.50596	0.53286	-0.02689
SO	-0.08707	-0.22143	-0.29901	0.43337	0.45720	-0.02383
SO_2	-0.24128	-0.58339	-0.85288	1.19499	1.24007	-0.04508

The variational theorem states that as the accuracy of the wavefunction improves, the energy for the system decreases. Since polarization functions cannot have a detrimental effect on the wavefunction, these increases in two-electron energies, must be offset by greater decreases in the kinetic and electron nuclear attraction components of the energy. The question that needs to be answered is which component of the energy factors more prominently in the reduction of the energy. From the set of data displayed in Table 5.1, it

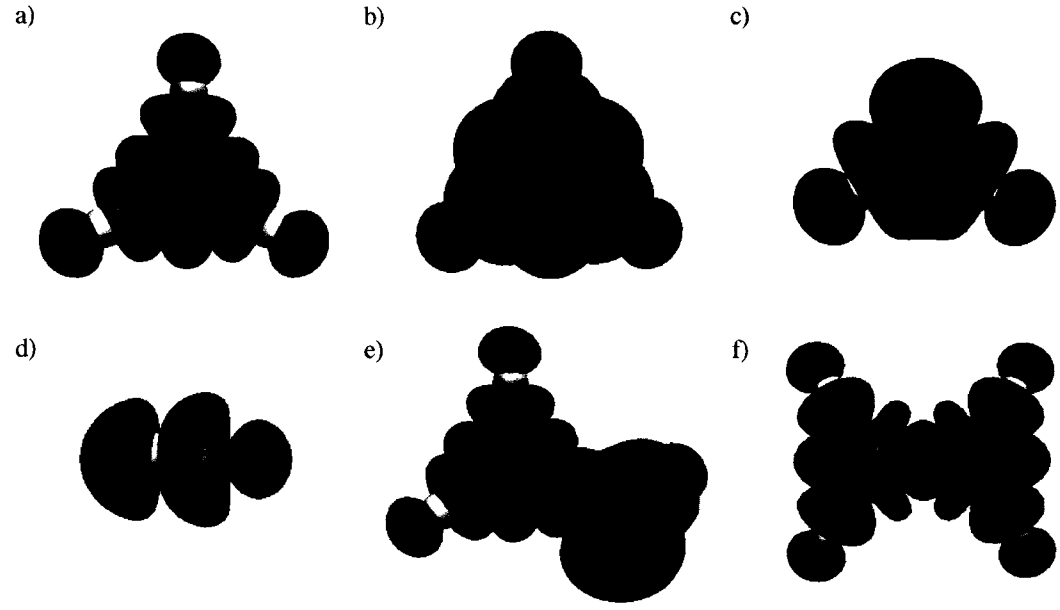

Figure 5.2: (Color) Electron density differences, $\Delta\rho^{(}2)(\boldsymbol{r})$, for a representative group of molecules from the G1 test set. a) Methane, CH_4, b) ammonia, NH_3, c) water, H_2O, d) hydrogen fluoride, HF, e) methanol, CH_3OH, f) ethene, C_2H_4. Green and red areas in the density difference indicate positive (+0.004) and negative (-0.004) values, respectively. All other colors present are indicative of atoms within the molecules.

is apparent that in majority of molecular systems, the stabilizing energy resulting from the attraction between the electrons and nuclei plays the major role in reducing the total energy of the system. This indicates that the electrons are attracted more strongly to the nuclei in the system but still does not provide a clear explanation as to why the introduction of polarization functions leads to a contraction of electrons in molecular systems.

5.2.3 Basis Set Dependence in the Electron Density

To develop a more complete picture as to what is occurring in these systems upon inclusion of polarization, we looked at the differences in electron densities for the seven previously mentioned basis set comparisons.

$$\Delta\rho^{i}(\boldsymbol{r}) = \rho^{\mathrm{Ref}_i}(\boldsymbol{r}) - \rho^{B_i}(\boldsymbol{r}) \tag{5.4}$$

Examples of these difference electron densities, $\Delta\rho^{(2)}(\boldsymbol{r})$, are displayed in Figure 5.2. Once again, the basis set comparison chosen for this display was case (2) as previously done in Table 5.1. In these density plots, the isovalues that are shown are ± 0.004. There was no theoretical reasoning for the choice of these particular values; they were simply chosen to provide a good visual representation of the positive (green) and negative (red) regions of $\Delta\rho(\boldsymbol{r})$. From the figure, it is evident that once the polarized functions are included in the construction of the wavefunction, an increase in the electron density within the bonding regions occurs. This is consistent with results obtained for the small subset of systems studied by Roos and Sigbahn amongst others.[145–148] However, herein, we have provided a great deal of evidence supporting this theory through the use of a wide range of basis set comparisons

5.2.4 Summary

Although these electron density differences do not tell the whole story, they provide a great deal of evidence as to why the electron repulsion energy is increasing in the molecules of the G1 test set. The inclusion of polarization functions allows for more accurate descriptions of the bonding regions and thus instead of increasing interelectronic separations with the inclusion of higher angular momenta orbitals, these orbitals overlap more effectively, providing a more accurate description of the electronic structure within a chemical bond. A great example of this is shown in Figure 5.2 (f), the ethene molecule. For the π-bond in this system, the p-orbitals would have to bend to effectively describe this type of bond; however, this is not possible. Therefore, once d-orbitals are incorporated into the basis set, they can combine with the p-orbitals to more effectively describe the overlap in the π-bond.

The idea that polarization functions increase electron density in bonding regions has been known for some time, at least for the small set of systems that have been described in the literature. However, to explore the validity of analyzing the origins of the basis antihole using electron densities, we separated the position intracule, $P(u)$, into its Coulomb, $J(u)$,

and exchange, $K(u)$, components. These fragments of the total intracule can be defined as

$$J(u) = \frac{1}{2}\int\int \rho(\boldsymbol{r})\rho(\boldsymbol{r}+\boldsymbol{u})\mathrm{d}\boldsymbol{r}\mathrm{d}\Omega_{\boldsymbol{u}} \tag{5.5}$$

and

$$K(u) = -\frac{1}{2}\sum_i\sum_j \int\int \chi_i(\boldsymbol{r})\chi_j(\boldsymbol{r})\chi_i(\boldsymbol{r}+\boldsymbol{u})\chi_j(\boldsymbol{r}+\boldsymbol{u}))\mathrm{d}\boldsymbol{r}\mathrm{d}\Omega_{\boldsymbol{u}} \tag{5.6}$$

where $\rho(\boldsymbol{r})$ is the electron density, $\chi_i(\boldsymbol{r})$ is the i^{th} spin orbital and $\Omega_{\boldsymbol{u}}$ denotes integration over the angular components of the vector $\boldsymbol{u}$. It is clear from these expressions that the Coulomb intracule is directly related to the electron density. It can be shown that the zeroth moment of the Coulomb and exchange components of the intracule are given by[46,47]

$$\int_0^\infty u^0 J(u)\mathrm{d}u = \frac{1}{2}N^2 \qquad\qquad \int_0^\infty u^0 K(u)\mathrm{d}u = -\frac{1}{2}N \tag{5.7}$$

where N is the number of electrons. With the position intracule given by the sum of the Coulomb and exchange intracules ($P(u) = J(u) + K(u)$), the ratio of the contribution of each of the components is

$$\frac{\int_0^\infty J(u)\mathrm{d}u}{\int_0^\infty K(u)\mathrm{d}u} = -N \tag{5.8}$$

Thus, the contribution to the total intracule from the Coulomb component is N times greater than that of the exchange component. Therefore, as the number of electrons within a system increases, the Coulomb intracule becomes the dominating factor, and because this component is directly related to the electron density, using the differences in electron density to study the basis antihole is reasonable.

Ideally one would look at the difference in the pair density for these comparisons; however, visualization of this function is not possible. Nonetheless, the electron density difference does an adequate job of explaining all of the observations in this study and from the evidence involving the Coulomb and exchange intracules above, this form of analysis is completely valid. The idea that atoms and molecules behave differently with molecules

showing increases in electron repulsion energy and atoms showing no obvious trend fits perfectly with this explanation. In molecules, the polarization functions improve the description of bonding regions leading to increases in electron density in the bond and the concomitant increase in repulsion energy and the presence of the basis antihole; whereas, in atomic systems which tend to be relatively symmetric, polarization functions would not cause significant differences. Any effect on an atomic system would be highly dependent on the electronic configuration of the specific atom as noted by the values of ΔE_{ee} in Table 5.1.

With the increase in the two-electron energy, the one-electron components of the energy must compensate for this decrease in order for the wavefunction to satisfy the variational theorem. The identity of the major contributor to this decrease was found to be the electron nuclear attraction component of the energy. However, the kinetic energy also demonstrated slight decreases. This suggests that since the electron density within the bonding region is increasing, the electron nuclear attraction would increase in magnitude (i.e. become more negative) as the electrons are being drawn closer to additional nuclei. In the case of the difference in kinetic energy, two competing effects would be observed. First, as electrons are drawn closer to nuclei as they appear to be based on the results in Figure 5.2, kinetic energy tends to increase which would result in a positive ΔE_T. But second, as the electrons are localizing in the bonding regions, the stronger attraction to two separate nuclei may compete with one another leading to a decrease in kinetic energy. These two competing effects could result in a ΔE_T smaller in magnitude than the corresponding ΔE_{eN}. One can consider an object with external potential forces being exerted on it in opposing directions; these opposing forces would lead to a hindrance of the kinetic energy of said object. There are some exceptions to this trend as noted by the data in Table 5.1 and more in-depth studies would have to be carried out to confirm or deny this hypothesis.

For the molecules in Figure 5.1 (left), as we move from case (3) to case (4) and finally to case (5), it is noted that the difference intracules become far more similar to their refer-

ence basis. These comparison cases involve increasing levels of functionalization starting with the 6-311++G basis. In cases (4) and (5), the '*unpolarized*' bases actually contain polarization functions, but do not contain the same level of polarization as their respective reference basis sets. Thus, slight improvements are noted upon the inclusion of further polarization functions, but the initial introduction of the higher angular momenta orbitals makes the most significant difference in improving the quality of the bond description.

5.3 Conclusion

The discovery of the basis antihole was somewhat surprising as it was believed that the addition of polarization functions to a system would lead to a decrease in repulsion energy and a concomitant separation of the electrons. However, as the basis antihole demonstrates, this is not the case in most molecular systems. We have shown here how the polarization functions improve the quality of the description of the bonding region. As the intracule can be directly related to the electron density through the Coulomb component, this in turn causes the electrons to get closer together leading to this increase in repulsion energy. To compensate for this increase in electron repulsion energy, and to obey the variational principle, it was determined that the electron nuclear attraction energy provides the greatest contribution in terms of decreasing the overall energy.

There have been some exceptions to the trend of increases in electronic repulsion and greater compensation by the electron nuclear attraction component, but these cases are rare (representing less than 1% of the cases studied). They appear to be most prevalent in systems containing atoms which are highly electronegative or electropositive such as fluorine, chlorine, and lithium. Regardless, this work demonstrated that there is a strong relationship between the occurrence of the basis antihole and increased electron density in the bonding regions due to the more accurate description of the bond through the inclusion of the polarization functions.

6 Optimizing Reaction Energetics Through the Linear Combination of Functional Groups (LCFG) Method

6.1 Introduction

This chapter diverges from the previous studies on electronic structure and focusses on a concept more broadly applicable to theoretical chemistry and the field of chemistry as a whole. Since the advent of the field in the 1920s, there have been a number of advancements in quantum chemistry which have led to highly accurate approximations to the solution of the Schrödinger equation. These include the development of the previously mentioned correlated methods such as configuration interaction (CI), coupled cluster (CC), Møller Plesset perturbation theory (MPPT), and density functional theory (DFT). These methods are commonly used today in the field of computational chemistry but their application is limited by an exponential increase in computational cost with system size. Therefore, highly accurate calculations on large molecules are still not feasible due to this scaling problem.

Regardless, experimental chemists often use computational chemistry as a supplement to their work. For instance, chemists involved in drug discovery and development often use computational techniques to determine what types of drugs to focus on in order to save time and money in the lab. For these same reasons, pharmaceutical companies often employ teams of theoreticians to enhance productivity and fiscal responsibility. Nonetheless, due to the high cost of accuracy in computational models, there are limitations to the advantages

that can be provided by theoretical work.

In this project, we aim to develop a program that is capable of optimizing reaction energetics with respect to substituents in a given reactant complex. Similarly, in 2006 Yang *et al.* reported their work on designing molecules through the optimization of atomic potentials.[149] In that report, they demonstrated the utility of the method by using it to determine the most polarizable molecule from a set of 25 constructed by linking all possible combinations of two identical sets of 5 substituents (-CH_3, -OH, -NH_2, -F, -Cl, and -SH). The method accurately predicted HS-SH as the most polarizable molecule of the 25. This results in significant time savings as the polarizability of each of the individual molecules need not be determined. These results provided the motivation behind the work that will be reported in this chapter. However, instead of optimizing a single state in terms of atomic potentials, we focussed on optimizing the energy difference, ΔE, between two states with respect to a set of substituents through a process that we refer to as a linear combination of functional groups (LCFG). It should be noted that the Rothlisberger group also performed similar calculations prior to those by Yang *et al.* that were applied in the design of a nonpeptidic anticancer drug candidate.[150]

6.2 Methodology

The aim of this project is to optimize reaction energetics of a particular reaction with respect to a functional group at a designable site in a molecule. Figure 6.2 shows a reaction coordinate showing the reactant state S_1 and two possible states for S_2: the transition state (S_{2a}) or the products (S_{2b}). Now, consider any process involving a reactant complex with a site that can be modified without affecting the type of reaction that occurs. To determine what functional group would optimize the energetics of such a reaction (minimize or maximize either ΔE_a or ΔE), one would have to perform calculations on the reactant and product (or transition) states of the molecule for each functional group. If one was interested in testing a wide range of functional groups, calculations of the highest accuracy

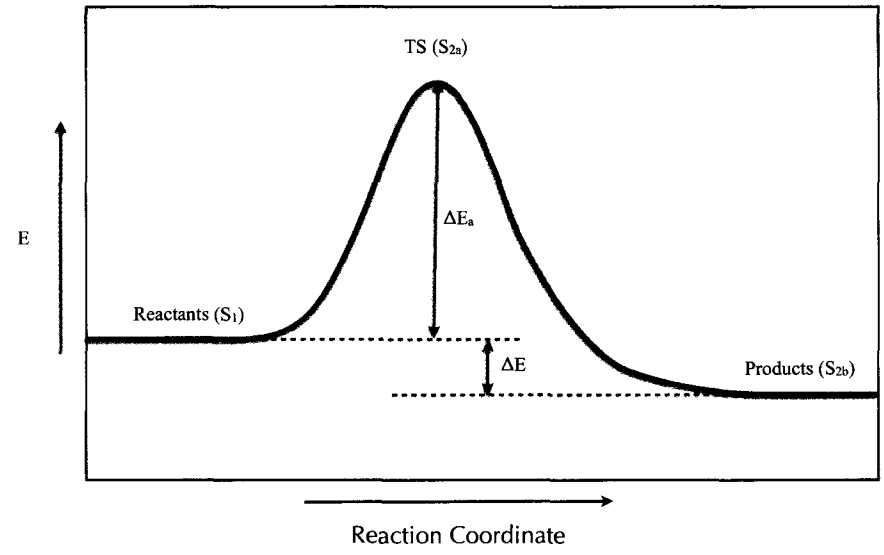

Figure 6.1: Reaction coordinate diagram for a general reaction defining the states of interest in the LCFG process.

would require an enormous amount of time for reactions involving molecules comprised of more than 5 or 6 heavy atoms. However, consider a large catalytic complex where the sizes of the functional groups are significantly smaller than the full molecule. In this case, recalculating all of the integrals involved in the fixed part of the system (which we will refer to as the reference system) would comprise the majority of the total calculation time despite the fact that these integrals are redundant. Thus, instead of performing separate calculations for each individual functional group, it would be far more efficient to perform a single calculation where all of the desired functional groups are superimposed at the same position in the molecule.

To develop such a method, one must allow each substituent to interact with the reference system while prohibiting interactions between the different functional groups. To achieve this, the energy expression can be partitioned into separate components for the reference system, E_{ref}, and the designable site (i.e. superimposed functional groups), $\sum E_a$, for both states of interest, S_1 and S_2. This can be represented mathematically as

$$\Delta E = \left(E_{ref}^{S_2} + \sum_{a=1} b_a E_a^{S_2} \right) - \left(E_{ref}^{S_1} + \sum_{a=1} b_a E_a^{S_1} \right), \qquad \sum_{a=1} b_a = 1 \tag{6.1}$$

where b_a is a coefficient defining the fraction of the energy contributed by individual functional groups. We may then minimize or maximize ΔE with respect to the linear coefficients, b_a; hence, the functional group pertaining to the largest coefficient would be that which optimizes the specific energetics of the process.

Since the reference system is fixed, the only components of the energy incorporated in $E_{ref}^{S_2}$ and $E_{ref}^{S_1}$ are those that only involve the atoms of the reference system. All other interactions, be they between the reference system and the functional group or between different orbitals within the functional group, would be included in $E_a^{S_2}$ or $E_a^{S_1}$. Every optimization performed in this study was carried out at the HF level of theory using the STO-3G basis (denoted by HF/STO-3G) as a reasonable *ab initio* starting point. Upon expanding the molecular orbitals in a basis of atomic orbitals, the HF energy, previously given by (1.12) and (1.56), can be expressed as

$$E = \sum_{\mu=1}^{K}\sum_{\nu=1}^{K} P_{\mu\nu}^{HF}(T_{\mu\nu} + V_{\mu\nu}^{eN}) + \sum_{\mu=1}^{K}\sum_{\nu=1}^{K}\sum_{\lambda=1}^{K}\sum_{\sigma=1}^{K} \Gamma_{\mu\nu\lambda\sigma}^{HF} V_{\mu\nu\lambda\sigma}^{ee} + \sum_{A=1}^{M}\sum_{B>A}^{M} \frac{Z_A Z_B}{R_{AB}} \quad (6.2)$$

where $T_{\mu\nu}$ and $V_{\mu\nu}^{eN}$ are elements of the kinetic and electron nuclear attraction integral matrices, respectively, while $V_{\mu\nu\lambda\sigma}^{ee}$ represents an element of the electron repulsion integral matrix. Finally, $P_{\mu\nu}^{HF}$ and $\Gamma_{\mu\nu\lambda\sigma}^{HF}$ are elements of the previously described charge density and two-particle density matrices. In order to separate the components of the energy, we can define the energy of the reference system as

$$E_{\text{ref}} = \sum_{\mu=1}^{K_{\text{ref}}}\sum_{\nu=1}^{K_{\text{ref}}} P_{\mu\nu}^{HF}(T_{\mu\nu}^{\text{ref}} + V_{\mu\nu}^{en,\text{ref}}) + \sum_{\mu=1}^{K_{\text{ref}}}\sum_{\nu=1}^{K_{\text{ref}}}\sum_{\lambda=1}^{K_{\text{ref}}}\sum_{\sigma=1}^{K_{\text{ref}}} \Gamma_{\mu\nu\lambda\sigma}^{HF} V_{\mu\nu\lambda\sigma}^{ee,\text{ref}} + \sum_{A=1}^{M_{\text{ref}}}\sum_{B>A}^{M_{\text{ref}}} \frac{Z_A Z_B}{R_{AB}} \quad (6.3)$$

where K_{ref} and M_{ref} refer to the set of basis functions describing the reference system and the set of nuclei in the reference system, respectively. For the energy pertaining to each of the functional groups, we must construct individual one- and two-electron matrices for

each functional group. These are given by

$$X^a_{\mu\nu} = \begin{cases} 0, & 1 \leq \mu \,\&\, \nu \leq K_{\text{ref}} \\ \langle \phi_\mu | \hat{O} | \phi_\nu \rangle, & \text{otherwise} \end{cases} \tag{6.4}$$

for the matrices of one-electron integrals, where $\hat{O}$ is the appropriate operator, and

$$Y^a_{\mu\nu\lambda\sigma} = \begin{cases} 0, & 1 \leq \mu \,\&\, \nu \,\&\, \lambda \,\&\, \sigma \leq K_{\text{ref}} \\ 2(\mu\nu|\lambda\sigma) - (\mu\sigma|\lambda\nu), & \text{otherwise} \end{cases} \tag{6.5}$$

for the two-electron integral matrix. Using these definitions, the energy contribution for each of the functional groups is given by

$$E_a = \sum_{\mu=1}^{K_a}\sum_{\nu=1}^{K_a} P^{HF}_{\mu\nu}(T^a_{\mu\nu} + V^{en,a}_{\mu\nu}) + \sum_{\mu=1}^{K_a}\sum_{\nu=1}^{K_a}\sum_{\lambda=1}^{K_a}\sum_{\sigma=1}^{K_a} \Gamma^{HF}_{\mu\nu\lambda\sigma} V^{ee,a}_{\mu\nu\lambda\sigma} + \sum_{A=1}^{M_a}\sum_{B>A}^{M_a} \frac{Z_A Z_B}{R_{AB}} - \sum_{A=1}^{M_{\text{ref}}}\sum_{B>A}^{M_{\text{ref}}} \frac{Z_A Z_B}{R_{AB}} \tag{6.6}$$

where K_a and M_a are the full set of basis functions and nuclei in the full chemical system with functional group, a. It should be noted that by using the indices K_{ref} and M_{ref}, it is assumed that the components of the matrices and the ordering of the nuclei are in such a way that these sums only run over the components that are associated with the reference system.

The one- and two-electron integral matrices are assembled according to (6.4) and (6.5) while the values of each of the integrals can easily be calculated using one of the many programs that performs quantum chemical calculations.[18] Where the problem lies, is in how to define the molecular orbital (MO) coefficient matrices, $\boldsymbol{C}$ to determine the contribution of each basis function to every molecular orbital. In order to discuss how the coefficients are determined, we must first introduce the concept of localized molecular orbitals (LMOs) versus the more traditional canonical molecular orbitals (CMOs). CMOs are the orbitals

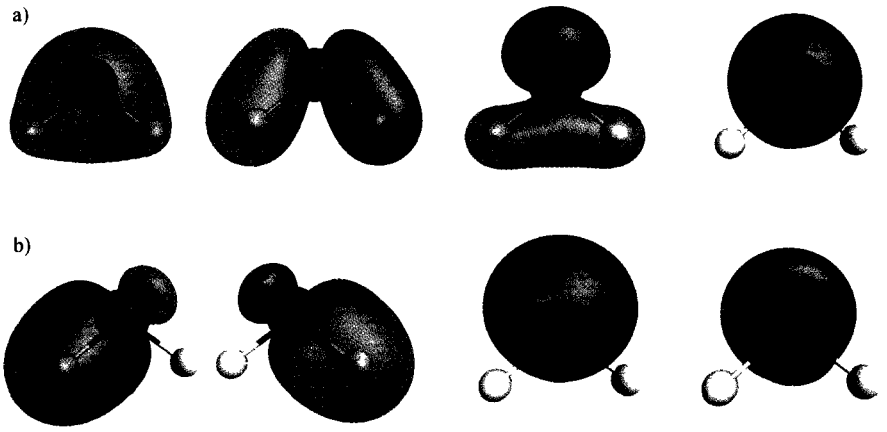

Figure 6.2: Comparison of the a) canonical, and b) localized molecular orbitals for the ground state of the water molecule calculated at the HF/STO-3G level of theory.

that are obtained as the eigenfunctions of the Fock operator. In general, these orbitals are delocalized over the entire chemical system and are highly dependent on the composition of the given molecule. LMOs, on the other hand, are far more conceptual; one can easily imagine what these orbitals would look like for any given system as they represent the bonds, lone pairs, and core orbitals within a molecule. Figure 6.2 shows the differences between CMOs and LMOs for the ground state of the water molecule at the HF/STO-3G level of theory.

The most important feature of LMOs is that they are highly transferable from one molecule to another, whereas with a CMO treatment, the molecular orbitals change drastically from one compound to the next. Figure 6.3 demonstrates the non-transferable nature of CMOs versus the high transferability of LMOs. The CMOs that are depicted in the figure range from the HOMO-3 up to HOMO whereas the displayed LMOs are the four orbitals that are contained in both the H_2O and HOF molecules (oxygen 1s core, O-H bond, and two oxygen lone pairs). Such localization allows for the transfer of atomic orbital coefficients from one molecule to the next for a specific LMO (e.g. lone pair of an oxygen atom).

As mentioned at the beginning of the discussion on molecular orbitals, the CMOs are obtained interatively by solving the Roothaan-Hall equations in an SCF procedure. In

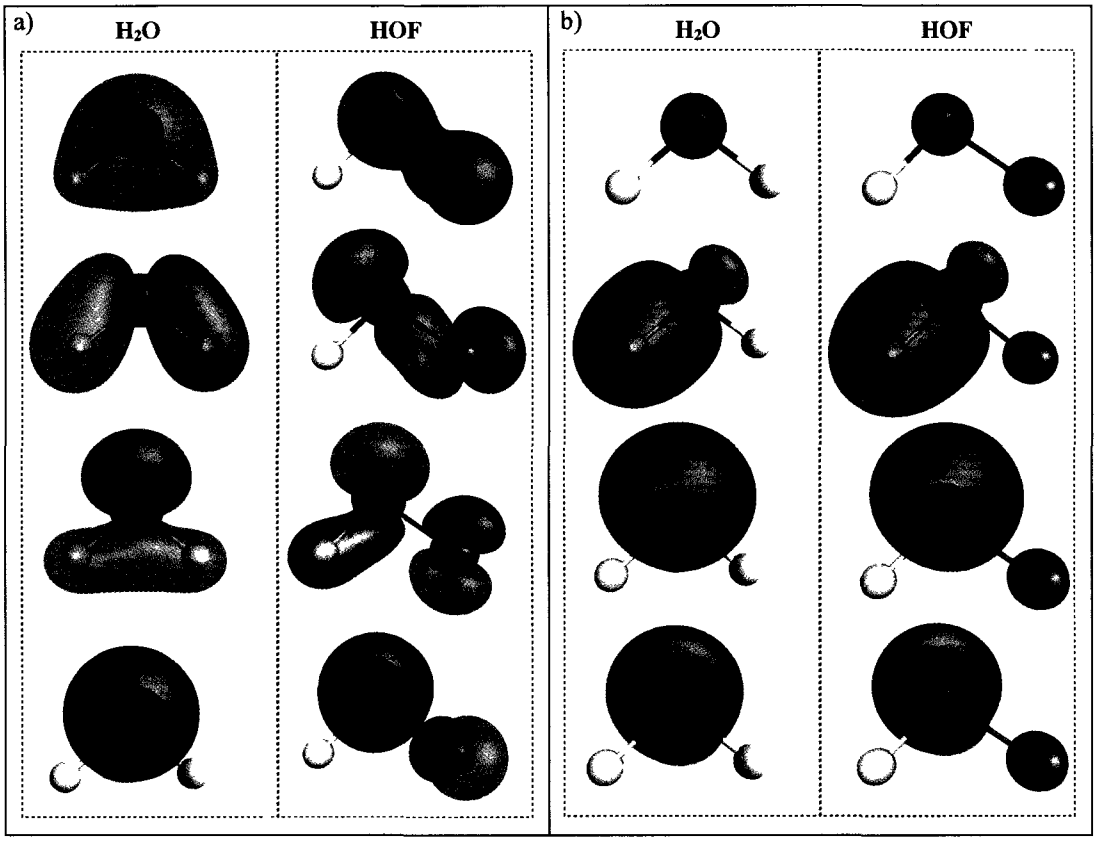

Figure 6.3: Comparison of the transferability of a) CMOs, and b) LMOs using the water molecule and hypofluorous acid as examples.

contrast, the LMOs are obtained by adding linear combinations of CMOs to obtain the most localized orbitals possible. This is possible due to the property of determinants that states that if one adds a multiple of column A to column B, the determinant will not change. Thus, for a two-electron system with a wave function given by a single Slater determinant as

$$\Psi(\boldsymbol{r_1}, \boldsymbol{r_2}) = \begin{vmatrix} \chi_1(\boldsymbol{r_1}) & \chi_2(\boldsymbol{r_1}) \\ \chi_1(\boldsymbol{r_2}) & \chi_2(\boldsymbol{r_2}) \end{vmatrix} \tag{6.7}$$

we can modify the columns by adding a multiple of column 1 to column 2 as follows

$$\Psi(\boldsymbol{r_1}, \boldsymbol{r_2}) = \begin{vmatrix} \chi_1(\boldsymbol{r_1}) & \chi_2(\boldsymbol{r_1}) + k\chi_1(\boldsymbol{r_1}) \\ \chi_1(\boldsymbol{r_2}) & \chi_2(\boldsymbol{r_2}) + k\chi_1(\boldsymbol{r_2}) \end{vmatrix} \tag{6.8}$$

without changing the wave function (where k is simply a coefficient denoting the addition of a multiple of column 1). One can work out the determinant above to prove the validity of this claim. This idea that one can combine different CMOs in various ways without affecting the accuracy of the wave function is the basis for the construction of LMOs. However, as one can imagine, there are countless ways to mix the CMOs to obtain new sets of molecular orbitals, especially in larger systems.

Lennard-Jones and Pople originally theorized that one could obtain localized orbitals by minimizing the interorbital repulsions which are given by[151,152]

$$4 \sum_{i} \sum_{j>i} \int \int |\phi_i(\boldsymbol{r_1})|^2 \frac{1}{r_{12}} |\phi_j(\boldsymbol{r_2})|^2 \, \mathrm{d}\boldsymbol{r_1} \, \mathrm{d}\boldsymbol{r_2} \tag{6.9}$$

where the factor of 4 stems from the fact that there are four interorbital repulsions from the electrons in a pair of molecular orbitals. This idea was the basis for the Edmiston and Ruedenberg (ER) localization method.[153] More correctly, in the ER localization scheme, the repulsions within a single orbital are maximized, but in doing so, one effectively minimizes the repulsions between different orbitals.

The ER localization method is one of the most popular today though there have been a number of other localization schemes[154–157] developed over the years such as that of Boys *et al.* , which maximizes the distance between centroids of charge in a molecule.[154,155] However, this method does fail to yield properly localized orbitals for some molecules.[1] For this reason, we have chosen to use the ER scheme; however, it should be noted, that the Boys method as well as the Pipek-Mezey method[157] were studied in the initial stages of the project but no significant differences in the LMOs were noted.

With the introduction to CMOs and LMOs complete, we now return to the discussion concerning the MO coefficient matrix. The LMOs of these partitioned systems can be divided into three categories: 1) the LMOs describing the core orbitals, lone pairs, and bonds within the reference system, 2) the LMO(s) describing the bond between the designable

site functional group and the reference system, and 3) the LMOs describing the core orbitals, lone pairs, and bonds within the designable site functional group. Describing the exact form of the coefficient matrices as well as where each piece of data is obtained either by written descriptions or through the use of mathematical expressions is non trivial, and thus we will instead demonstrate this pictorially in Figure 6.4.

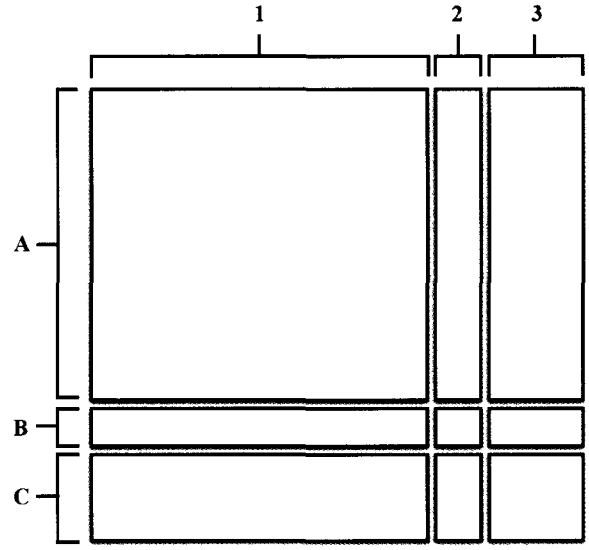

Figure 6.4: Fragmentation of the MO coefficient matrix. (A)-(C) Atomic orbital basis functions describing the reference system, the reference system atom attached to the functional site, and the functional group atoms, respectively. (1)-(3) LMOs describing reference system orbitals, reference system/functional group bond, and functional group orbitals, respectively.

The simplest, and perhaps, most efficient way to define the MO coefficients of the reference system (Region A1 in Figure 6.4), is to perform a calculation on the reference system with the empty valence being capped with a hydrogen atom. Hydrogen is likely the least biased choice for a capping agent as it is not electron withdrawing or electron donating and its small size allows for a simple description of the atom in terms of basis set size. This is similar to the method employed in QM/MM and ONIOM calculations in order to complete the valence of any bonds that are broken in the partitioning process.[158–160]

All coefficients pertaining to the reference system basis functions that are used in the description of the LMOs (Region A1) for the reference system are obtained through this

initial calculation using the hydrogen capping agent. The remaining LMO coefficients will either be supplied through a pre-built library of coefficients or set to zero. As the orbitals in these systems are localized, the contribution of atoms (and thus their basis functions) that are not involved in the bond or lone pair that the orbital is describing is often negligible anyway. This suggests that omitting the orbital contribution from distant atoms will not result in large energetic errors.

Two different approaches of assembling the MO coefficient matrices were employed in this study and they are represented in Figure 6.5 with regions shaded in light green denoting MO coefficients that are provided by the initial SCF calculation. The regions shaded in dark green denote those that are provided from a predefined library and white regions indicate the coefficients that are set to zero. These two methods, Method I (MI) and Method II (MII), will be compared in the results and discussion section of this chapter. Ideally, one would prefer to use Method II as it requires less information to be included in the library.

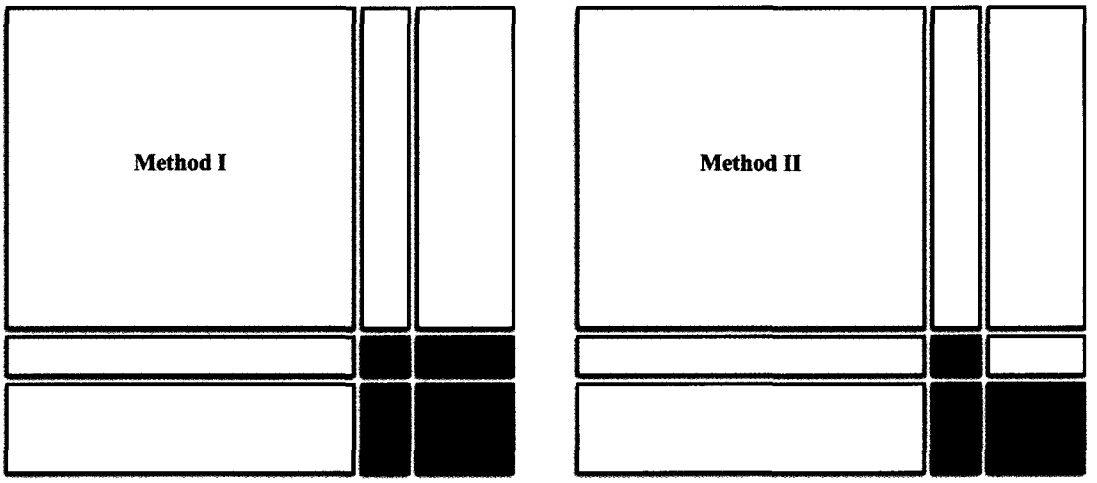

Figure 6.5: Pictorial representation of the two methods for constructing the coefficient matrices. Shaded regions indicate the origin of the coefficients as follows: → coefficients provided from initial calculation on reference system capped with H atom, ■ → coefficients provided from the predefined library, and □ → coefficients set to zero.

The results presented in the next section are obtained using the energy expressions from (6.1)-(6.6) where the density and two-particle density matrices are formed from the two aforementioned methods of constructing the MO coefficient matrix. Recall that in HF

theory, these two matrices can be related to the MO coefficients by

$$P_{\mu\nu} = 2\sum_{a=1}^{N/2} c_{\mu a}^{*} c_{\nu a} \tag{6.10}$$

$$\Gamma_{\mu\nu\lambda\sigma} = \frac{1}{4}(2P_{\mu\nu}P_{\lambda\sigma} - P_{\mu\sigma}P_{\lambda\nu}) \tag{6.11}$$

The construction of the library of coefficients is a huge undertaking. Thus, instead of focussing on the development of this library, the focus of this project was to develop the fundamental process for these optimizations. Thus, for the two methods displayed in Figure 6.5, any coefficients that are specified as being provided by the library were instead obtained from a calculation on the true molecule. One might suggest that this introduces an advantageous bias; however, one must remember that these orbitals are localized and demonstrate very little differences from one molecule to the next. This reaction affords the opportunity for a proof-of-concept investigation whereby we can determine the level of accuracy retained by truncating the MO coefficient matrix.

For the purposes of this study, the GAMESS software package[161] was used to calculate all of the one- and two-electron integrals while the optimization procedures were carried out using Mathematica.[76] All of the calculations presented in the next section were performed using the STO-3G basis set. Atomic units are used throughout unless otherwise stated.

6.3 Results and Discussion

The LCFG method has been tested on the deprotonation of the HO-X molecule, where X denotes the designable site containing the superimposed functional groups. This process was chosen as it represents a reasonably simple test case to determine the validity of the method. As this reaction is a simple deprotonation, one cannot specify a transition state, and thus, the optimization was carried out with the goal of maximizing the difference between the energies of the product (S_f) and reactant (S_i) states as a function of the

substituent in the X position.

In reality, one would often want to maximize ΔE for an exothermic reaction or minimize it for an endothermic process to obtain an estimate of the most stable product; however, the choice of minimizing or maximizing may in principle be left to the user. We have used our code to predict the order of reaction energies, ΔE, from highest to lowest. When a large number of functional groups is superimposed at the designable site, one would not care about the exact order of reaction energies; however, it would likely be of interest to determine the functional groups that would lead to a few of the highest or lowest ΔE values.

For this optimization, a set consisting of five functional groups was superimposed at the X site in the O-X bond. These substituents include -H, -F, -Cl, -CH_3, and -NH_2 which were chosen to give a set of functional groups with varying electronegativities. The energy results for this optimization are summarized in Table 6.1 where HF, MI and MII refer to calculations obtained from a full HF benchmark calculation and the LCFG calculations using MO coefficient matrices based on Methods I and II, respectively. From this data, it can be noted that the energy values obtained from these LCFG optimizations contain a significant amount of error compared to the actual HF calculations. However, as all of the systems contain significant errors, the only concern is whether or not the errors are relative and lead to a retention of the order of ΔE values. One must realize that the sole purpose of this program is to determine the optimal substituent(s) for a given reaction. Thus, quantitative energetics are not required for a successful application.

From the data listed in Table 6.1, it can be noted that for each of the three methods, the order of the reaction energies from lowest to highest is as follows:

HF -Cl < -F < -NH_2 < -CH_3 < -H

MI -Cl < -H < -F < -NH_2 < -CH_3

MII -F < -CH_3 < -NH_2 < -Cl < -H

Table 6.1: Results of the LCFG optimization for the deprotonation of HO-X

				Order of ΔE		
Substituent (X)	ΔE^{HF}	ΔE^{MI}	ΔE^{MII}	HF	MI	MII
-Cl	0.72076	-0.46596	0.13137	1	1	4
-F	0.82116	-0.39085	0.72762	2	3	1
$-NH_2$	0.83662	0.10802	0.25630	3	4	3
$-CH_3$	0.84283	0.13143	0.26460	4	5	2
-H	0.90088	-0.46523	-0.46523	5	2	5

Comparing the results from Method II to those from the true HF calculations, it is clear that this method is ineffective in the prediction of the optimal substituent(s), at least for this particular reaction. This is not an unexpected result as this method does not provide as much information as the coefficient matrix used in Method I.

At first glance, it may appear as though Method I also performed poorly in terms of predicting the best substituents to minimize/maximize the reaction energetics; however, one must consider how the coefficients for these systems were obtained. All of the atomic orbital coefficients for the functional group LMOs (that are not set to zero) were obtained directly from calculations on the specific compound (HO-X), while those for the fixed reference were obtained from a calculation involving the reference system, -OH, capped with a hydrogen atom. Thus, the MO coefficients used in the optimization of the HOH complex are exact (with the exception of the omitted coefficients). This leads to a strong bias for the -H substituent in the optimization and results in a spurious placement of it within the ordering in Table 6.1 for MI and MII.

When considering the results of the optimization without the biased -H substituent, one can note that the reaction energies obtained from the LCFG/MI calculations are identical

to those obtained from the true HF calculations.

HF	-Cl	<	-F	<	$-NH_2$	< $-CH_3$
MI	-Cl	<	-F	<	$-NH_2$	< $-CH_3$

These findings demonstrate great promise for the idea of algorithmically optimizing a reactant complex for a specific reaction process and serve as an important proof-of-concept for the idea.

6.4 Future Work and Conclusions

Despite the simplicity of the test case studied here, the LCFG method of optimizing reaction energetics appears to merit further study. Obviously, we would like to expand the applications of this code to be suitable for any type of reaction. But first, there remains work that can be performed to optimize the code.

Presently, much of the work carried out in these optimizations is done manually. The integrals as well as the localized molecular orbitals for the reference system are initially calculated in GAMESS[161] after which they are imported into Mathematica[76] where the optimization is conducted. Additionally, as LMOs are not automatically arranged according to the schematic in Figure 6.3, one must manually modify the coefficient matrices to arrange the molecular orbitals in the proper order. For efficient use of this program, each step of this process should be automated. In the future, we plan to develop this code as a stand alone program in Fortran to maximize the cost savings for the method; however, the method as is was deemed sufficient for this proof-of-concept project.

As previously mentioned, the predefined library of coefficients must be carefully constructed. This library will be formed in such a way to remove the bias for the reactant complex containing a hydrogen atom at the designable site. The exact method for determining the MO coefficients for this library needs to be explored. Some possible options

include performing calculations on a wide range of molecules containing the substituent of interest after which an average or weighted average of the MO coefficients would be used to determine the appropriate values of the library to minimize error. Alternatively, one could simply optimize these coefficients in order to minimize the difference between the actual HF energy and that which is obtained through the LCFG method. These optimizations could be carried out for a given substituent in a wide range of chemical environments to obtain coefficients that would be unbiased to a particular class of molecules. The construction of said library is a major undertaking and will require a great deal of time and effort.

The end goal of this project is to have a fully functional program that can optimize a reactant complex with respect to functional groups present at multiple designable sites within the molecule. In a multiple site optimization, cost savings of the method would increase dramatically making for the most efficient use of this code.

Finally, as mentioned in the introduction, the correlation energy, which is not included at the HF level of theory, is often on the same order of magnitude as reaction energies. The results reported here have been on HF calculations using minimal basis sets; however, in order for this method to be useful as a complement to experimental chemistry, it must be adapted in the future for use with a correlated method. Kohn-Sham (KS) density functional theory (DFT) is a method which we see as a potential candidate for an accurate method as, much like HF, an SCF routine is used to determine the contribution of each basis function to the KS orbitals. Although KS orbitals technically have no physical meaning since DFT is not a wave function theory, it is still possible to obtain localized KS orbitals to use in this method. Alternative correlated methods, such as the MPPT, CI, and CC levels of theory are post-HF methods which employ the HF wavefunction as well as additional corrections. The implementation of these methods would likely be more complicated than with DFT; however, if this program is deemed successful, these post-HF methods could also be incorporated.

Herein, we have described the development of a novel method known as the linear combination of functional groups and its application in optimizing reaction energetics. For the simple test case of the deprotonation of the HO-X molecule, this optimization scheme has performed surprisingly well. Although this test case is simplistic due to the small size of the reactant, it does pose problems as the products introduce a charge on the atom neighboring the functional groups. In later applications of this code, reaction sites would likely be separated from the designable site by more than a single bond. It would be interesting to study a series of reactions to determine the maximum distance that the designable site can be separated from the reaction site where the method can still accurately predict the optimal substituent.

It must be reiterated that this project is still in the stages of infancy. There is a great deal of work that can still be done in this area; however, the results that have been obtained thus far have demonstrated great potential for the idea. There will always be some adjustment to the method that can be made to improve the predictive accuracy, but it is essential to begin at the simplest starting point to avoid the addition of any unnecessary, time-consuming steps. This is the point to which the program has been described in this chapter; however, if, upon the inclusion of the library coefficients, the accuracy proves to be inadequate, one can always modify the method of fragmenting the energy expression or allow for relaxation of the predetermined LMOs of the functional group. Nonetheless, further research is essential to determine what methods will prove most effective and which ones need reconsidering.

7 Conclusion

This thesis has highlighted the details of two separate research projects: the first, which was covered in Chapters 2-5, involved the study of electronic structure while the second, described in Chapter 6, pertained to the development of a novel method for the optimization of reaction processes. This chapter will serve to summarize the major conclusions that were drawn from the data generated in this research and discuss future avenues of research involving these projects.

7.1 Summary

Chapters 2 and 3 detailed the development of new probability densities that provide novel ways of studying electronic structure. The intex and angular intex densities have been developed for s-type orbitals and have been used to study the distribution of electrons in two-electron systems. These two densities have each been employed to elucidate information regarding correlation effects and the nature of the secondary Coulomb hole in addition to the general electronic structure of such systems.

In order to make these densities applicable to the study of the electronic structure of molecules, the expressions for the intex and angular intex integrals must be expanded for the use of orbitals with higher angular momenta. Once these expressions are obtained, the intex density and angular intex densities can be used for analyses of a wide range of atomic and molecular systems. It would be interesting to observe the intex correlation hole of molecules and use it to analyze the secondary Coulomb holes in these molecular systems

and note how they compare to those of atomic systems.

The intex density, described in Chapter 2, demonstrated that HF methods do not favour large electronic separations in all configurations as the Coulomb hole, $\Delta P(u)$, suggests. Instead, the intex correlation hole demonstrates that this probability is intrinsically linked to the centre of mass variable, R, and correlated treatments appear to favour large values of u for electronic configurations where $u \approx 2R$.

However, from Chapter 3, we know that this assessment is also incomplete. When averaging over all angles in the system, it does provide an accurate description of the effects of correlation; however, the angular-dependent intex density, $X(R, u, \theta_{Ru})$ has demonstrated that this observation is dependent on the angle between the $\boldsymbol{R}$ and $\boldsymbol{u}$ vectors. When this angle is equal to $\pi/2$ (or 90°) and the electrons are equidistant from the nucleus, HF treatments are more probable both when averaging over all values of R and u (i.e. $A^{HF}(\pi/2) > A^{Exact}(\pi/2)$), but also at all configurations with large u regardless of the value of the centre of mass radius. However, as θ_{Ru} is decreased towards 0 (or increased towards π), the probability in correlated treatments becomes greater on average and we begin to see a preference in correlated treatments of the configurations where $u \approx 2R$. Nonetheless, it has been noted that at small values of R and large values of u, there is a greater probability of systems having these configurations under the HF method than a correlated treatment, regardless of the value of θ_{Ru}. Thus, this angular work has not only provided a new way of looking at electron pairs, but has demonstrated that the secondary Coulomb hole results from all possible relative configurations of the R and u vectors; however, the largest contributors to the effect are those configurations where the angle between said vectors is approaching $\pi/2$ radians.

Chapter 4 acted as a final and summary chapter for the studies on the secondary Coulomb hole. By studying the effect of the external potential on the secondary Coulomb hole, we were able to determine the dependence of the hole on the form of the nuclear potential. From the data obtained thus far, it appears that an attractive external potential is required

for correlation to lead to the contraction of distant electrons. With a very noticeable secondary negative region present for excited states of two electron systems, it is believed that the secondary hole is a result of nuclear screening. All of the data obtained thus far supports this theory; however, it remains to determine the intracule for 3-ballium at the UHF level of theory. If the secondary Coulomb hole does exist for this system, it would contradict this hypothesis concerning shielding; however, as previously explained, it is not expected that the hole will exist for ballium. Understanding the secondary Coulomb hole is essential for a more accurate understanding of the HF model and its deficiencies. Having a complete understanding of the method could potentially lead to the development of more efficient correlated methods. As current correlated methods such as CI and CC are purely mathematically motivated, this greater understanding of the HF and exact position intracules could lead to the determination of the correlation energy through physically motivated methods such as intracule functional theory.

In Chapter 5, we detailed the analysis of an effect similar to the Coulomb hole which results from the comparison of the effects on interelectronic separations using basis sets with and without polarization functions. It had been previously noted that polarization functions led to a contraction of electron pairs, but there was no explanation as to why this occurs. One might expect that the addition of polarization functions would provide more flexibility for electronic motion and lead to a concomitant increase in interelectronic separations. However, through the study of each component of the energy in polarized and unpolarized basis sets as well as the Coulomb hole and differences in the electron density $\Delta\rho(\boldsymbol{r})$, it was determined that by incorporating polarization functions, these orbitals cause electrons to shift towards the bonding regions to improve the description of chemical bonds in molecules. For this reason, this effect appears to be a feature of molecular systems while there appears to be no such trend for the atomic systems. Through this study, we were able to correlate the behaviour in the position intracule (basis antihole) with the increase in electron density in the bonding regions of molecules.

While the first four results and discussion chapters focussed on the analysis of electronic structure, Chapter 6 focussed on a separate project involving the development of a program capable of optimizing reaction energetics with respect to a set of functional groups superimposed at a designable site within the molecule. We have demonstrated the utility of this program through the optimization of a deprotonation reaction of an HO-X molecule where X represents the functional site which is optimized. Although this reaction is very simple, the theory involved in this code should apply to a reactant complex of any size. As mentioned in that chapter, the foundation for this program has been established but there are still many areas which can be explored to expand the applicability of the code and improve its predictive capabilities.

Appendix A

In Chapter 4, we developed correlations between the strength of the secondary Coulomb hole and different properties of the intracule that are related to the diffuseness of said density. The correlations presented in that chapter could essentially be applied to any atom or molecule while maintaining their relevance. Here, we present two new correlations, the first of which is really only relevant for atoms, while the second would only apply to a set of ions in an isoelectronic series.

For one of the previous correlations, we had noted that the first moment of the position intracule, $\langle u \rangle$, yielded the average value of u in that system. For a system with two electrons, when both of the electrons are considered simultaneous, they tend to adopt different radii in order to avoid one another. Thus, we can consider two new moments which give the average inner radius, $\langle r_< \rangle$, and the average outer radius, $\langle r_> \rangle$. These values have been previously defined by Koga as[162]

$$\langle r_< \rangle = \int_0^\infty \int_0^\infty \rho(r_1, r_2) \times \mathrm{Min}(r_1, r_2)\, \mathrm{d}r_1\, \mathrm{d}r_2 \tag{1}$$

$$\langle r_> \rangle = \int_0^\infty \int_0^\infty \rho(r_1, r_2) \times \mathrm{Max}(r_1, r_2)\, \mathrm{d}r_1\, \mathrm{d}r_2 \tag{2}$$

We will denote the difference between these two radii as Δr_{io} given simply by

$$\Delta r_{io} = \langle r_> \rangle - \langle r_< \rangle \tag{3}$$

This new variable describes the average radial separation of the two electrons in the system.

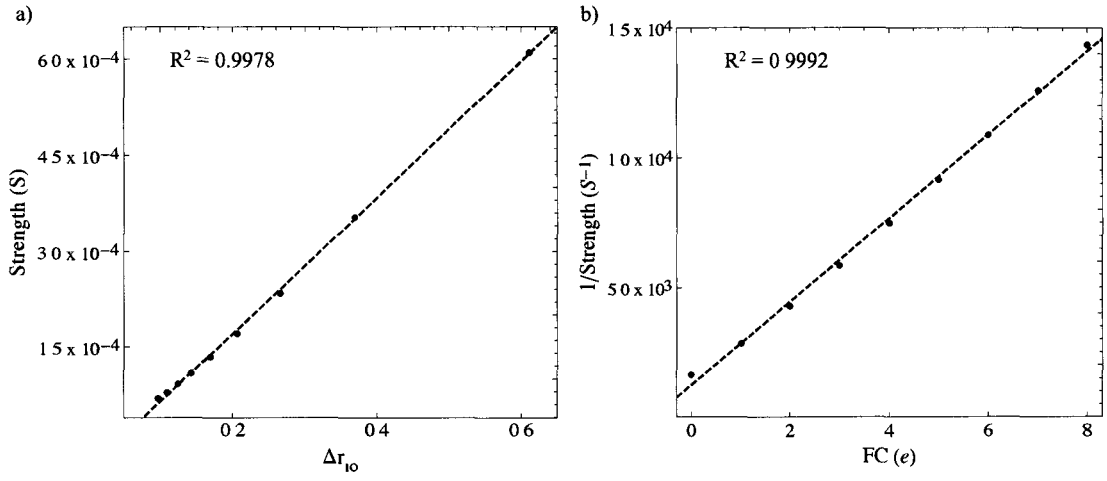

Figure A.1: Correlation between a) the average radial separation and the strength of the secondary Coulomb hole, and b) the formal charge (FC) of the ion and the inverse of the secondary hole strength.

The relationship between Δr_{io} and the strength of the secondary Coulomb hole is given in Figure 1a. One can see that the trend is linear and indicates that as the electrons increase their radial separation, the size of the secondary hole increases. These data substantiate the idea that HF theory overestimates screening when the electrons are far apart.

As mentioned earlier, the second correlation that will be discussed here is only relevant for a given isoelectronic series. This relationship concerns the formal charge (FC) on the ion with the inverse of the strength of the secondary hole (i.e. S^{-1}). The formal charge is expressed in atomic units in terms of the elementary charge e which in SI units is equal to $1.602 \times 10^{-19} C$. The results of this correlation are given in Figure 1b. This relationship is analogous to those that were explored in Chapter 4 as the electron density would be less diffuse as the ionic charge is increased. Thus, as there is a much smaller probability that the electrons will be far apart, the strength of the secondary Coulomb hole decreases as was noted in the previously studied relationships.

Appendix B

In the study of polarization effects presented in Chapter 5, all contributors to the energy were analyzed to determine which components compensated for the increase in electron repulsion energy to lead to the overall decrease in the total energy required by the variational theorem. Tabulated below are all of the energy differences for the seven basis set comparisons for each individual element of the energy.

Table B.1: ΔE_{tot} for the seven basis set comparisons.

	ΔE_{tot}						
System	Case 1	Case 2	Case 3	Case 4	Case 5	Case 6	Case 7
Al	-0.00279	-0.00213	-0.00213	-0.00170	-0.00003	-0.00337	-0.00391
Ar	-0.00159	0.00000	0.00000	0.00000	0.00000	0.00000	0.00000
B	-0.00255	-0.00308	-0.00304	-0.00072	-0.00001	-0.00322	-0.00374
Be	-0.00018	0.00000	0.00000	0.00000	0.00000	0.00000	0.00000
C	-0.00302	-0.00302	-0.00300	-0.00067	-0.00001	-0.00314	-0.00365
Cl	-0.00502	-0.00356	-0.00356	-0.00097	-0.00200	-0.00385	-0.00645
F	-0.00410	-0.00272	-0.00270	-0.00077	-0.00115	-0.00279	-0.00453
He	0.00000	0.00000	0.00000	0.00000	0.00000	0.00000	0.00000
Li	-0.00014	0.00000	0.00000	0.00000	0.00000	0.00000	0.00000
Mg	-0.00039	0.00000	0.00000	0.00000	0.00000	0.00000	0.00000
N	-0.00435	0.00000	0.00000	0.00000	0.00000	0.00000	0.00000
Na	-0.07491	0.00000	0.00000	0.00000	0.00000	0.00000	0.00000
Ne	-0.00053	0.00000	0.00000	0.00000	0.00000	0.00000	0.00000
O	-0.00362	-0.00272	-0.00265	-0.00079	-0.00115	-0.00283	-0.00453
P	-0.00120	0.00000	0.00000	0.00000	0.00000	0.00000	0.00000
S	-0.00454	-0.00319	-0.00319	-0.00119	-0.00198	-0.00375	-0.00631
Si	-0.00335	-0.00257	-0.00256	-0.00154	-0.00004	-0.00364	-0.00418
BeH	-0.00477	-0.00403	-0.00393	-0.00044	-0.00010	-0.10138	-0.10103
CH	-0.01560	-0.01540	-0.01520	-0.00206	-0.00040	-0.01852	-0.02128
$CH_2(^1A_1)$	-0.02314	-0.02333	-0.02312	-0.00288	-0.00041	-0.02278	-0.02664

Table B.1: (*Continued.*)

	ΔE_{tot}						
System	Case 1	Case 2	Case 3	Case 4	Case 5	Case 6	Case 7
$CH_2(^3B_1)$	-0.01374	-0.01410	-0.01418	-0.00153	-0.00064	-0.01362	-0.01661
CH_3	-0.01781	-0.01817	-0.01823	-0.00219	-0.00089	-0.01821	-0.02163
CH_3Cl	-0.04410	-0.04320	-0.04230	-0.00569	-0.00281	-0.04706	-0.04775
CH_3SH	-0.06323	-0.06255	-0.06199	-0.00755	-0.00328	-0.06310	-0.06809
CH_4	-0.02118	-0.02091	-0.02072	-0.00266	-0.00076	-0.02242	-0.02435
Cl_2	-0.05111	-0.04678	-0.04547	-0.00811	-0.00836	-0.05404	-0.06021
ClF	-0.04455	-0.03658	-0.03678	-0.01137	-0.00610	-0.03608	-0.05322
ClO	-0.06385	-0.05844	-0.05785	-0.01084	-0.00808	-0.05780	-0.07172
CN	-0.04205	-0.04257	-0.04210	-0.00414	-0.00268	-0.04228	-0.04977
CO	-0.07011	-0.06857	-0.06811	-0.00604	-0.00388	-0.07003	-0.07651
CO_2	-0.11789	-0.11859	-0.11873	-0.00961	-0.00824	-0.11782	-0.13630
CS	-0.06486	-0.06517	-0.06464	-0.00782	-0.00302	-0.06532	-0.07262
F_2	-0.02774	-0.01817	-0.01777	-0.00630	-0.00446	-0.01880	-0.02728
H_2	-0.00454	-0.00450	-0.00451	-0.00055	-0.00001	-0.00414	-0.00499
H_2CCH_2	-0.03432	-0.03534	-0.03534	-0.00431	-0.00265	-0.03458	-0.04383
H_2CO	-0.06104	-0.05882	-0.05976	-0.00616	-0.00388	-0.06021	-0.06809
H_2NNH_2	-0.06433	-0.05938	-0.06004	-0.00612	-0.00242	-0.07228	-0.06513
H_2O	-0.03814	-0.03704	-0.03779	-0.00414	-0.00172	-0.04629	-0.04061
H_2S	-0.04814	-0.04679	-0.04668	-0.00562	-0.00190	-0.04355	-0.05081
H_3CCH_3	-0.04072	-0.04006	-0.03979	-0.00486	-0.00160	-0.04282	-0.04644
H_3COH	-0.05914	-0.05582	-0.05657	-0.00661	-0.00326	-0.06159	-0.06300
HCCH	-0.02869	-0.02955	-0.02969	-0.00337	-0.00295	-0.02862	-0.03770
HCl	-0.02924	-0.02856	-0.02835	-0.00361	-0.00160	-0.02745	-0.03185
HCN	-0.04799	-0.04916	-0.04850	-0.00456	-0.00309	-0.04858	-0.05716
HCO	-0.06357	-0.06275	-0.06307	-0.00625	-0.00395	-0.06357	-0.07177
HF	-0.02795	-0.02477	-0.02484	-0.00308	-0.00172	-0.03090	-0.02718
HOCl	-0.05987	-0.05408	-0.05368	-0.00987	-0.00620	-0.05900	-0.06677
HOOH	-0.06720	-0.05983	-0.05988	-0.00771	-0.00416	-0.07035	-0.06558
Li_2	-0.00068	-0.00018	-0.00017	-0.00001	-0.00001	-0.00009	-0.00012
LiF	-0.01331	-0.00661	-0.00427	-0.00379	-0.00018	-0.01246	-0.01072
LiH	-0.00192	-0.00113	-0.00114	-0.00028	-0.00004	-0.00233	-0.00164
N_2	-0.07491	-0.07527	-0.07503	-0.00682	-0.00322	-0.07534	-0.08800
Na_2	-0.00028	-0.00032	-0.00031	-0.00033	-0.00010	-0.00017	-0.00022
NaCl	-0.00858	-0.00723	-0.00712	-0.00289	-0.00066	-0.00800	-0.00944
NH	-0.01960	-0.01867	-0.01831	-0.00226	-0.00039	-0.16107	-0.02051
NH_2	-0.03238	-0.03176	-0.03169	-0.00386	-0.00075	-0.11049	-0.03524
NH_3	-0.03393	-0.03218	-0.03267	-0.00267	-0.00027	-0.04060	-0.03583

Table B.1: (*Continued.*)

	ΔE_{tot}						
System	Case 1	Case 2	Case 3	Case 4	Case 5	Case 6	Case 7
NO	-0.07253	-0.06952	-0.06930	-0.00684	-0.00430	-0.07337	-0.08029
O_2	-0.06921	-0.05875	-0.05811	-0.00807	-0.00470	-0.30773	-0.06690
OH	-0.02494	-0.02364	-0.02367	-0.00293	-0.00153	-0.02732	-0.02647
P_2	-0.06901	-0.06938	-0.06842	-0.01443	-0.00382	-0.07323	-0.08059
PH_2	-0.04294	-0.04001	-0.04005	-0.00521	-0.00132	-0.03781	-0.04414
PH_3	-0.05810	-0.05384	-0.05383	-0.00594	-0.00128	-0.04929	-0.05728
S_2	-0.07843	-0.07515	-0.07395	-0.01615	-0.00900	-0.23349	-0.09399
Si_2	-0.02620	-0.03514	-0.03398	-0.01296	-0.00131	-0.02126	-0.03560
Si_2H_6	-0.09872	-0.09221	-0.09155	-0.00914	-0.00241	-0.07941	-0.09628
$SiH_2(^1A_1)$	-0.03276	-0.03042	-0.03028	-0.00340	-0.00061	-0.02727	-0.03221
$SiH_2(^3B_1)$	-0.02799	-0.02605	-0.02597	-0.00445	-0.00081	-0.02381	-0.02936
SiH_3	-0.04390	-0.04064	-0.04061	-0.00508	-0.00104	-0.03497	-0.04399
SiH_4	-0.05724	-0.05288	-0.05267	-0.00525	-0.00109	-0.04370	-0.05508
SiO	-0.07734	-0.06417	-0.06557	-0.01306	-0.00329	-0.05908	-0.07967
SO	-0.09578	-0.08707	-0.08810	-0.01927	-0.00881	-0.08291	-0.10749
SO_2	-0.26486	-0.24128	-0.24080	-0.04580	-0.01806	-0.22806	-0.28326

Table B.2: ΔE_T for the seven basis set comparisons.

	ΔE_T						
System	Case 1	Case 2	Case 3	Case 4	Case 5	Case 6	Case 7
Al	-0.08343	0.00814	0.00818	-0.00410	0.00006	0.00807	0.00372
Ar	-0.33576	0.00000	0.00000	0.00000	0.00000	0.00000	0.00000
B	-0.00372	0.00536	0.00587	-0.00182	0.00003	0.00568	0.00374
Be	-0.00196	0.00000	0.00000	0.00000	0.00000	0.00000	0.00000
C	0.00549	0.00505	0.00538	-0.00145	0.00003	0.00527	0.00361
Cl	-0.29022	0.00847	0.00847	-0.00299	0.00399	0.00846	0.00871
F	-0.19701	0.00493	0.00511	-0.00134	0.00178	0.00573	0.00537
He	0.00000	0.00000	0.00000	0.00000	0.00000	0.00000	0.00000
Li	0.00463	0.00000	0.00000	0.00000	0.00000	0.00000	0.00000
Mg	-0.04042	0.00000	0.00000	0.00000	0.00000	0.00000	0.00000
N	-0.08240	0.00000	0.00000	0.00000	0.00000	0.00000	0.00000
Na	0.00053	0.00000	0.00000	0.00000	0.00000	0.00000	0.00000
Ne	-0.11270	0.00000	0.00000	0.00000	0.00000	0.00000	0.00000
O	-0.14661	0.00463	0.00501	-0.00127	0.00183	0.00527	0.00513
P	-0.21532	0.00000	0.00000	0.00000	0.00000	0.00000	0.00000
S	-0.24823	0.00844	0.00844	-0.00348	0.00375	0.00796	0.00787
Si	-0.12944	0.00882	0.00891	-0.00445	0.00005	0.00818	0.00397
BeH	-0.00372	0.00538	0.00472	-0.00020	0.00081	0.09114	0.09273
CH	-0.00336	-0.00319	-0.00166	-0.00236	-0.00032	-0.02098	-0.00216
$CH_2(^1A_1)$	-0.02014	-0.01322	-0.01107	-0.00219	-0.00143	-0.03913	0.00868
$CH_2(^3B_1)$	-0.05282	-0.00990	-0.01017	0.00316	-0.00459	-0.03244	0.01384
CH_3	-0.06179	-0.01469	-0.01443	0.00495	-0.00392	-0.04587	0.02189
CH_3Cl	-0.47581	-0.07913	-0.07256	-0.00700	-0.01004	-0.17653	-0.03800
CH_3SH	-0.46683	-0.08676	-0.08226	-0.00806	-0.01011	-0.21867	-0.04743
CH_4	-0.06402	-0.01789	-0.01521	0.00837	-0.00287	-0.06149	0.03332
Cl_2	-0.86124	-0.17659	-0.17194	-0.05284	-0.01428	-0.26833	-0.24268
ClF	-0.71928	-0.13091	-0.13387	-0.05708	-0.01488	-0.14834	-0.21393
ClO	-0.76687	-0.19780	-0.19656	-0.06779	-0.02480	-0.26294	-0.26937
CN	-0.20272	-0.10480	-0.10092	-0.00979	-0.00790	-0.12377	-0.07186
CO	-0.22360	-0.06952	-0.06994	-0.00507	-0.00692	-0.09716	-0.02562
CO_2	-0.42445	-0.00924	-0.10992	-0.01896	-0.01178	-0.19627	-0.08192
CS	-0.43968	-0.11710	-0.11130	-0.01860	-0.00767	-0.21935	-0.10384
F_2	-0.50506	-0.05463	-0.05430	-0.00476	-0.00592	-0.05074	-0.08725
H_2	0.00314	0.00415	0.00453	0.00097	-0.00013	0.00344	0.00499
H_2CCH_2	-0.11991	-0.03422	-0.03303	0.00373	-0.00181	-0.09061	0.03318
H_2CO	-0.26588	-0.06940	-0.07357	-0.00863	-0.00504	-0.14340	-0.02177

Table B.2: (*Continued.*)

	ΔE_T						
System	Case 1	Case 2	Case 3	Case 4	Case 5	Case 6	Case 7
H_2NNH_2	-0.29085	-0.06109	-0.06422	-0.01341	-0.00357	-0.17172	0.03339
H_2O	-0.18602	-0.02611	-0.02834	-0.01484	0.00204	-0.07870	0.00664
H_2S	-0.37452	-0.03825	-0.03697	-0.00865	-0.00179	-0.12820	-0.04201
H_3CCH_3	-0.13620	-0.03720	-0.03340	0.00958	-0.00612	-0.12779	0.05759
H_3COH	-0.27405	-0.06351	-0.06431	-0.01208	-0.00489	-0.14304	0.00453
HCCH	-0.10815	0.00438	0.00461	-0.00992	-0.01430	-0.06900	-0.02314
HCl	-0.37973	-0.02179	-0.02073	-0.00827	-0.00360	-0.08213	-0.02479
HCN	-0.13413	-0.04086	-0.03671	-0.00390	-0.00783	-0.08517	-0.02314
HCO	-0.25845	-0.07557	-0.07771	-0.01051	-0.00612	-0.12867	-0.03628
HF	-0.22976	-0.01730	-0.01800	-0.01473	-0.00110	-0.04266	-0.00868
HOCl	-0.66075	-0.13372	-0.13325	-0.04772	-0.01524	-0.19021	-0.17698
HOOH	-0.43554	-0.08140	-0.08259	-0.04233	-0.00313	-0.15202	-0.05830
Li_2	0.00293	0.00056	0.00050	-0.00033	-0.00010	-0.00149	0.00014
LiF	-0.19178	-0.02145	-0.00477	-0.00393	-0.00107	-0.03243	-0.04733
LiH	0.00673	0.00157	0.00148	0.00011	0.00004	-0.00441	0.00326
N_2	-0.25661	-0.07752	-0.07548	-0.01333	0.00209	-0.13794	-0.03058
Na_2	0.00789	0.00087	0.00088	0.00096	0.00099	0.00697	0.00973
NaCl	-0.28767	-0.00405	-0.00737	-0.00687	0.00279	-0.00277	-0.01481
NH	-0.08900	-0.01096	-0.00925	-0.00609	0.00187	0.10219	-0.00074
NH_2	-0.09861	-0.01863	-0.01790	-0.00781	0.00163	0.05831	0.01057
NH_3	-0.11813	-0.02272	-0.02404	-0.00041	0.00156	-0.07815	0.03153
NO	-0.45017	-0.16052	-0.16282	-0.02723	-0.00734	-0.24078	-0.12917
O_2	-0.55703	-0.13201	-0.12788	-0.04406	-0.00842	-0.67596	-0.11104
OH	-0.16367	-0.01282	-0.01265	-0.01335	0.00273	-0.04040	0.00002
P_2	-0.68117	-0.13313	-0.12530	-0.05494	-0.01125	-0.29387	-0.16110
PH_2	-0.27689	-0.01483	-0.00779	0.00075	-0.08812	-0.12829	-0.03290
PH_3	-0.31334	-0.02342	-0.02252	-0.00429	-0.00045	-0.12829	-0.03290
S_2	-0.88673	-0.20359	-0.19534	-0.06919	-0.02111	-0.55062	-0.26344
Si_2	-0.38593	-0.04325	-0.03706	-0.04049	-0.00642	-0.30412	-0.06558
Si_2H_6	-0.45735	-0.00722	-0.00311	-0.00963	0.00336	-0.19714	-0.01318
$SiH_2(^1A_1)$	-0.16707	-0.00879	-0.00758	-0.00502	0.00067	-0.05150	-0.01013
$SiH_2(^3B_1)$	-0.18378	-0.00019	0.00053	-0.00681	0.00175	-0.04122	-0.00511
SiH_3	-0.18446	0.00290	0.00364	-0.00533	0.00304	-0.05846	-0.00074
SiH_4	-0.19887	-0.00324	-0.00112	-0.00381	0.00347	-0.08305	-0.00522
SiO	-0.38220	-0.08018	-0.09134	-0.04157	-0.00377	-0.08206	-0.13815
SO	-0.72189	-0.22143	-0.23172	-0.08270	-0.02005	-0.29361	-0.31366
SO_2	-1.33445	-0.58339	-0.58478	-0.14535	-0.03904	-0.77499	-0.73453

Table B.3: ΔE_{eN} for the seven basis set comparisons.

	ΔE_{eN}						
System	Case 1	Case 2	Case 3	Case 4	Case 5	Case 6	Case 7
Al	0.05600	-0.03512	-0.03558	0.01887	-0.00018	-0.02327	-0.01247
Ar	0.35105	0.00000	0.00000	0.00000	0.00000	0.00000	0.00000
B	0.00360	-0.00687	-0.00860	0.00532	-0.00001	-0.00632	-0.00298
Be	0.00722	0.00000	0.00000	0.00000	0.00000	0.00000	0.00000
C	-0.01067	-0.00573	-0.00683	0.00405	-0.00165	-0.25209	-0.25533
Cl	0.29334	-0.02004	-0.02003	0.00860	-0.00862	-0.01560	-0.01802
F	0.19474	-0.00569	-0.00648	0.00361	-0.00225	-0.00604	-0.00497
He	0.00000	0.00000	0.00000	0.00000	0.00000	0.00000	0.00000
Li	-0.00357	0.00000	0.00000	0.00000	0.00000	0.00000	0.00000
Mg	0.03288	0.00000	0.00000	0.00000	0.00000	0.00000	0.00000
N	0.08751	0.00000	0.00000	0.00000	0.00000	0.00000	0.00000
Na	-0.00121	0.00000	0.00000	0.00000	0.00000	0.00000	0.00000
Ne	0.11165	0.00000	0.00000	0.00000	0.00000	0.00000	0.00000
O	0.15256	-0.00568	-0.14619	0.00389	-0.00260	-0.00555	-0.00518
P	0.22724	0.00000	0.00000	0.00000	0.00000	0.00000	0.00000
S	0.24735	-0.02423	-0.02417	0.01117	-0.00945	-0.01564	-0.01873
Si	0.11347	-0.02947	-0.03011	0.01660	-0.00009	-0.01908	-0.01070
BeH	-0.01537	-0.02246	-0.02170	-0.00088	-0.00165	-0.25209	-0.25533
CH	-0.04475	-0.04260	-0.04609	0.00146	-0.00029	-0.02148	-0.05172
$CH_2(^1A_1)$	-0.05931	-0.07093	-0.07545	-0.00662	0.00069	-0.03878	-0.10751
$CH_2(^3B_1)$	0.01617	-0.03552	-0.03300	-0.00726	0.00322	-0.00593	-0.06835
CH_3	0.01870	-0.03934	-0.03786	-0.01054	0.00155	-0.00107	-0.08793
CH_3Cl	0.32388	-0.10776	-0.11545	-0.02803	-0.00280	-0.04422	-0.18763
CH_3SH	0.21117	-0.21907	-0.22544	-0.03800	-0.00521	-0.08996	-0.30249
CH_4	0.01775	-0.03814	-0.04272	-0.01715	0.00106	0.00799	-0.10427
Cl_2	0.57235	-0.13461	-0.13388	-0.03565	-0.04534	-0.01549	-0.22294
ClF	0.51010	-0.06743	-0.04740	-0.01842	-0.01515	-0.04397	-0.08028
ClO	0.50315	-0.09446	-0.07891	0.01207	-0.01148	-0.02676	-0.09061
CN	-0.02695	-0.12726	-0.13255	-0.01296	-0.00373	-0.10706	-0.19345
CO	-0.13948	-0.28497	-0.27155	-0.02720	-0.01499	-0.26967	-0.36420
CO_2	-0.19679	-0.54085	-0.48628	-0.03042	-0.03187	-0.47403	-0.62947
CS	0.00485	-0.35027	-0.36962	-0.03745	-0.01829	-0.23562	-0.44689
F_2	0.29190	-0.06147	-0.04853	-0.02274	-0.01194	-0.07660	-0.09789
H_2	-0.01403	-0.01559	-0.01614	-0.00205	0.00007	-0.01388	-0.01745
H_2CCH_2	0.00582	-0.10053	-0.09950	-0.02159	-0.00991	-0.04292	-0.20507
H_2CO	0.00053	-0.21199	-0.18740	-0.01837	-0.01300	-0.13948	-0.28788

Table B.3: (*Continued.*)

	ΔE_{eN}						
System	Case 1	Case 2	Case 3	Case 4	Case 5	Case 6	Case 7
H_2NNH_2	0.05684	-0.17348	-0.15255	-0.01466	-0.00602	-0.12159	-0.29617
H_2O	0.07013	-0.10374	-0.08990	0.00590	-0.00856	-0.08459	-0.14308
H_2S	0.16931	-0.21351	-0.21708	-0.02505	-0.00728	-0.08710	-0.24271
H_3CCH_3	0.03840	-0.07886	-0.08652	-0.02967	0.00168	0.00628	-0.20193
H_3COH	0.08957	-0.13564	-0.11982	-0.01282	-0.00627	-0.07792	-0.22574
HCCH	-0.02547	-0.14987	-0.15024	-0.00550	0.00281	-0.07468	-0.14645
HCl	0.27663	-0.12289	-0.12338	-0.00870	-0.00303	-0.04216	-0.14256
HCN	-0.11803	-0.21345	-0.21843	-0.02471	-0.00716	-0.17481	-0.26848
HCO	-0.02229	-0.21313	-0.19555	-0.01213	-0.01368	-0.16238	-0.28101
HF	0.14956	-0.06472	-0.05457	0.00717	-0.00446	-0.07130	-0.07131
HOCl	0.40143	-0.13917	-0.11746	-0.01899	-0.01249	-0.12324	-0.17717
HOOH	0.14490	-0.18122	-0.15379	-0.00657	-0.01301	-0.17415	-0.23275
Li_2	0.00203	-0.00250	-0.00244	0.00037	-0.00015	-0.00084	-0.00108
LiF	0.18878	0.03261	-0.01444	-0.02191	-0.00032	0.12396	0.07409
LiH	-0.01983	-0.00957	-0.00937	-0.00288	-0.00041	-0.01193	-0.01410
N_2	-0.12363	-0.31241	-0.31798	-0.02232	-0.01935	-0.25463	-0.42637
Na_2	-0.01727	-0.01123	-0.01154	-0.00526	-0.00093	-0.02293	-0.02575
NaCl	0.15251	-0.13930	-0.12250	-0.01662	-0.01833	-0.08268	-0.14987
NH	0.03843	-0.05040	-0.05338	0.00358	-0.00295	-0.20267	-0.06368
NH_2	0.00446	-0.09152	-0.09152	0.00003	-0.00386	-0.15557	-0.13124
NH_3	0.01762	-0.09035	-0.08391	-0.00975	-0.00470	-0.05573	-0.16066
NO	0.12296	-0.16704	-0.15678	-0.00598	-0.01154	-0.10230	-0.24613
O_2	0.23968	-0.14914	-0.14619	-0.00269	-0.01314	0.34515	-0.22421
OH	0.10383	-0.06356	-0.05959	0.01072	-0.00623	-0.04859	-0.07578
P_2	0.02632	-0.59634	-0.62523	-0.09065	-0.03384	-0.48214	-0.76372
PH_2	0.04940	-0.23035	-0.23372	-0.01994	-0.00486	-0.11553	-0.23509
PH_3	0.06193	-0.30050	-0.30484	-0.04487	-0.00356	-0.14328	-0.31772
S_2	0.40438	-0.36533	-0.38258	-0.03473	-0.05340	-0.23419	-0.48611
Si_2	0.15724	-0.37625	-0.39770	-0.04719	-0.01201	0.19795	-0.34860
Si_2H_6	-0.14636	-0.63157	-0.64723	-0.07256	-0.02074	-0.28199	-0.66490
$SiH_2(^1A_1)$	-0.06323	-0.20851	-0.21313	-0.01931	-0.00281	-0.13299	-0.21849
$SiH_2(^3B_1)$	0.03143	-0.15941	-0.16146	0.20919	-0.00589	-0.06939	-0.13655
SiH_3	-0.06226	-0.24702	-0.24843	-0.00664	-0.00885	-0.11268	-0.24276
SiH_4	-0.12677	-0.31094	-0.31902	-0.03602	-0.01035	-0.14573	-0.32874
SiO	-0.30890	-0.48996	-0.44031	-0.05593	-0.02614	-0.40936	-0.51458
SO	0.19488	-0.29901	-0.24780	0.01461	-0.02997	-0.17556	-0.26583
SO_2	-0.21171	-0.85288	-0.76423	-0.15915	-0.07968	-0.60523	-0.97211

Table B.4: ΔE_{ee} for the seven basis set comparisons

	ΔE_{ee}						
System	Case 1	Case 2	Case 3	Case 4	Case 5	Case 6	Case 7
Al	0.02465	0.02485	0.02527	-0.01648	0.00009	0.01183	0.00484
Ar	-0.01688	0.00000	0.00000	0.00000	0.00000	0.00000	0.00000
B	-0.00243	-0.00158	-0.00031	-0.00422	-0.00003	-0.00257	-0.00450
Be	-0.00543	0.00000	0.00000	0.00000	0.00000	0.00000	0.00000
C	0.00216	-0.00234	-0.00155	-0.00328	-0.00003	-0.00334	-0.00483
Cl	-0.00814	0.00800	0.00799	-0.00657	0.00263	0.00329	0.00286
F	-0.18339	-0.00195	-0.00132	-0.00304	-0.00069	-0.00247	-0.00493
He	0.00000	0.00000	0.00000	0.00000	0.00000	0.00000	0.00000
Li	-0.00119	0.00000	0.00000	0.00000	0.00000	0.00000	0.00000
Mg	0.00714	0.00000	0.00000	0.00000	0.00000	0.00000	0.00000
N	-0.00554	0.00000	0.00000	0.00000	0.00000	0.00000	0.00000
Na	0.00068	0.00000	0.00000	0.00000	0.00000	0.00000	0.00000
Ne	0.00051	0.00000	0.00000	0.00000	0.00000	0.00000	0.00000
O	-0.00957	-0.00166	-0.00007	-0.00341	-0.00037	-0.00255	-0.00448
P	-0.01312	0.00000	0.00000	0.00000	0.00000	0.00000	0.00000
S	-0.00366	0.01262	0.01255	-0.00888	0.00371	0.00392	0.00455
Si	0.01262	0.01808	0.01864	-0.01369	0.00000	0.00725	0.00255
BeH	0.01097	0.01305	0.01304	0.00064	0.00074	0.05957	0.06158
CH	0.03251	0.03039	0.03255	-0.00115	0.00021	0.02393	0.03260
$CH_2(^1A_1)$	0.05631	0.06082	0.06340	0.00593	0.00033	0.05514	0.07219
$CH_2(^3B_1)$	0.02291	0.03132	0.02899	0.00257	0.00071	0.02475	0.03790
CH_3	0.02528	0.03587	0.03405	0.00341	0.00148	0.02874	0.04441
CH_3Cl	0.10782	0.14369	0.14571	0.02934	0.01002	0.17369	0.17789
CH_3SH	0.19244	0.24327	0.24571	0.03851	0.01205	0.24552	0.28183
CH_4	0.02508	0.03512	0.03720	0.00613	0.00106	0.03108	0.04660
Cl_2	0.23777	0.26441	0.26035	0.08039	0.05126	0.36916	0.40541
ClF	0.16462	0.16176	0.14450	0.06413	0.02392	0.15623	0.24100
ClO	0.19987	0.23382	0.21763	0.04487	0.02820	0.23189	0.28827
CN	0.18762	0.18949	0.19137	0.01861	0.00895	0.18856	0.21554
CO	0.29298	0.28592	0.27338	0.02623	0.01804	0.29681	0.31332
CO_2	0.50334	0.52160	0.47747	0.03977	0.03541	0.55248	0.57508
CS	0.36997	0.40220	0.41628	0.04823	0.02294	0.38966	0.47810
F_2	0.18542	0.09792	0.08506	0.06120	0.01340	0.10853	0.15790
H_2	0.00635	0.00694	0.00709	0.00054	0.00005	0.00631	0.00748
H_2CCH_2	0.07977	0.09942	0.09718	0.01355	0.00907	0.09894	0.12805
H_2CO	0.20431	0.22257	0.20121	0.02084	0.01416	0.22267	0.24156

Table B.4: (*Continued.*)

	ΔE_{ee}						
System	Case 1	Case 2	Case 3	Case 4	Case 5	Case 6	Case 7
H_2NNH_2	0.16967	0.17519	0.15673	0.02195	0.00717	0.22103	0.19765
H_2O	0.07675	0.09282	0.08044	0.00480	0.00481	0.11701	0.09583
H_2S	0.15707	0.20498	0.20737	0.02808	0.00717	0.17175	0.23391
H_3CCH_3	0.05708	0.07600	0.08013	0.01523	0.00283	0.07869	0.09790
H_3COH	0.12534	0.14333	0.12756	0.01828	0.00789	0.15937	0.15821
HCCH	0.10494	0.11594	0.11594	0.01205	0.00855	0.11507	0.13189
HCl	0.07387	0.11612	0.11677	0.01336	0.00503	0.09684	0.13550
HCN	0.20417	0.20514	0.20664	0.02405	0.01190	0.21140	0.23446
HCO	0.21717	0.22595	0.21018	0.01639	0.01584	0.22748	0.24553
HF	0.05225	0.05725	0.04773	0.00447	0.00384	0.08306	0.05281
HOCl	0.19946	0.21881	0.19703	0.05684	0.02153	0.25445	0.28138
HOOH	0.22344	0.20279	0.17650	0.041219	0.01190	0.25582	0.22547
Li_2	-0.00564	0.00177	0.00177	-0.00005	0.00024	0.00224	0.00082
LiF	-0.01031	-0.01777	0.01494	0.02204	0.00120	-0.10399	-0.03747
LiH	0.01118	0.00687	0.00674	0.00250	0.00024	0.01401	0.00920
N_2	0.30533	0.31466	0.31843	0.02883	0.01404	0.31721	0.36895
Na_2	0.00909	0.01004	0.01035	0.00396	-0.00016	0.01579	0.01581
NaCl	0.12659	0.13612	0.12275	0.02060	0.01487	0.07745	0.15523
NH	0.03097	0.04268	0.04432	0.00025	0.00069	-0.06059	0.04391
NH_2	0.06178	0.07838	0.07773	0.00393	0.00148	-0.01323	0.08544
NH_3	0.06658	0.08089	0.07528	0.00748	0.00287	0.09329	0.09330
NO	0.25467	0.25804	0.25030	0.02637	0.01457	0.26971	0.29501
O_2	0.24813	0.22240	0.21596	0.03869	0.01686	0.02308	0.26835
OH	0.03490	0.05274	0.04857	-0.00030	0.00197	0.06167	0.04930
P_2	0.58584	0.66010	0.68211	0.13116	0.04127	0.70279	0.84423
PH_2	0.18455	0.20517	0.20778	0.02252	0.00279	0.16584	0.21443
PH_3	0.24904	0.27008	0.27354	0.04323	0.00274	0.22228	0.29334
S_2	0.40392	0.49377	0.50396	0.08777	0.06551	0.55133	0.65556
Si_2	0.20249	0.38436	0.40078	0.07471	0.01713	0.08491	0.37858
Si_2H_6	0.50499	0.54658	0.55879	0.07305	0.01497	0.39972	0.58180
$SiH_2(^1A_1)$	0.19754	0.18688	0.19042	0.02093	0.00153	0.15722	0.19641
$SiH_2(^3B_1)$	0.12436	0.13356	0.13496	-0.01856	0.00333	0.08681	0.11229
SiH_3	0.20283	0.20348	0.20418	0.00689	0.00478	0.13617	0.19951
SiH_4	0.26841	0.26130	0.26747	0.03458	0.00579	0.18509	0.27888
SiO	0.61375	0.50597	0.46608	0.08444	0.02662	0.43234	0.57306
SO	0.43124	0.43337	0.39142	0.04882	0.04121	0.38626	0.47201
SO_2	1.28130	1.19499	1.10820	0.25870	0.10066	1.15216	1.42337

Table B.5: ΔE_J for the seven basis set comparisons.

	ΔE_J						
System	Case 1	Case 2	Case 3	Case 4	Case 5	Case 6	Case 7
Al	0.02953	0.03170	0.03216	-0.01309	0.00047	0.02098	0.01530
Ar	-0.02483	0.00000	0.00000	0.00000	0.00000	0.00000	0.00000
B	0.00391	0.00658	0.00811	-0.00324	0.00016	0.00553	0.00508
Be	-0.00507	0.00000	0.00000	0.00000	0.00000	0.00000	0.00000
C	0.00734	0.00496	0.00590	-0.00236	0.00016	0.00384	0.00370
Cl	-0.00692	0.01642	0.01641	-0.00488	0.00497	0.01207	0.01514
F	0.00136	0.00432	0.00498	-0.00153	0.00019	0.00384	0.00359
He	0.00000	0.00000	0.00000	0.00000	0.00000	0.00000	0.00000
Li	-0.00030	0.00000	0.00000	0.00000	0.00000	0.00000	0.00000
Mg	0.00699	0.00000	0.00000	0.00000	0.00000	0.00000	0.00000
N	-0.01051	0.00000	0.00000	0.00000	0.00000	0.00000	0.00000
Na	0.00079	0.00000	0.00000	0.00000	0.00000	0.00000	0.00000
Ne	-0.00069	0.00000	0.00000	0.00000	0.00000	0.00000	0.00000
O	-0.00778	0.00478	0.00639	-0.00167	0.00060	0.00404	0.00442
P	-0.01852	0.00000	0.00000	0.00000	0.00000	0.00000	0.00000
S	-0.00175	0.02085	0.02079	-0.00638	0.00622	0.01312	0.01756
Si	0.01621	0.02502	0.02563	-0.01120	0.00057	0.01587	0.01247
BeH	0.01976	0.02072	0.02068	0.00124	0.00101	0.10939	0.01120
CH	0.04693	0.04634	0.04891	-0.00066	0.00094	0.05045	0.06566
$CH_2(^1A_1)$	0.07190	0.07739	0.08081	0.00457	0.00072	0.06865	0.09020
$CH_2(^3B_1)$	0.03597	0.04638	0.04353	0.00390	0.00127	0.03978	0.05604
CH_3	0.04470	0.05753	0.05545	0.00553	0.00247	0.04976	0.07098
CH_3Cl	0.12545	0.17137	0.17377	0.03071	0.01086	0.20050	0.20979
CH_3SH	0.22541	0.28666	0.28924	0.04010	0.01373	0.28559	0.32897
CH_4	0.04896	0.06121	0.06371	0.00864	0.00169	0.05565	0.07827
Cl_2	0.22093	0.26247	0.25899	0.07600	0.05033	0.36838	0.40022
ClF	0.15029	0.16129	0.14297	0.06170	0.02277	0.15273	0.23832
ClO	0.18469	0.23591	0.21841	0.03838	0.02944	0.23010	0.28506
CN	0.18447	0.18892	0.19106	0.01965	0.00959	0.19093	0.21862
CO	0.32227	0.31774	0.30391	0.02906	0.02168	0.33015	0.35024
CO_2	0.56286	0.58603	0.53723	0.04346	0.04190	0.62199	0.64705
CS	0.38919	0.43003	0.44587	0.05024	0.02614	0.41649	0.51305
F_2	0.18072	0.09802	0.08418	0.06028	0.01195	0.10841	0.15600
H_2	0.01270	0.01387	0.01419	0.00108	0.00009	0.01261	0.01496
H_2CCH_2	0.11650	0.14076	0.13836	0.01769	0.01175	0.13953	0.18073
H_2CO	0.23925	0.26365	0.23991	0.02421	0.01714	0.26276	0.28858

Table B.5: (*Continued.*)

	ΔE_J						
System	Case 1	Case 2	Case 3	Case 4	Case 5	Case 6	Case 7
H_2NNH_2	0.19273	0.20704	0.18674	0.02150	0.00857	0.25940	0.23164
H_2O	0.08634	0.10693	0.09269	0.00381	0.00572	0.13880	0.10881
H_2S	0.17776	0.23280	0.23526	0.02818	0.00821	0.19651	0.26190
H_3CCH_3	0.09994	0.12301	0.12766	0.01939	0.00426	0.12315	0.15488
H_3COH	0.15358	0.17888	0.16116	0.01966	0.00551	0.19547	0.19751
HCCH	0.13725	0.15077	0.15070	0.01478	0.01069	0.15348	0.17213
HCl	0.07931	0.12928	0.12990	0.01320	0.00551	0.10920	0.14888
HCN	0.23862	0.24235	0.24465	0.02766	0.01478	0.25096	0.27852
HCO	0.24623	0.25967	0.24260	0.01940	0.01938	0.26232	0.28525
HF	0.05709	0.06488	0.05387	0.00450	0.00457	0.09666	0.05872
HOCl	0.19312	0.22655	0.20333	0.05328	0.02170	0.26436	0.28575
HOOH	0.23097	0.21998	0.19067	0.03915	0.01252	0.28159	0.23828
Li_2	-0.00412	0.00213	0.00213	-0.00009	0.00022	0.00239	0.00100
LiF	-0.02101	-0.02358	0.01466	0.02377	0.00152	-0.12584	-0.04707
LiH	0.01547	0.00910	0.00895	0.00286	0.00041	0.01805	0.01219
N_2	0.33541	0.35249	0.35734	0.03169	0.01731	0.35589	0.41634
Na_2	0.01038	0.01041	0.01074	0.00405	-0.00039	0.01678	0.01748
NaCl	0.12116	0.13806	0.12388	0.02099	0.01537	0.07331	0.15635
NH	0.03954	0.05646	0.05802	0.00037	0.00151	-0.02342	0.05839
NH_2	0.07628	0.09811	0.09731	0.00307	0.00282	0.02861	0.10631
NH_3	0.08093	0.10012	0.09399	0.00727	0.00373	0.11663	0.11431
NO	0.25017	0.26098	0.25192	0.02609	0.01681	0.27621	0.29982
O_2	-0.00778	0.23364	0.22707	0.04105	0.01954	-0.05137	0.28349
OH	0.04389	0.06762	0.06261	0.00028	0.00335	0.07999	0.06484
P_2	0.60454	0.69314	0.71700	0.13905	0.04581	0.74086	0.89172
PH_2	0.21329	0.23842	0.24120	0.02515	0.00551	0.19650	0.25074
PH_3	0.28874	0.31376	0.31720	0.04541	0.00453	0.25992	0.33720
S_2	0.40501	0.51042	0.52193	0.09289	0.07331	0.53035	0.68754
Si_2	0.20958	0.41286	0.43078	0.08331	0.01964	0.05455	0.41168
Si_2H_6	0.61038	0.65622	0.66851	0.07979	0.01940	0.49859	0.69613
$SiH_2(^1A_1)$	0.22190	0.21151	0.21543	0.02153	0.00236	0.17936	0.22069
$SiH_2(^3B_1)$	0.15193	0.16402	0.16558	-0.01225	0.00497	0.11854	0.14952
SiH_3	0.25146	0.25265	0.25361	0.01300	0.00690	0.18313	0.25447
SiH_4	0.33262	0.32346	0.32995	0.03877	0.00760	0.24116	0.34314
SiO	0.63872	0.53286	0.48933	0.08902	0.02962	0.45190	0.60407
SO	0.44457	0.45720	0.41221	0.05468	0.04787	0.40861	0.50568
SO_2	1.31330	1.24010	1.14690	0.26041	0.11142	1.19350	1.47770

Table B.6: ΔE_K for the seven basis set comparisons.

	ΔE_K						
System	Case 1	Case 2	Case 3	Case 4	Case 5	Case 6	Case 7
Al	-0.00488	-0.00685	-0.00689	-0.00339	-0.00037	-0.00915	-0.01046
Ar	0.00795	0.00000	0.00000	0.00000	0.00000	0.00000	0.00000
B	-0.00633	-0.00816	-0.00841	-0.00098	-0.00019	-0.00810	-0.00958
Be	-0.00036	0.00000	0.00000	0.00000	0.00000	0.00000	0.00000
C	-0.00518	-0.00731	-0.00745	-0.00092	-0.00018	-0.00718	-0.00853
Cl	-0.00121	-0.00842	-0.00842	-0.00169	-0.00233	-0.00878	-0.01228
F	-0.00320	-0.00627	-0.00630	-0.00151	-0.00088	-0.00631	-0.00852
He	0.00000	0.00000	0.00000	0.00000	0.00000	0.00000	0.00000
Li	-0.00090	0.00000	0.00000	0.00000	0.00000	0.00000	0.00000
Mg	0.00015	0.00000	0.00000	0.00000	0.00000	0.00000	0.00000
N	0.00497	0.00000	0.00000	0.00000	0.00000	0.00000	0.00000
Na	-0.00011	0.00000	0.00000	0.00000	0.00000	0.00000	0.00000
Ne	0.00120	0.00000	0.00000	0.00000	0.00000	0.00000	0.00000
O	-0.00179	-0.00644	-0.00646	-0.00174	-0.00097	-0.00659	-0.00891
P	0.00540	0.00000	0.00000	0.00000	0.00000	0.00000	0.00000
S	-0.00191	-0.00823	-0.00824	-0.00250	-0.00250	-0.00920	-0.01302
Si	-0.00359	-0.00694	-0.00699	-0.00249	-0.00047	-0.00862	-0.00991
BeH	-0.00878	-0.00767	-0.00764	-0.00060	-0.00027	-0.04982	-0.05037
CH	-0.01442	-0.01595	-0.01636	-0.00049	-0.00073	-0.02652	-0.03306
$CH_2(^1A_1)$	-0.01559	-0.01657	-0.01741	0.00135	-0.00039	-0.01352	-0.01801
$CH_2(^3B_1)$	-0.01306	-0.01506	-0.01453	-0.00133	-0.00056	-0.01504	-0.01814
CH_3	-0.01942	-0.02166	-0.02140	-0.00212	-0.00100	-0.02102	-0.02657
CH_3Cl	-0.01763	-0.02768	-0.02807	-0.00138	-0.00084	-0.02681	-0.03191
CH_3SH	-0.03298	-0.04338	-0.04353	-0.00159	-0.00168	-0.04008	-0.04714
CH_4	-0.02387	-0.02609	-0.02651	-0.00251	-0.00064	-0.02457	-0.03167
Cl_2	0.01684	0.00194	0.00136	0.00439	0.00093	0.00077	0.00519
ClF	0.01434	0.00048	0.00153	0.00244	0.00115	0.00350	0.00268
ClO	0.01518	-0.00210	-0.00079	0.00659	-0.00124	0.00179	0.00321
CN	0.00315	0.00056	0.00031	-0.00104	-0.00064	-0.00237	-0.00308
CO	-0.02929	-0.03183	-0.03054	-0.00283	-0.00364	-0.03335	-0.03693
CO_2	-0.05952	-0.06443	-0.05976	-0.00368	-0.00649	-0.06951	-0.07196
CS	-0.01921	-0.02784	-0.02960	-0.00202	-0.00320	-0.02683	-0.03495
F_2	0.00470	-0.00010	0.00088	0.00092	0.00145	0.00012	0.00190
H_2	-0.00635	-0.00694	-0.00709	-0.00054	-0.00005	-0.00631	-0.00748
H_2CCH_2	-0.03673	-0.04135	-0.04118	-0.00414	-0.00267	-0.04059	-0.05268
H_2CO	-0.03494	-0.04108	-0.03870	-0.00337	-0.00299	-0.04009	-0.04702

Table B.6: (*Continued.*)

	ΔE_K						
System	Case 1	Case 2	Case 3	Case 4	Case 5	Case 6	Case 7
H_2NNH_2	-0.02306	-0.03185	-0.03001	0.00045	-0.00141	-0.03837	-0.03399
H_2O	-0.00959	-0.01412	-0.01223	0.00099	-0.00091	-0.02180	-0.01299
H_2S	-0.02069	-0.02782	-0.02788	-0.00010	-0.00104	-0.02476	-0.02798
H_3CCH_3	-0.04286	-0.04700	-0.04754	-0.00415	-0.00143	-0.04446	-0.05698
H_3COH	-0.02824	-0.03555	-0.03360	-0.00138	-0.00177	-0.03610	-0.03930
HCCH	-0.03231	-0.03482	-0.03476	-0.00274	-0.00215	-0.03842	-0.04024
HCl	-0.00544	-0.01316	-0.01304	0.00016	-0.00048	-0.01237	-0.01338
HCN	-0.03445	-0.03721	-0.03801	-0.00361	-0.00288	-0.03957	-0.04406
HCO	-0.02907	-0.03373	-0.03241	-0.00301	-0.00343	-0.03484	-0.03973
HF	-0.00484	-0.00764	-0.00614	-0.00003	-0.00073	-0.01360	-0.00591
HOCl	0.00634	-0.00775	-0.00630	0.00356	-0.00017	-0.00991	-0.00438
HOOH	-0.00753	-0.01719	-0.01418	0.00204	-0.00053	-0.02577	-0.01281
Li_2	-0.00152	-0.00036	-0.00037	0.00004	0.00002	-0.00015	-0.00018
LiF	0.01071	0.00581	0.00028	-0.00173	-0.00031	0.02186	0.00960
LiH	-0.00429	-0.00223	-0.00221	-0.00036	-0.00007	-0.00404	-0.00299
N_2	-0.03008	-0.03784	-0.03891	-0.00285	-0.00327	-0.03867	-0.04739
Na_2	-0.00129	-0.00037	-0.00039	-0.00009	0.00023	-0.00099	-0.00167
NaCl	0.00542	-0.00194	-0.00113	-0.00039	-0.00049	0.00414	-0.00112
NH	-0.00857	-0.01377	-0.01370	-0.00012	-0.00082	-0.03717	-0.01448
NH_2	-0.01450	-0.01973	-0.01958	0.00085	-0.00134	-0.04184	-0.02087
NH_3	-0.01434	-0.01923	-0.01871	0.00021	-0.00087	-0.02334	-0.02101
NO	0.00450	-0.00294	-0.00163	0.00028	-0.00223	-0.00650	-0.00481
O_2	-0.00338	-0.00124	-0.01112	-0.00237	-0.00268	0.07445	-0.01514
OH	-0.00899	-0.01488	-0.01403	-0.00058	-0.00138	-0.01832	-0.01554
P_2	-0.01870	-0.03304	-0.03490	-0.00789	-0.00454	-0.03807	-0.04749
PH_2	-0.02874	-0.03325	-0.03342	-0.00263	-0.00272	-0.03067	-0.03630
PH_3	-0.03969	-0.04368	-0.04367	-0.00218	-0.00180	-0.03764	-0.04386
S_2	-0.00108	-0.01665	-0.01798	-0.00511	-0.00781	0.02098	-0.03198
Si_2	-0.00709	-0.02850	-0.02999	-0.00859	-0.00251	0.03036	-0.03310
Si_2H_6	-0.10539	-0.10963	-0.10972	-0.00674	-0.00443	-0.09887	-0.11433
$SiH_2(^1A_1)$	-0.02436	-0.02463	-0.02501	-0.00059	-0.00083	-0.02213	-0.02428
$SiH_2(^3B_1)$	-0.02758	-0.03047	-0.03062	-0.00631	-0.00163	-0.03173	-0.03723
SiH_3	-0.04863	-0.04917	-0.04944	-0.00612	-0.00212	-0.04696	-0.05497
SiH_4	-0.06422	-0.06216	-0.06249	-0.00419	-0.00181	-0.05608	-0.06427
SiO	-0.02497	-0.02689	-0.02326	-0.00457	-0.00300	-0.01956	-0.03102
SO	-0.01333	-0.02383	-0.02079	-0.00586	-0.00666	-0.02235	-0.03368
SO_2	-0.03196	-0.04508	-0.03871	-0.00171	-0.01075	-0.04131	-0.05437

Bibliography

[1] Levine, I. N. *Quantum Chemistry*, 6th ed.; Pearson Education: New Jersey, 2009.

[2] Heitler, W.; London, F. *Z. Phys.* **1927**, *44*, 455.

[3] Heisenberg, W. *Z. Phys.* **1927**, *43*, 172.

[4] Schrödinger, E. *Ann. Phys.* **1926**, *79*, 361.

[5] Szabo, A.; Ostlund, N. S. *Modern Quantum Chemistry, Introduction to Advanced Electronic Structure Theory*; Dover Publications: New York, 1989.

[6] Born, M.; Oppenheimer, J. R. *Ann. Physik* **1927**, *84*, 457.

[7] Hartree, D. R. *Proc. Camb. Philos. Soc.* **1927**, *24*, 89.

[8] Slater, J. C. *Phys. Rev* **1930**, *35*, 210.

[9] Fock, V. *Z. Phys.* **1930**, *61*, 126.

[10] Slater, J. C.; Verma, H. C. *Phys. Rev.* **1929**, *34*, 1293.

[11] Slater, J. C. *Phys. Rev.* **1930**, *35*, 509.

[12] Roothaan, C. C. J. *Rev. Mod. Phys.* **1951**, *23*, 69.

[13] Hall, G. G. *Proc. Royal Soc. (London)* **1951**, *A205*, 541.

[14] Pople, J. A.; Nesbet, R. K. *J. Chem. Phys.* **1954**, *22*, 571.

[15] Roothaan, C. C. J. *Rev. Mod. Phys.* **1960**, *32*, 179.

[16] Woon, D. E.; Dunning, T. H. *J. Chem. Phys.* **1993**, *98*, 1358.

[17] Kendall, R. A.; Dunning, T. H.; Harrison, R. J. *J. Chem. Phys.* **1992**, *96*, 6796.

[18] Shao, Y. et al. *Phys. Chem. Chem. Phys.* **2006**, *8*, 3172–3191.

[19] Löwdin, P.-O. *Adv. Chem. Phys.* **1959**, *2*, 207.

[20] Møller, C.; Plesset, M. S. *Phys. Rev.* **1934**, *46*, 618.

[21] Sherrill, C. D.; Schaefer, H. F. In *Advances in Quantum Chemistry*; Löwdin, P. O., Ed.; Academic Press: San Diego, 1999; pp 143–269.

[22] Cizek, J. *J. Chem. Phys.* **1966**, *45*, 4256.

[23] Hohenberg, P.; Kohn, W. *Phys. Rev.* **1964**, *136*, B864.

[24] Kohn, W.; Sham, L. J. *Phys. Rev.* **1965**, *140*, A1133.

[25] Parr, R. G.; Yang, W. *Density Functional Theory of Atoms and Molecules*; Oxford University Press: U.S.A., 1994.

[26] Schultz, N.; *et al.*, *J. Phys. Chem. A* **2005**, *109*, 4388.

[27] N.E. Schultz, t. *J. Phys. Chem. A* **2005**, *109*, 11127.

[28] Zhao, Y.; Truhlar, D. G. *J. Chem. Theory Comput.* **2005**, *1*, 415.

[29] Becke, A. D. *J. Chem. Phys.* **1993**, *98*, 5648.

[30] Hylleraas, E. *Z. Phys.* **1929**, *54*, 347.

[31] Kinoshita, T. *Phys. Rev.* **1957**, *105*, 1490.

[32] Kutzelnigg, W.; Klopper, W. *J. Chem. Phys.* **1991**, *94*, 1985.

[33] Klopper, W.; Manby, F. R.; Ten-No, S.; Valeev, E. F. *Int. Rev. Phys. Chem.* **2006**, *25*, 427.

[34] Lester, W. A.; Krauss, M. *J. Chem. Phys.* **1966**, *44*, 207.

[35] Per, M. C.; Russo, S. P.; Snook, I. K. *J. Chem. Phys.* **2009**, *130*, 134103.

[36] Coulson, C. A.; Neilson, A. H. *Proc. Phys. Soc. (London)* **1961**, *78*, 831–837.

[37] Coleman, A. J. *Int. J. Quantum Chem. Symp.* **1967**, *1*, 457.

[38] Thakkar, A. J.; Smith, V. H. *Chem. Phys. Lett.* **1976**, *42*, 476–481.

[39] Boyd, R. J.; Sarasola, C.; Ugalde, J. M. *At. Mol. Opt. Phys.* **1988**, *21*, 2555–2561.

[40] Gill, P. M. W.; Crittenden, D. L.; O'Neill, D. P.; Besley, N. A. *Phys. Chem. Chem. Phys.* **2006**, *8*, 15–25.

[41] Thakkar, A. J. In *Density Matrices and Density Functionals*; Erdahl, R. M., Smith, V. H., Eds.; Reidel: Dordrecht, 1987; pp 553–581.

[42] Boyd, R. J.; Ugalde, J. M. In *Computational Chemistry*; Fraga, S., Ed.; Elsevier: Amsterdam, 1992; pp 273–299.

[43] Valderrama, E. In *Many-Electron Densities and Reduced Density Matrices*; Cioslowski, J., Ed.; Kluwer Academic: New York, 2000; pp 231–248.

[44] Davidson, E. R. *Reduced Density Matrices in Quantum Chemistry*; Academic: New York, 1976.

[45] Koga, T. In *Many-Electron Densities and Reduced Density Matrices*; Cioslowski, J., Ed.; Kluwer Academic: New York, 2000; pp 267–298.

[46] Gill, P. M. W.; Lee, A. M.; Nair, N.; Adamson, R. D. *J. Mol. Struct. (Theochem)* **2000**, *506*, 303–312.

[47] Lee, A. M.; Gill, P. M. W. *Chem. Phys. Lett* **1999**, *313*, 271.

[48] O'Neill, D. P.; Gill, P. M. W. *Phys. Rev. A* **2003**, *68*, 022505.

[49] Gill, P. M. W.; O'Neill, D. P.; Besley, N. A. *Theor. Chem. Acc.* **2003**, *109*, 241.

[50] Besley, N. A.; O'Neill, D. P.; Gill, P. M. W. *J. Chem. Phys.* **2003**, *118*, 2033.

[51] Gill, P. M. W.; Besley, N. A.; O'Neill, D. P. *Int. J. Quantum Chem.* **2004**, *100*, 2033.

[52] Besley, N. A.; Gill, P. M. W. *J. Chem. Phys.* **2004**, *120*, 7290.

[53] Besley, N. A.; Lee, A. M.; Gill, P. M. W. *Mol. Phys.* **2002**, *100*, 1763.

[54] Pearson, J. K.; Crittenden, D. L.; Gill, P. M. W. *J. Chem. Phys.* **2009**, *130*, 164110.

[55] Gill, P. M. W.; Besley, N. A.; O'Neill, D. P. *Int. J. Quantum Chem.* **2004**, *100*, 166.

[56] Thakkar, A. J.; Moore, N. J. *Int. J. Quantum Chem.* **1981**, *20*, 393–400.

[57] Galvez, F. J.; Buendia, E.; Sarsa, A. *J. Chem. Phys.* **1999**, *111*, 3319.

[58] Pearson, J. K.; Gill, P. M. W.; Ugalde, J. M.; Boyd, R. J. *Mol. Phys.* **2009**, *107*, 1089–1093.

[59] Wang, J.; Tripathi, A. N.; Smith, V. H. *J. Chem. Phys.* **1992**, *97*, 9188.

[60] Wang, J.; Tripathi, A. N.; Smith, V. H. *J. Phys. B* **1993**, *26*, 205.

[61] Engel, T.; Reid, P. *Physical Chemistry*, 2nd ed.; Prentice Hall, 2010.

[62] Loos, P. F.; Gill, P. M. W. *Mol. Phys.* **2010**, *108*, 2527.

[63] Gill, P. M. W.; O'Neill, D. P.; Besley, N. A. *Theor Chem. Acc.* **2003**, *109*, 241.

[64] Gill, P. M. W.; Besley, N. A.; O'Neill, D. *Int. J. Quantum Chem.* **2004**, *100*, 166.

[65] Schmidt, M. W.; Ruedenberg, K. *J. Chem. Phys.* **1979**, *71*, 3951.

[66] Koga, T. *Theor. Chem. Acc.* **2000**, *105*, 96–99.

[67] Koga, T. *J. Chem. Phys.* **2001**, *114*, 72–75.

[68] Koga, T.; Matsuyama, H. *J. Chem. Phys.* **1998**, *108*, 3424–3430.

[69] Matsuyama, H.; Koga, T. *Chem. Phys. Lett.* **1999**, *300*, 515.

[70] Koga, T.; Matsuyama, H.; Romera, E.; Dehesa, J. S. *Phys. Rev. A* **1998**, *57*, 4212.

[71] Romera, E. *J. Phys. B: At. Mol. Opt. Phys.* **2002**, *35*, L309–L314.

[72] Cioslowski, J.; Liu, G. *J. Chem. Phys* **1998**, *109*, 8225.

[73] Hylleraas, E. A. *Z. Phys.* **1930**, *65*, 209.

[74] Koga, T.; Kasai, Y.; Thakkar, A. J. *Int. J. Quantum. Chem* **1993**, *46*, 689–699.

[75] Koga, T. *J. Chem. Phys.* **1996**, *104*, 6308–6312.

[76] Mathematica 7. Wolfram Research, Inc., 2008.

[77] Loos, P.-F.; Gill, P. M. W. *Phys. Rev. A* **2010**, *81*, 052510.

[78] Curl, R. F.; Coulson, C. A. *Proc. Phys. Soc.* **1965**, *85*, 647.

[79] Boyd, R. J.; Coulson, C. A. *J. Phys. B* **1973**, *B6*, 782.

[80] Boyd, R. J. *Theoret. Chim. Acta* **1974**, *33*, 79–86.

[81] Loos, P.-F.; Gill, P. M. W. *Chem. Phys. Lett.* **2010**, *500*, 1.

[82] Hoegaasen, H.; Richard, J.-M.; Sorbal, P. *Am. J. Phys.* **2010**, *78*, 86–93.

[83] Nakashima, H.; Nakatsuji, H. *J. Chem. Phys.* **2007**, *127*, 224104.

[84] Nakashima, H.; Nakatsuji, H. *J. Chem. Phys.* **2008**, *128*, 154107.

[85] Nakashima, H.; Hijikata, Y.; Nakatsuji, H. *J. Chem. Phys.* **2008**, *128*, 154108.

[86] Kurokawa, Y. I.; Nakashima, H.; Nakatsuji, H. *Phys. Chem. Chem. Phys.* **2008**, *10*, 4486.

[87] Proud, A. J.; Pearson, J. K. *J. Chem. Phys.* **2010**, *133*, 134113.

[88] Wang, J.; Kim, K. S.; Baerends, E. J. *J. Chem. Phys.* **2010**, *132*, 204102.

[89] Lennard-Jones, J. E.; Pople, J. A. *Phil. Mag.* **1952**, *43*, 581.

[90] Banyard, K. E.; Ellis, D. J. *Mol. Phys.* **1972**, *24*, 1291.

[91] Banyard, K. E.; Ellis, D. J. *J. Phys. B: At. Mol. Phys.* **1975**, *8*, 2311.

[92] Rehmus, P.; Kellman, M. E.; Berry, R. S. *Chem. Phys.* **1978**, *31*, 239.

[93] Boyd, R. J.; Yee, M. C. *J. Chem. Phys.* **1982**, *77*, 3578–3582.

[94] Ugalde, J. M.; Boyd, R. J. *Int. J. Quantum Chem.* **1985**, *27*, 439–449.

[95] Ugalde, J. M.; Boyd, R. J.; Perkyns, J. S. *J. Chem. Phys.* **1987**, *87*, 1216–1219.

[96] Koga, T. *J. Chem. Phys.* **2002**, *117*, 10493.

[97] Koga, T. *Chem. Phys. Lett.* **2003**, *10*, 565–570.

[98] Koga, T. *Theor. Chem. Acc.* **2003**, *110*, 79.

[99] Koga, T.; Matsuyama, H. *J. Phys. B: At. Mol. Opt. Phys.* **2005**, *38*, 3687–3692.

[100] Koga, T. *J. Chem. Phys.* **2004**, *120*, 7145.

[101] Matsuyama, H.; Koga, T. *Theor. Chem. Acc.* **2004**, *111*, 25.

[102] Koga, T.; Matsuyama, H. *J. Chem. Phys.* **2004**, *120*, 7831.

[103] Koga, T. *Theor. Chem. Acc.* **2004**, *112*, 431.

[104] Matsuyama, H.; Koga, T. *Theor. Chem. Acc.* **2004**, *112*, 435.

[105] Kominos, Y.; Nicolaides, C. A. *Phys. Rev. A* **1994**, *50*, 3782.

[106] Nicolaides, C. A.; Kominos, Y. *Int. J. Quantum Chem.* **1998**, *67*, 321.

[107] Kominos, Y.; Nicolaides, C. A. *Int. J. Quantum Chem.* **1999**, *71*, 25.

[108] Koga, T.; Matsuyama, H.; Thakkar, A. J. *Chem. Phys. Lett* **2011**, *512*, 287–289.

[109] Loos, P. F. *Phys. Rev. A* **2010**, *81*, 032510.

[110] Loos, P. F.; Gill, P. M. W. *J. Chem. Phys.* **2010**, *132*, 234111.

[111] Loos, P. F.; Gill, P. M. W. *Phys. Rev. A* **2010**, *81*, 052510.

[112] Hollett, J. W.; McKemmish, L. K.; Gill, P. M. W. *J. Chem. Phys* **2011**, *134*, 224103.

[113] Boyd, R. J. *Can. J. Phys.* **1975**, *53*, 592.

[114] Boyd, R. J.; Coulson, C. A. *J. Phys. B* **1973**, *6*, B864.

[115] Slamet, M.; Sahni, V. *Phys. Rev. A* **1995**, *51*, 2815.

[116] de Saavedra, F. A.; Porras, I.; Buendía, E.; Gálvez, F. J. *J. Phys. B.* **1995**, *28*, 3123.

[117] Kais, S.; Herschbach, D. R.; Levine, R. D. *J. Chem. Phys.* **1989**, *91*, 7791.

[118] Kestner, N. R.; Sinanoglu, O. *Phys. Rev.* **1962**, *128*, 2687.

[119] Ragot, S. *J. Chem. Phys.* **2008**, *128*, 164104.

[120] Manzano, D.; Plastnio, A. R.; Dehesa, J. S.; Koga, T. *J. Phys. A: Math. Theor.* **2010**, *43*, 275301.

[121] Katriel, J.; Roy, S.; Springborg, M. *J. Chem. Phys.* **2005**, *123*, 104104.

[122] Amovilli, C.; March, N. H. *Phys. Rev. A* **2003**, *67*, 022509.

[123] Gori-Giorgi, P.; Savin, A. *J. Chem. Theory Comput.* **2007**, *3*, 796.

[124] Gill, P. M. W.; O'Neill, D. P. *J. Chem. Phys.* **2005**, *122*, 094110.

[125] Kais, S.; Herschbach, D. R.; Handy, N. C.; Murray, C. W.; Laming, G. J. *J. Chem. Phys.* **1993**, *99*, 417.

[126] Abramowitz, M.; Stegun, I. A. *Handbook of Mathematical Functions*; Dover: New York, 1965.

[127] Ryabinkin, I. G.; Staroverov, V. N. *Phys. Rev. A* **2010**, *81*, 032509.

[128] Alavi, A. *J. Chem. Phys.* **2000**, *113*, 7735.

[129] Ghosh, S.; Gill, P. M. W. *J. Chem. Phys.* **2005**, *122*, 154108.

[130] Thompson, D. C.; Alavi, A. *Phys. Rev. B* **2002**, *66*, 235118.

[131] Jung, J.; Alvarellos, J. E. *J. Chem. Phys.* **2003**, *118*, 10825.

[132] Jung, J.; Garcia-Gonzalez, P.; Alvarellos, J. E.; Godby, R. W. *Phys. Rev. A* **2004**, *69*, 052501.

[133] Thompson, D. C.; Alavi, A. *Phys. Rev. B* **2004**, *69*, 201302.

[134] Thompson, D. C.; Alavi, A. *J. Phys.: Condens. Matter* **2004**, *16*, 7979.

[135] Thompson, D. C.; Alavi, A. *J. Chem. Phys* **2005**, *122*, 124107.

[136] Boyd, R. J.; Coulson, C. A. *J. Phys. B* **1973**, *6*, 782.

[137] Boyd, R. J.; Katriel, J. *Int. J. Quantum Chem.* **1974**, *8*, 255.

[138] Ugalde, J. M.; Boyd, R. J.; Perkins, J. S. *J. Chem. Phys.* **1987**, *87*, 1216.

[139] Thakkar, A. J. *J. Phys. B* **1987**, *20*, 3939.

[140] Banyard, K. E.; Keeble, D. R. T.; Drake, G. W. F. *J. Phys. B* **1992**, *25*, 3405.

[141] Boys, S. F. *Proc. R. Soc. London.* **1950**, *A200*, 542.

[142] Hollett, J. M.; Gill, P. M. W. *Phys. Chem. Chem. Phys.* **2011**, *13*, 2972.

[143] Pople, J. A.; Head-Gordon, M.; Fox, D. J.; Raghavachari, K.; Curtiss, A. *J. Chem. Phys.* **1989**, *90*, 5622.

[144] Dunning, T. H.; Peterson, K. A.; Wilson, A. K. *J. Chem. Phys.* **1989**, *90*, 1007.

[145] Roos, B.; Siegbahn, P. *Theor. Chim. Acta* **1971**, *21*, 368–380.

[146] Breitenstein, M.; Dannohl, H.; Meyer, H.; Seeger, R.; Seeger, U.; Zittlau, W. *Int. Rev. Phys. Chem.* **1983**, *3*, 335.

[147] Hall, M. B. In *Electron Distributions and the Chemical Bond*; Coppens, P., Hall, M. B., Eds.; Plenum Press: New York, 1982.

[148] Kunze, K. L.; Hall, M. B. *J. Am. Chem. Soc.* **1986**, *108*, 5122–5127.

[149] Wang, M.; Hu, X.; Beratan, D. N.; Yang, W. *J. Am. Chem. Soc.* **2006**, *128*, 3228.

[150] von Lilenfeld, O. A.; Lins, R. D.; Rothlisberger, U. *Phys. Rev. Lett.* **2005**, *95*, 153002.

[151] Lennard-Jones, J. E.; Pople, J. A. *Proc. Roy. Soc. (London)* **1950**, *A202*, 166.

[152] Lennard-Jones, J. E.; Pople, J. A. *Proc. Roy. Soc. (London)* **1951**, *A210*, 190.

[153] Edmiston, C.; Ruedenberg, K. *Rev. Mod. Phys.* **1963**, *35*, 457.

[154] Boys, S. F. *Rev. Mod. Phys.* **1960**, *32*, 296.

[155] Foster, J. M.; Boys, S. F. *Rev. Mod. Phys.* **1960**, *32*, 300.

[156] von Niessen, W. *J. Chem. Phys.* **1972**, *47*, 971.

[157] Pipek, J.; Mezey, P. G. *J. Chem. Phys.* **1989**, *90*, 4916.

[158] Lin, H.; Truhlar, D. G. *Theor. Chem. Acc.* **2007**, *117*.

[159] Singh, U. C.; Kollman, P. A. *J. Comput. Chem.* **1986**, *7*, 718.

[160] Svensson, M.; Humbel, S.; Froese, R. D. J.; Matsubara, T.; Sieber, S.; Morokuma, K. *J. Phys. Chem.* **1996**, *100*, 19357.

[161] Schmidt, M. W.; Baldridge, K. K.; Boatz, J. A.; Elbery, S. T.; Gordon, M. S.; Jensen, J. H.; Koseki, S.; Matsunaga, N.; Nguyen, K. A.; Su, S. J.; Windus, T. L.; Dupuis, M.; Montgomery, J. A. *J. Comput. Chem.* **1993**, *14*, 1347–1363.

[162] Koga, T. *J. Chem. Phys.* **2004**, *121*, 3939.